Harmonic State Space Model of Three Phase Thyristor Controlled Reactor

Jordan Rel C. Orillaza

A thesis presented for the degree of
Doctor of Philosophy
in
Electrical and Computer Engineering
at the
University of Canterbury,
Christchurch, New Zealand.

April 2012

ABSTRACT

Harmonic domain models have been developed for Thyristor Controller Reactors (TCR) and other power electronic devices. Recently, these models have been extended to describe not just the steady-state harmonic interactions but harmonic transients as well. However, these dynamic models consistently do not incorporate models for controls. On the other hand, for the TCR as a FACTS Controller, dynamic models are available in which only the fundamental frequency component of the Controller is included; excluding harmonic interactions presumes that these do not affect the dynamics of the Controller. This thesis describes the development of a Harmonic State Space (HSS) model of a three phase TCR. As an extended state space description, this model describes the dynamics of the Controller while capturing harmonic interactions. It also includes the effect of switching instant variation which significantly improves the effectiveness of the model and allows the controller feedback characteristics to be included. The result of this model was validated with a purely time-domain simulation in PSCAD/EMTDC. Using the HSS to model a power system with TCR, it is illustrated that harmonic interactions play a significant role in the dynamics of the system. It is observed that for the specific system analysed, the least-damped pole-pair which dominates the dynamics of the system is associated with the 5^{th} harmonic. Failure to include interactions with this specific harmonic produces an inaccurate dynamic description.

Preliminary to the development of HSS model, a linearised harmonic domain model of a TCR which establishes the harmonic interactions across the device is also developed. Results of this model are validated with a time-domain simulation. This characterisation paves the way for a reduced harmonic state space model that is used in the HSS model.

The principles and procedures established in this thesis can be applied to the development of models for other FACTS Controllers or HVDC links.

CONTENTS

LIST OF FIGURES

LIST OF TABLES

NOMENCLATURE

DHD	Dynamic Harmonic Domain
EHD	Extended Harmonic Domain
EMP	Exponentially Modulated Periodic
FACTS	Flexible AC Transmission System
FFT	Fast-Fourier Transform
FTM	Frequency Transfer Matrix
HAM	Harmonic Admittance Matrix
HD	Harmonic Domain
HDAM	Harmonic Domain Admittance Matrix
HDDTF	Harmonic Domain Dynamic Transfer Function
HSS	Harmonic State Space
HTF	Harmonic Transfer Function
LTI	Linear Time Invariant
LTP	Linear Time Periodic
LTV	Linear Time Variant
MDHD	Modified Dynamic Harmonic Domain
PAM	Pulse Amplitude Modulation
PSS	Partial Steady-State
PT	Partial Transient
RHP	Right-Hand-Plane
RMS	root-mean-square

SIV	Switching Instant Variation
SVC	Static VAR Compensator
TCR	Thyristor Controlled Reactor
VAR	Volt Ampere Reactive
α	thyristor switch-on
β	thyristor switch-off
$\delta(f)$	harmonic vector for the Dirac delta or sampling function
$\delta_T(t)$	Dirac delta or sampling function
$\mathbb{C}$	set of complex numbers
$\mathbb{Z}$	set of integers
$\mathcal{D}\{\cdot\}$	operation to convert a vector to a diagonal matrix
$\mathcal{H}\{\cdot\}$	operation to convert a vector to a Hankel matrix
$\mathcal{T}\{\cdot\}$	operation to convert a vector to a Toeplitz matrix
$\mathbf{\Delta}(f)$	frequency transfer matrix for the Dirac delta or sampling function
$\mathbf{\Gamma}(t)$	modulation vector to transform a harmonic domain vector to a time domain signal
$\mathbf{\Lambda}$	general symbol for a frequency transfer matrix
ω_0	fundamental angular frequency
ω_n	natural angular frequency
ω_p	angular frequency of reflected pole
$\Psi_0(t)$	switching function with fixed switching instants
h	highest harmonic number in the model
H_c	characteristic harmonics
h_c	a characteristic harmonic
r_k	sequence number (i.e. positive, negative, or zero) of the k^{th} harmonic
s	complex frequency, complex argument of Laplace transform
s_k	complex frequency modulated by the k^{th} harmonic

$X(\omega)$	harmonic domain signal or vector of harmonic domain coefficients
$x(t)$	time domain signal
$X_\psi(\omega)$	three-phase harmonic domain signal or vector of harmonic domain coefficients
$x_\psi(t)$	three phase time domain signal

Chapter 1

INTRODUCTION

1.1 THYRISTOR CONTROLLED REACTORS

Thyristor Controlled Reactor (TCR) installations have been around for a few decades now. Possibly the first publication related to the use of thyristors for producing variable inductance was in 1967 by Sen, Biringer and Segsworth [61]. ABB [2] reports that their predecessor's (ASEA) first Static VAR Compensator (SVC) installation was a 20kV/60MVAR system at an electric arc furnace in Sweden in 1970. The same document estimates that at present, 138,000 MVAR of controllable shunt reactive power has been installed worldwide. With the TCR's capability of providing quick and continuous-valued reactive power support that is essential to the operation of the power system, its proliferation is expected to continue. As a first-generation Flexible AC Transmission System (FACTS) Controllers[†], there is value in applying new techniques to develop new models for this Controller.

1.2 HARMONIC INTERACTIONS IN A CONTROLLER

As an electronically-controlled variable-reactance device, various linear models for the harmonic interactions across the TCR are available. Based on the switching function of the thyristors, these models describe the current harmonics generated by the device and the resulting harmonic distortion in the bus voltage. The switching instants of the thyristors are known to be nonlinearly dependent to the applied voltage. Hence, existing linearised models are limited to use predetermined switching instants which affects the overall accuracy of these models. A better model has to incorporate the effect of voltage distortion on switching instants.

Recently, a number of dynamics models have been presented to describe not just the steady state of the individual harmonics but the dynamics of these harmonics, as well. It is conspicuous that these dynamics models do not include the description of the

[†]Similar with Hingorani and Gyugyi's [30] convention, "Controller" with capital C refers to a "FACTS Controller" as opposed to the lowercase "controller" that refers to a particular component in a feedback system

controller which is of critical importance to the dynamics of the system. Better results would be obtained if the effect of switching instant variation were incorporated and controller models are included.

Various models for TCR as a Controller are also available. The most common application is for voltage control which is either an end in itself or possibly an intermediate procedure to satisfy more complex requirements in the system [42]. The RMS of the bus voltage which is essentially a measure of the fundamental frequency voltage, is controlled by a reference voltage, V_{ref}, which is a DC signal. As a DC-signal Controller, available TCR models leave out the effects of harmonic interactions. Similarly, applications for power factor correction and load balancing where real and reactive power are controlled, only the effective fundamental frequency power are considered, hence harmonic interactions are again ignored in most models. Disregard for harmonic interaction in Controller models assumes that harmonic interactions do not affect the dynamics of the Controller.

1.3 RESEARCH OBJECTIVES

As a first generation FACTS Controller, the TCR's mature technology makes it a suitable platform to develop a novel modelling procedure. The primary objective of this research is to develop a dynamic model for TCR that is suitable for analysing small-signal stability of a system with FACTS Controller. This model should be able to accommodate the description of a controller which is known to significantly affect the dynamic response of the system; at the same time, it should capture the harmonic interaction across the device. Even as a linearised model, it is imperative that the effect of voltage distortion on the thyristor switching is included in the model. As a model that is in the form of a Linear Time Invariant system model, analysis techniques such as pole-zero locations and step response will be applicable to it.

It is also an important objective of this research that simulation results from the developed harmonic domain model be validated with another simulation which is time-domain based. While there is subjectivity in validating results from these different procedures, insights could still be drawn regarding the performance of the developed model.

Although the primary task is to develop a model for observing harmonic interaction across the device, it is envisaged that the same modelling procedure could be extended to model two or more power electronic controllers that are electrically close to each other.

1.4 THESIS OUTLINE

Chapter 2 describes the advances in the development of linearised model for power electronics apparatus in the power system. As previously observed in [73], there are two streams of progress in this area, namely, models for analysing harmonics, and models for analysing controls. This chapter traces them both and highlights that the direction is for these two streams to converge to a model of the system with power electronics that describes the small-signal stability while taking into account the harmonic interactions. This is the essence of the Harmonic State Space (HSS) model being advanced in this thesis.

Prior to the development of a full HSS model, the harmonic interaction across the TCR is analytically described by developing a linearised harmonic domain model. Chapter 3 presents the development of a linearised harmonic domain model of a three phase TCR. It describes in detail the harmonic interaction from voltage distortion and from switching angle modulation to line current variation. This model is used as basis before proceeding with a HSS model of the TCR.

The full development of a HSS model prior to the integration of controls is presented in Chapter 4. The HSS structure is presented together with a proposal to use only the characteristic harmonics for the purpose of reducing the size and complexity of the model.

The HSS model for a TCR with voltage control procedure is presented in Chapter 5. In addition to the model presented in the preceding chapter, a small-signal frequency transfer matrix for the actuator, the voltage meter and the controller are presented. The pole locations in the resulting models are analysed to provide insights into the stability of the system. The results of the HSS model is validated with a time-domain simulation.

This thesis closes with a final chapter summarising the contributions of this research and describing areas of future work that can be derived from this work.

Chapter 2

RELATED WORK

2.1 INTRODUCTION

This chapter presents an overview of the literature related to the HSS model development in this thesis. It aims to put in perspective the motivations that led to this research. It provides an overview of linearised models before it proceeds to the main section on dynamic models. The discussion on dynamic models traces the advances in FACTS Controller models suitable for small-signal stability studies that culminate in the HSS model presented in this thesis.

2.2 LINEARISED MODELS

While there is little doubt that thyristor based power electronic circuits are both time variant and non-linear, there is great value in models that linearise their behaviour. This allows access to an enormous range of efficient linear algebra methods, and allows the use of powerful classical control and analysis techniques.

Systems with fully controlled (and fixed) switching instants predictably switch from one linear combination of components to another, and form a special class of systems known as Linear Time Variant (LTV). In general, they can be described by the equation set:

$$\dot{x}(t) = A(t)x(t) + B(t)u(t) \tag{2.1a}$$

$$y(t) = C(t)x(t) + D(t)u(t) \tag{2.1b}$$

To be LTV, the time variation of $A(t)$, $B(t)$, $C(t)$, and $D(t)$ must be independent of x and u. A fixed switching instant, IGBT-based circuit would meet this criteria. However, in a TCR or HVDC circuit, thhyristor switch-off is dependent on state-variables — the thyristor currents — which makes the matrices A,B,C, and D functions of time and x, rendering the circuit relationships truly non-linear. Even in a fully controlled IGBT-based converter, if the switching instants are controlled by a controller that measures

system variables, then the system is non-linear. This inherent non-linearity of typical FACTS Controllers has until now hampered the development and use of good linearised models.

Even a nonlinear system responds linearly with a small-signal input applied about a stable operating point. Linearisation refers to finding a linear approximation of the model about an operating point. Small-signal stability studies are carried out on linearised model as an important initial test prior to more detailed large-signal stability studies. This process can be fast and efficient.

The dynamic behaviour of a power system can be described as a multivariable differential equation that takes the general form of 2.2

$$\begin{aligned} \dot{x}_i &= f_i(x_1, x_2, \ldots, x_n, u_1, u_2, \ldots, u_m, t) \\ \dot{\boldsymbol{x}} &= \boldsymbol{f}(\boldsymbol{x}, \boldsymbol{u}, t) \end{aligned} \tag{2.2}$$

where $\boldsymbol{x}(t)$[†] and $\boldsymbol{u}(t)$ refer to the vector of n-state variables and the vector of m-inputs, respectively. Complementary to this, a measurement equation takes the following form:

$$\begin{aligned} y_j &= g_j(x_1, x_2, \ldots, x_n, u_1, u_2, \ldots, u_m, t) \\ \boldsymbol{y} &= \boldsymbol{g}(\boldsymbol{x}, \boldsymbol{u}, t) \end{aligned} \tag{2.3}$$

It is not difficult to show[‡] that after linearising this set of equations about an initial state, a set of linearised state-space equation can be written in standard form as follows:

$$\begin{aligned} \Delta\dot{\boldsymbol{x}} &= \boldsymbol{A}\Delta\boldsymbol{x} + \boldsymbol{B}\Delta\boldsymbol{u} \\ \Delta\boldsymbol{y} &= \boldsymbol{C}\Delta\boldsymbol{x} + \boldsymbol{D}\Delta\boldsymbol{u} \end{aligned} \tag{2.4}$$

where $\boldsymbol{A}$, $\boldsymbol{B}$, $\boldsymbol{C}$, and $\boldsymbol{D}$ are the Jacobian matrices for $\boldsymbol{f}$ with respect to $\boldsymbol{x}$, $\boldsymbol{f}$ with respect to $\boldsymbol{u}$, $\boldsymbol{g}$ with respect to $\boldsymbol{x}$ and $\boldsymbol{g}$ with respect to $\boldsymbol{u}$, respectively. Equation 2.4 provides the framework for writing the linearised mathematical description of the system.

There is a wealth of useful techniques that can be applied to linearised models. Primarily, system models can be developed by interconnecting various submodels. Block diagram algebra is a well-known procedure and is described in any control engineering book such as [47] and [22]. Equally important but not as commonly available in texts is an algorithm for automatically interconnecting state-space blocks. This was presented in the development of a comprehensive HVDC model in [53].

Wood, Hume and Osauskas [73], [31] in 2000 reviewed models for HVDC and FACTS Controllers, and observed that linearised models whether derived analytically or through

[†]For the rest of the thesis, a bold typeface indicates a matrix or vector.

[‡]This is presented in detail in various texts such as by Kundur in 1994 [36]

extensive simulations can be classified according to purpose, namely, models for harmonic analysis, or models for control analysis. Historically, there is indeed a clear distinction between these categories, however recent developments trend toward diminishing that distinction. This is the main objective of this thesis — that linearised harmonic domain models for the purpose of control analysis shall include complete descriptions of the harmonic interactions. The succeeding subsections present the various models that are described in the literature.

2.3 LINEARISED MODELS FOR HARMONIC ANALYSIS

As early as 1976, Gyugyi [25] introduced a set of existence functions that facilitates the description of the components of an output voltage (or current) from the components of an input voltage (or current). In matrix form, an existence matrix, $\boldsymbol{H}(t)$ describes the transfer from $\boldsymbol{v}_i(t)$ to $\boldsymbol{v}_o(t)$.

$$\boldsymbol{v}_i(t) = \boldsymbol{H}(t)\boldsymbol{v}_o(t) \tag{2.5}$$

Gyugyi originally used this to describe the frequency changes across a converter. It is easy to appreciate that if the elements of the vectors, $\boldsymbol{v}_i(t)$ and $\boldsymbol{v}_o(t)$, are the harmonic components of the input and the output, respectively, then the existence function effectively describes the frequency modulation across the converter.

The existence function was later adopted by Wood in 1984 [76] to analyse switching power converters. The existence function (existence matrix) was referred to as switching function (switching matrix) as it was extensively used to analyse switching circuits. The rest of the linearised models that follow, with the aim of describing harmonic interactions apply this procedure in some way.

In 1989, Bohmann and Lasseter [10] introduced a Harmonic Admittance Matrix (HAM) based on switching functions for circuits such as a TCR. The limitation of this model is that switching instants have to be pre-calculated before generating the switching matrix.

Also in 1989, an important modeling development was presented by Larsen, Baker and McIver [38], where they presented a linearised model of the complex harmonic interaction across the AC and DC networks in an HVDC system. They described the harmonic transfers between a set of inputs (i.e. AC-side voltage, DC-side current and modulated firing angle) to a set of outputs (i.e. DC-side voltage and AC-side current) as shown in 2.6 with a set of matrices where each harmonic matrix was extracted from a converter simulation using numerical methods. This could be one of the earliest attempts to incorporate a control signal (i.e. modulated firing angle) into the harmonic transfers. Another important contribution of this publication is that it highlights the effectiveness of using sequence components in a three phase harmonic model, exem-

plifying the difference in frequency shifts associated with positive sequence harmonics and negative sequence harmonics.

$$\begin{bmatrix} \Delta V_{dc} \\ \Delta I_{+ve} \\ \Delta I_{-ve} \end{bmatrix} = \begin{bmatrix} VVP & VVN & VI & VB \\ IPVP & IPVN & IPI & IPB \\ INVP & INVN & INI & INB \end{bmatrix} \begin{bmatrix} \Delta V_{+ve} \\ \Delta V_{-ve} \\ \Delta I_{dc} \\ \Delta \beta \end{bmatrix} \tag{2.6}$$

Wood, Hume and Osauskas [73] picked up from Larsen, et al. by using the same set of harmonic transfers but improved on it by deriving analytically each harmonic matrix. Instead of focusing on the rigors of the derivation, this publication described the mechanisms involved in the harmonic transfers which gave a better appreciation of the harmonic interactions involved. Hume's thesis in 2002 [31], included the details of the analytical model of the HVDC converter.

Prior to that, Osauskas and Wood in 1998 [52] applied a similar approach to derive individual transfers for a three phase TCR. They analytically derived the transfers from both voltage distortion and firing angle modulation to current distortion. This model has been a strong influence in the linearised harmonic domain model that is presented in Chapter 3.

Other worthy publications, specifically for TCR includes Acha's linearised model for the TCR [3] where the TCR is described as a Norton admittance matrix that includes the cross-couplings between harmonics of the currents and the voltage. However, the process of calculating the harmonics of the current involves multiple transformations between time-domain and frequency domain and the use of Fast-Fourier Transform (FFT) calculation. In 1996, Rico, Acha and Miller improved on it, by using switching functions to derive the harmonic Norton equivalent of the TCR. The assumption however is that the switching function is not affected by low or moderate distortion (i.e. in voltages). Although, this produced good results according to their purpose, there is still a need to address the effect of voltage distortion on switching instants.

The next major advance in TCR harmonic modelling was the Harmonic Domain Admittance Matrix (HDAM) by Noda, Semlyen and Iravani in 2004 [48]. They presented the derivation of HDAM for the nonlinear and switching elements to be incorporated into the Jacobian of the system for a Newton-Raphson iterative solution. The problem with switching instants being affected by voltage distortion can be addressed by using the values of the previous iteration to solve the present switching instants. Related to this, Lima, Semlyen and Iravani [39] described a detailed iterative calculation of HDAM of a TCR as a function of distorted voltage, and switching instants.

2.3.1 Extended Harmonic Domain

In the past decade or so, resulting from the proliferation of power electronic devices, it became apparent that the traditional Harmonic Domain (HD)[††] models which describe the harmonics in steady-state could be extended to describe the harmonics in transients as well. These models are alternately termed as either Extended Harmonic Domain (EHD) or Dynamic Harmonic Domain (DHD). They quantify individual harmonics during transients with the possibility of defining new indices with applications in the development of more robust protection and control schemes [58].

In 2003, Rico, Madrigal and Acha [58] presented the Extended Haromonic Domain (EHD) and applied it to a pulse-width modulation (PWM) STATCOM model. The core equations that are used in this descriptions stem from the state-space equations for time-periodic systems:

$$\begin{aligned} \dot{x}(t) &= a(t)x(t) + b(t)u(t) \\ y(t) &= c(t)x(t) + d(t)u(t) \end{aligned} \tag{2.7}$$

where $a(t)$,$b(t)$,$c(t)$ and $d(t)$ are periodic functions.

Without going into the details, if the state and input variables can be written as Exponentially Modulated Periodic (EMP), 2.7 can be written in matrix equations as

$$\begin{aligned} \dot{\boldsymbol{X}} &= (\boldsymbol{A} - \boldsymbol{N})\boldsymbol{X} + \boldsymbol{B}\boldsymbol{U} \\ \boldsymbol{Y} &= \boldsymbol{C}\boldsymbol{X} + \boldsymbol{D}\boldsymbol{U} \end{aligned} \tag{2.8}$$

where input ($\boldsymbol{U}$), output($\boldsymbol{Y}$) and state variable($\boldsymbol{X}$) are vectors of harmonic components (i.e. DC, fundamental and harmonic components) in complex variables. The ABCD parameters are Toeplitz matrices whose elements are the Fourier coefficients of the periodic switching or transfer function. N is a diagonal matrix whose elements are functions of the fundamental angular frequency, ω_0 and the harmonic number. The derivation of 2.8 is described in Sec. 4.3 and in Appendix E.

With their case study on the STATCOM, aside from analysing individual harmonics during transients, they introduced Dynamic Electrical Indices for power (i.e. apparent $S(t)$, active $P(t)$, reactive $Q(t)$, and distortion $D(t)$), voltage $V_{rms}(t)$ and current $I_{RMS}(t)$ are all varying in time.

Very recently in 2010, Vyakaranam, Madrigal, Villaseca and Rarick [69] presented an EHD model for each of the more common FACTS controllers, namely a SVC, a TCSC,

[††]The term *Harmonic Domain (HD)* refers to the loose but general subset of the frequency domain where models and analyses are confined to integral multiples of the fundamental frequency. This is as opposed to the HD described in some literature such as [8] which refers to the iterative three phase power flow analysis that takes into account the voltage and current distortions and their effect on switching instants and converter controls, among many other things.

a Static Synchronous Series Compensator (SSSC) and a Unified Power Flow Controller (UPFC). Although this work is highly commendable in terms of breadth, all the models assumed fixed switching instants for the converters.

Back in 2008, Chavez and Ramirez [15] introduced the Dynamic Harmonic Domain (DHD) which they described as slightly different from the earlier EHD. However, the formulation is fundamentally the same and any perceived difference by the authors can be considered incidental. This was applied to travelling wave analysis for a three phase transmission line supplying a nonlinear load. They have likewise briefly described time-varying apparent power with clear reference to the dynamic indices introduced in [58]. One of the highlights in this investigation is that non-harmonic frequencies are readily present as resonance conditions in the system with long transmission lines, and that the DHD can be extended to futher analyse this phenomenon; this they pursued separately.

In 2010, Chavez [18] presented a conference paper on Modified Dynamic Harmonic Domain (MDHD) that accommodates interharmonics into the DHD by using fine frequency interval (i.e. fraction of the integer steps). At about the same time, Ramirez in a 2011 publication [56] independently described the MDHD for analysing interharmonics. These provide a glimpse of where research on EHD and DHD is heading.

There has also been an attempt to incorporate controllers into the DHD models. Garcia and Madrigal in 2009 [23] presented a DHD model for TCR-FC that included a Proportional-Integral (PI) controller. This was updated in 2011 [24] highlighting the use of companion harmonic circuit models for power electronics devices in the power systems. These papers made significant contribution in the dynamics analysis of harmonics in the power systems, however since it used Numerical Integration Substition (NIS) [19], it was not necessary for them to have time-invariant A, B, C and D matrices for the DHD formulation. These matrices can be updated at every time-step solution. Hence, there is still an opportunity to develop a DHD model with time-invariant A, B, C and D matrices.

2.4 LINEARISED MODELS FOR CONTROL ANALYSIS

Until recently there have been basically two types of dynamic model that are being applied to systems with switching apparatus including FACTS Controllers. The first one which is described in Section 2.4.1 is the classical model where the TCR is modelled as a linearised reactance (or susceptance) as a function of the switching angle. The second one which is described in Section 2.4.2 uses the fundamental frequency model Controller.

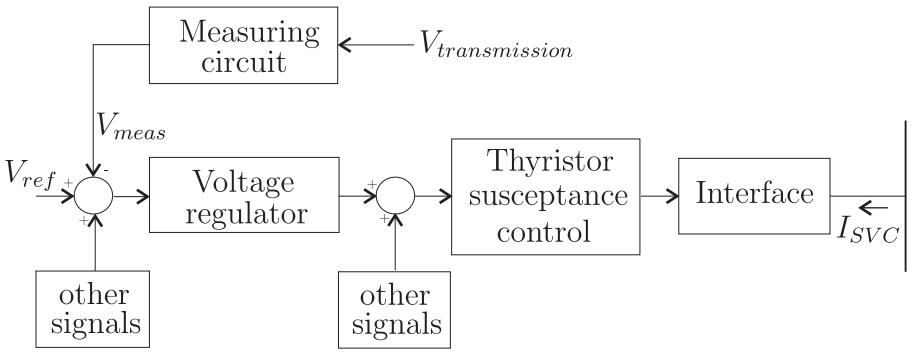

Figure 2.1: IEEE Basic Nonlinear Model 1 for Dynamic Performance

2.4.1 Classical Model

In 1994, IEEE Special Stability Controls Working Group published SVC models for dynamic performance simulation [32]. There were two models in the report. The first one which is shown in Fig. 2.1 indicates the connection of the major blocks namely, voltage regulator, measuring circuit, thyristor susceptance control, and interface. The second one which is not shown integrates a more sophisticated procedure to introduce a slope (typically referred to as droop) across the control range of the V-I characteristic of the SVC. This slope is included in most installations which produces advantages such as (i) reduced required reactive power rating, (ii) preventing the SVC from reaching its reactive power limit too frequently, and (iii) facilitating the sharing of reactive power among multiple compensators in parallel [42]. This droop, however, is not implemented in this thesis as there is no perceived additional gain in relation to the development of modelling technique that is being pursued.

The dynamic model for each of these blocks is described in detail in the report which mostly consists of rational transfer functions. The exception is for the thyristor susceptance control model where the relationship between the variable susceptance, B, and the firing angle, α, is described by the nonlinear equation in 2.9, and a linearisation procedure was applied.

$$B_{TCR} = B_{max}\left(1 - \frac{2\alpha}{\pi} - \frac{1}{\pi}sin(2\alpha)\right) \tag{2.9}$$

For a long time, this basic model has been acknowledged as the industry standard and is referred here as the Classical Model. Milano in 2010 [45] and Jiang in 2011 [33] still used this small-signal model. However, the major drawback to this is that the switching behaviour of the thyristor is not explicitly included.

2.4.2 Generalized Averaging Method and Dynamic Phasors

State-space averaging has been used to design and analyse power electronic converters. However, as highlighted by Kassakian, Schlecht and Verghese [34], this method assumes both small ripple and slow variation in the voltage and current signals of interest. These assumptions make it suitable for the analysis of high-frequency switching converters such as PWM converters. Due to this limitation, a generalised averaging method was proposed in 1991 by Sanders, Noworolski, Liu and Verghese [59], which has since been referred to Generalized Averaging Method. This method is based on a time-dependent Fourier series representation for a sliding window of a given waveform. The primary motivation was to be able to analyse resonant power converters since state-space averaging is limited to small-ripple applications (e.g. PWM converters)

In 1997, Mattavelli, Verghese and Stankovic [44] referred to the procedure as phasor dynamics to highlight the time-varying nature of the signals in phasor description. Shortly thereafter, the term *Dynamic Phasors* as a modelling procedure was adopted in a number of their succeeding publications [43], [64] and has been consistently used by other publications up to the present.

The formulation is anchored in the following expression:

$$x(t-T+s) = \sum_{k} \langle x \rangle_k(t) e^{jk\omega_s(t-T+s)} \tag{2.10}$$

where the sum is over all integers (k), ω_s and T are the fundamental frequency and period, respectively, and $s \in (0, T]$. $\langle x \rangle_k(t)$ is the k^{th} harmonic coefficient. Similar to the phasor transform, the principle is that we introduce a frame of reference in which a time-varying signal can be viewed as a constant signal. The major difference is that the traditional phasor transform assumes a steady-state sinusoidal signal (or sum thereof) and transforms it to a constant signal; dynamic phasors on the other hand, accommodate non-periodic signals and result in a time-varying (i.e. dynamic) phasor.

Without going into too much detail, the dynamic equation related to dynamic phasors is described as follows:

$$\frac{d}{dt}x(t) = f\{(x(t), u(t)\} \tag{2.11}$$

$$\frac{d}{dt}\langle x \rangle_k = -jk\omega_s \langle x \rangle_k + \langle f(x,u) \rangle_k \tag{2.12}$$

Dynamic phasor models generally include models that capture the dynamics of individual harmonics as acknowledged by Almér and U. T. Jöhnsson [5]. However in practice, dynamic phasor models only include the relatively large Fourier coefficients [59] which in most cases refer to the DC component (i.e. the adoption of the term "averaging"). For systems driven with a periodic signal, the fundamental frequency of the driving function which is the main frequency of the model is included. For the rest of this thesis,

dynamic phasor model is used to refer to the fundamental frequency-only model to differentiate it from the Harmonic State Space (HSS) model where additional harmonics are always included.

Investigations using averaging or dynamic phasors repeatedly acknowledge that additional harmonic terms significantly improve the models [59], or at least recommend that effects of important harmonics should be included in the models [44].

Worth mentioning is the series of publications from Centro de Pesquisas de Energia Elétrica (CEPEL). Pilotto, Alves and Watanabe in 2000 [54] described the use of switching function to represent the harmonic interaction in a TCR. In 2008, they used the same switching matrix as they developed analytical nonlinear and linear dynamic models of a TCR [6]. They proceeded to derive a detailed dynamic model for the TCR system. However, when they incorporated the switched reactor model into the rest of the dynamic components of the model, the switching matrix was truncated to the DC component only. Around the same period, Gomes and Martins (also from CEPEL) together with Stankovic in 2006 [62] described a dynamic phasor model of SVCs suitable for high frequency analysis with significantly detailed model for the control. Similar to the rest, only the fundamental frequency phasors were included in the analysis. However this paper acknowledged in its conclusion that a model with harmonic phasors (as compared to fundamental frequency-only model) has to be used in order to observe if there is any adverse interaction in the higher frequency between FACTS Controllers and the network. Even back in 1999, Caliskan, Verghese and Stankovic in 1999 [14] seriously proposed to include multifrequency interaction in power electronic models. However since their application that time was for a PWM DC-DC converter, their model only included the DC and the fundamental frequency.

Although it was not specifically acknowledged in the paper as a dynamic phasor model, Osauskas and Wood in 2003 published a small-signal dynamic model of an HVDC system. They applied interconnection technique to build a state-space model of the HVDC from component submodels. Although they have previously derived the harmonic transfers of the HVDC converter, the focus of this dynamic model is on 2 to 200 Hz range on the DC side, hence, the elements of the transfer matrix are approximated as constants seen from the DC side.

An attempt to include multifrequency interaction in a dynamic phasor model was presented in 2005 by He and Cai [29]. Quoting from [44] that a TCSC dynamic phasor model has to include more than the fundamental frequency, they extended the TCSC model to include the 3rd and 5th harmonics as the dominant Fourier coefficients. However control model was not included in their description. This leads us to the next class of models where both harmonic interactions and controls are included in the models.

2.5 LINEARISED MODEL FOR BOTH HARMONIC AND CONTROL ANALYSES

This section describes a number of models which incorporate both harmonic interactions and control. The first one using discrete topology was presented a long time ago was scarcely developed due to its perceived complexity. The next are various models proposed by various authors which present a transfer-function based approach to power electronics modelling. The last one presented is the Harmonic State Space model which is equivalent to the EHD that was described earlier, but this time controls are integrated in the model.

2.5.1 Discrete Topology Method

In 1989, Bohmann and Lasseter [10] described a state-variable procedure to predict resonance condition of a TCR circuit. This was closely followed in 1990 [11] with a procedure to analyse the stability of a TCR circuit taking into account harmonic interactions across the device. This was a genuine breakthrough in this area. The procedure includes the computation of the state transition matrix $\Phi(t, t_0)$ from the state matrix $A(t)$. The procedure is that the periodic $A(t)$ is divided into n topologies with fixed switching instants. The state transition matrix and eventually the state variable solution can be written as factored exponentials

$$\dot{x} = A(t)x \tag{2.13}$$

$$x(t) = \Phi(t, t_0)x_0 \tag{2.14}$$

$$x(T) = \prod_{i=1}^{n} exp(A_i(\tau_i))x_0 \tag{2.15}$$

where $x(t)$ is the state-variable solution at any time, t; $x(T)$ is the solution at the end of the period, T; n is the number of discrete topologies or circuit configurations within the period; and τ_i is the length in seconds of the i^{th} interval. It is emphasised that A_i is a constant matrix as opposed to the periodic $A(t)$. The stability of the system can be analysed by observing the characteristic roots or eigenvalues (λ_j) of the state variable function wherein stability is expected while $|\lambda_j| < 1$.

To illustrate the TCR model, the four discrete topologies that form each period are shown in Fig. 2.2. For each topology, a constant matrix, A_i and the periodic solution, $x(p)$ is computed as factored exponentials (2.15). This procedure which was referred to as discrete topology method was picked up by Tang and Meliopoulus in 1997 [65] with a proposal for a systematic procedure to build the state space matrix using Nodal equations. As an alternative to the usual procedure of determining the subintervals from the steady-state periodic solution also known as the base case, the period can be divided into a fixed large number of intervals.

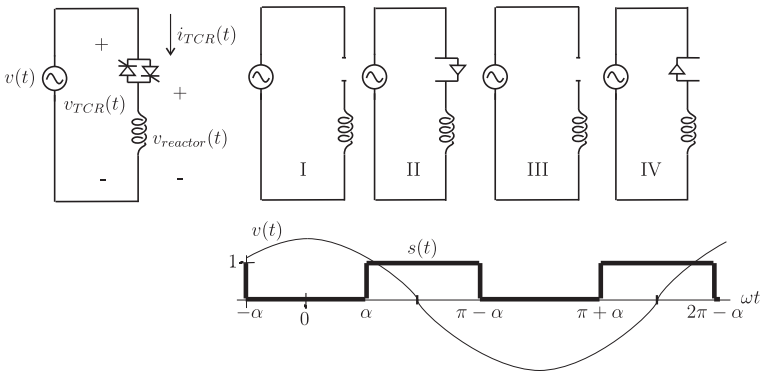

Figure 2.2: Discrete Topologies for TCR

This procedure however is limited to models where switching instants are fixed and there is no provision for the fact that thyristors' switching instants vary with voltage distortion. This may be sufficient for steady-state models whose switching instants are solved separately. In addition, this approach is susceptible for increased complexity since the number of discrete topologies quickly builds up with additional switching devices having switching times which are expected to be independent among devices.

2.5.2 Harmonic Transfer Function

In 2000 Mollerstedt presented his thesis [46] on the dynamic analysis of harmonics in electrical systems. This analysis was facilitated by building Harmonic Transfer Functions (HTF) . Every block in the power system including power system components and controllers were described in terms of state-space equations exactly the same as expressed in the EHD. As the purpose of the analysis is geared towards steady-state harmonics, the time-varying harmonic dynamics were dropped and a steady-state HTF was calculated. These HTF blocks were used to build power system models that include train converters.

Practically equivalent to this is Noda, Semlyen and Iravani's Harmonic Domain Dynamic Transfer Function (HDDTF) [49] which was published in 2003 and was subsequently followed by Ramirez, Semlyen and Iravani in 2005 [57]. As transfer function-based models that capture the dynamics of the harmonics superimposed on a steady-state solution, these models are very promising for various types of stability analysis. In addition, their modularity makes it suitable for modelling large power networks as highlighted by examples in [49] and [48].

In 2004, Wood and Osauskas [74] presented an analytically-derived transfer function based model for a STATCOM. Starting from the harmonic transfers described by Larsen, et al. [38] where the modulated firing angle is defined as an input to the harmonic transfer, the loop was closed by modelling firing angle modulation through a PLL controller.

These various models effectively capture the harmonic interaction of systems including controllers, however as steady-state models, there is still opportunity to extend these to capture the dynamics of the power system.

2.5.3 Harmonic State Space

The Harmonic State Space (HSS) traces its roots from Wereley's thesis in 1991 [72]. He presented a formal analogy between Linear Time Invariant (LTI) and Linear Time Periodic (LTP) systems. Since it was originally intended for control engineering application in helicopter technology, it was left largely unnoticed by power systems engineers. The HSS formulation is exactly the same as was earlier described in the EHD and DHD formulation, however the HSS was never referred to among the EHD and DHD publications.

Recently, there has been direct references to HSS in power systems engineering such as those of Mollerstedt [46] and Love [40]. The term HSS has been adopted throughout this document as a matter of convenience since the initial motivation to pursue this research were from publications on HSS. More importantly, it is an acknowledgement of the earliest known contribution [72].

This thesis is dedicated to the HSS description of a TCR with the intention to observe both the transients and steady-state solution of individual harmonics. Likewise, eigenvalue analysis can also be performed from the state matrix of the HSS. Unlike transfer-function based models which assumes zero initial conditions, an HSS model accommodates analysis from any initial condition.

2.6 CONCLUSIONS

Traditionally, there was clear distinction between time-domain (TD) and frequency-domain (FD) models and analyses in power systems. FD methods are used to highlight the harmonic characteristics and harmonic interactions in the system, while TD methods are used to understand the transients in the system. However with increasing power electronics penetration in the system, it is increasingly becoming unsound to look at these two domains distinctly from each other. Acknowledging this, an IEEE task force was convened recently to survey available techniques to interface TD and FD methods. In 2010, an IEEE Task Force on Simulation Tools published a report on *Interfacing Techniques for Time-Domain and Frequency-Domain Simulation Methods* [67]. Among those assessed, the DHD (which is identified as equivalent to HSS in this thesis) method and the Wavelet Transform were recognized as capable of producing results simultaneously in time or frequency domain without postprocessing.

This chapter reviewed a number of modelling and analysis techniques that pave the way for analysing FACTS Controllers in the HSS Domain. With greater challenges

to keep the power system operate in a stable manner, and with increasing number of power electronics being connected, the HSS domain shows a huge promise.

Chapter 3

LINEARISED HARMONIC DOMAIN TCR MODEL

3.1 INTRODUCTION

Harmonic domain models provide a comprehensive description of harmonic interactions across power electronic devices. These models can be derived either in the frequency-domain or in the time-domain [66]. In the latter case, harmonic characteristics are extracted from time-domain results using Fast Fourier Transform (FFT) [8]. The model presented in this chapter is a linearised harmonic domain of a three phase Thyristor Controlled Reactor (TCR) which is developed solely in the frequency-domain and uses a transfer function approach. Power electronic devices are naturally nonlinear because the input voltage affects the instants of device switching. Linearised models are pursued so that the wealth of techniques applicable to linear models can be conveniently used.

Chapter 2 summarises the development of harmonic domain models for TCR circuits. Among them, of specific note is the linearised harmonic domain model for an HVDC by Larsen, Baker and McIver, [38] whose overall Frequency Transfer Matrix (FTM) is shown in 2.6. They observed that positive sequence harmonics shifts in one direction while negative sequence harmonics shifts in another direction. This is important in the sense that in developing a linearised model for the harmonic transfers, separate linearised models can be written for each sequence component harmonic transfers involved. Applying Larsen, et. al's linearised harmonic domain model to a TCR which does not have a DC side, the overall transfer becomes:

$$\begin{bmatrix} \Delta I_{+ve} \\ \Delta I_{-ve} \end{bmatrix} = \begin{bmatrix} IPVP & IPVN & IPA \\ INVP & INVN & INA \end{bmatrix} \begin{bmatrix} \Delta V_{+ve} \\ \Delta V_{-ve} \\ \Delta \alpha \end{bmatrix} \tag{3.1}$$

This chapter linearises the nonlinear harmonic transfers from voltage distortion and switching instant variation (also known as firing angle modulation) to the resulting current distortion. Specifically, the positive sequence current distortion can be modelled as linearised transfers from the input distortion (i.e. positive sequence voltage distortion, negative sequence voltage distortion and the switching instant variation).

Likewise, the linearised transfers from the same set of input distortion to the negative sequence current distortion are modelled separately. Analytic derivation for each individual FTMs (susbmtrices) in 3.1 are described in this chapter. The general procedure in deriving the FTM starts by determining the mathematical expression describing the input-output relation in time-domain. This is followed by a time-domain to frequency-domain (i.e. harmonic frequencies only) transform of the equation as shown in 3.2.

$$w(t) = v(t)u(t) \Longleftrightarrow \boldsymbol{W}(f) = \boldsymbol{V}(f) \otimes \boldsymbol{U}(f) \tag{3.2}$$

The convolution in 3.2 can be implemented as a matrix multiplication, such that $\boldsymbol{U}(f)$ is the vector of input frequencies and a FTM replaces $\boldsymbol{V}(f)$. The structure of this FTM is explained in Sec. 3.3.

A similar linearised harmonic domain model was derived by Osauskas and Wood in 1998 [52], where frequency transfers from voltage and switching instant distortions to current distortion were derived using direct algebraic equations. This chapter however offers an alternative procedure to derive similar transfers. The hypothesis is that the approach presented here can be systematically extended to the Harmonic State Space model that is developed in Chapter 4.

The first few sections are devoted to describing the signal notation for single phase and three phase signals and matrix representations that are used in the chapter and for most of the thesis. Following this, Section 3.6 describes the typical operation of a TCR by presenting typical voltage and current plots in with emphasis on the switching instants and conduction periods. Section 3.7 presents the model development for a single phase TCR while Section 3.8 extends it to a three phase TCR. The harmonic characteristics of the TCR described by this model is validated with another set of harmonics derived from a purely time-domain solution. The last section presents an assessment of the model and its contribution towards the development of a harmonic state-space model.

3.2 HARMONIC SIGNAL REPRESENTATION

A time domain periodic signal is transformed to an equivalent frequency domain signal by Fourier series expansion [35] which is represented in the frequency domain as a harmonic coefficient vector:

$$x(t) = \sum_{k \in \mathbb{Z}} X_k e^{jk\omega_0 t} \tag{3.3}$$

where X_k[†] $\in \mathbb{C}$, ω_0 is the fundamental angular frequency in rad/s and k is the harmonic number.

The transform from time domain to frequency or harmonic domain explicitly described as

$$x(t) \Longleftrightarrow \boldsymbol{X}(\omega) \tag{3.4}$$

is facilitated by defining a modulation vector, $\boldsymbol{\Gamma}(t)$ as follows:

$$\boldsymbol{\Gamma}(t) = \begin{bmatrix} e^{-jh\omega_0 t} & \dots & e^{-j2\omega_0 t} & e^{-j\omega_0 t} & 1 & e^{j\omega_0 t} & e^{j2\omega_0 t} & \dots & e^{jh\omega_0 t} \end{bmatrix} \tag{3.5}$$

This allows 3.3 to be written as

$$x(t) = \boldsymbol{\Gamma}(t)\boldsymbol{X} \tag{3.6}$$

where

$$\boldsymbol{X}(\omega) = \begin{bmatrix} X_{-h} & \dots & X_{-2} & X_{-1} & X_{DC} & X_1 & X_2 & \dots & X_h \end{bmatrix}^T$$

Uppercase characters are used to denote harmonic-domain variables with the argument (ω) dropped for brevity; as opposed to lowercase characters which are used for time-domain variables. Each element of the vector is a complex quantity. Technically, the DC component of the signal is a scalar quantity but for uniformity, a complex variable with zero imaginary component is used. It is important to emphasise that the harmonic domain representation is a vector of infinite length. Practical models truncate the vector to a reasonably high harmonic number (h) based on the signal roll-off.

3.3 FREQUENCY TRANSFER MATRIX

3.3.1 Special Matrices for Frequency Transfer Matrix

The linearised harmonic domain model presented in this chapter takes a transfer matrix approach. Specifically, every harmonic response vector results from the product of a Frequency Transfer Matrix (FTM) and an input harmonic vector. It is imperative to define and describe the structures of some special matrices that are used throughout this thesis. Specifically, diagonal, Toeplitz and Hankel matrices are defined. Toeplitz and Hankel matrices are originally defined as infinitely-dimensioned [12], however with truncation up to the highest harmonic in this model, the square matrices here are of finite rank.

[†]Depending on the modeling tool, each complex quantity expressed as real and imaginary components may be processed as separate elements in a two-element array. That is, $X = [X_{re}; X_{imag}]$.

Diagonal Matrix Given a sequence $\{\boldsymbol{a}_n\}_{n\in[0,h]}$ of complex numbers, the diagonal matrix associated with this sequence is a square matrix of rank $h+1$, whose diagonal elements are composed of the elements of $\{\boldsymbol{a}_n\}$ and whose off-diagonal elements are all zeros as shown in 3.7.

$$\begin{aligned}\boldsymbol{D} &= \mathcal{D}\{\boldsymbol{a}_n\}_{n\in[0,h]} \\ &= \begin{bmatrix} a_0 & & & \\ & a_1 & & \\ & & \ddots & \\ & & & a_h \end{bmatrix} \\ \boldsymbol{D}_{k,l} &= \begin{cases} a_n, & \text{for } k = l \\ 0, & \text{for } k \neq l \end{cases}\end{aligned} \tag{3.7}$$

Toeplitz Matrix Given a sequence $\{\boldsymbol{a}_n\}_{n\in[-h,h]}$ of complex numbers, the Toeplitz matrix associated with this sequence is a square matrix of rank $h+1$ with constant diagonals as shown in 3.8.

$$\begin{aligned}\boldsymbol{T} &= \mathcal{T}\{\boldsymbol{a}_n\}_{n\in[-h,h]} \\ &= \begin{bmatrix} a_0 & a_{-1} & \cdots & a_{-h} \\ a_1 & \ddots & \ddots & \ddots \\ \vdots & \ddots & \ddots & a_{-1} \\ a_h & \ddots & a_1 & a_0 \end{bmatrix} \\ \boldsymbol{T}_{k,l} &= \boldsymbol{T}_{k+1,l+1}\end{aligned} \tag{3.8}$$

Alternately, given a pair of sequences $\{\boldsymbol{a}_n, \boldsymbol{b}_n\}_{n\in[0,h]}$, the Toeplitz matrix associated with this pair of sequences is a square matrix of rank $h+1$ as shown in 3.9

$$\begin{aligned}\boldsymbol{T} &= \mathcal{T}\{\boldsymbol{a}_n, \boldsymbol{b}_n\}_{n\in[0,h]} \\ &= \begin{bmatrix} a_0 & b_1 & \cdots & b_h \\ a_1 & \ddots & \ddots & \ddots \\ \vdots & \ddots & \ddots & b_1 \\ a_h & \ddots & a_1 & a_0 \end{bmatrix}\end{aligned} \tag{3.9}$$

where a_0 dominates over b_0 when $a_0 \neq b_0$.

Hankel Matrix Given a sequence $\{\boldsymbol{a}_n\}_{n\in[0,2h]}$, the Hankel Matrix associated with this sequence is a square matrix of rank $h+1$ with constant positive slope diagonals as shown in 3.10.

$$\begin{aligned}\boldsymbol{H} &= \mathcal{H}\{\boldsymbol{a}_n\}_{n\in[0,2h]} \\ &= \begin{bmatrix} a_0 & a_1 & \cdots & a_h \\ a_1 & \iddots & \iddots & a_{h+1} \\ \vdots & \iddots & \iddots & \vdots \\ a_h & a_{h+1} & \cdots & a_{2h} \end{bmatrix} \\ \boldsymbol{H}_{k,l} &= \boldsymbol{H}_{k-1,l+1}\end{aligned} \tag{3.10}$$

3.3.2 Frequency Transfer Matrices for Operations

Mathematical operations can be performed on harmonic vectors as Frequency Transfer Matrices (FTM). These operations can be broadly classified as either unary operations or binary operations[‡]. In a unary operation such as differentiation or integration, a single harmonic vector operand is involved. Time delay is considered as a special unary operation where a scalar quantity (i.e. the time delay in seconds) is specified in addition to the lone operand. FTMs for unary operations are implemented as diagonal matrices with structures similar to 3.7. There is no frequency shift involved but the magnitude and phase changes are expressed as complex number elements in the FTM. On the other hand a binary operation such as convolution involves two harmonic vectors as operands. This operation is implemented as a product between an FTM from the first operand and the harmonic vector of the second operand. With signal representations truncated to the h^{th} harmonic, harmonic vectors are of length $2h+1$ and the following operation FTM's are of rank $2h+1$. These are summarised as follows:

Harmonically Decoupled FTM The most basic transfer that can be described using FTM is between two harmonically decoupled signals. Given a pair of harmonic vectors: input $\boldsymbol{U}$ and output $\boldsymbol{W}$, if these vectors are harmonically decoupled, then the FTM $\boldsymbol{V}$ which describes the transfer is described as:

$$\begin{aligned}\boldsymbol{W} &= \boldsymbol{V}\boldsymbol{U} \\ \boldsymbol{V} &\triangleq \mathcal{D}\{v_n\}_{n\in[-h,h]}\end{aligned} \tag{3.11}$$

This applies to impedance and admittance if the voltage and currents are coupled at the same harmonic frequency and not with any other harmonics. The integration, the

[‡]any operation between multiple operands is treated as a cascade of binary operations

differentiation, and the time-shift FTMs presented as follows are special cases of this type of matrix.

Integration FTM Given a harmonic vector $\boldsymbol{U}$ with fundamental angular frequency denoted as ω_0, the integral of this vector, and the corresponding FTM, ($\boldsymbol{\Lambda}_{\int}$) is described as:

$$\begin{aligned} y(t) &= \int u(t)dt \\ Y_n &= \frac{1}{jn\omega_0}U_n \\ \boldsymbol{\Lambda}_{\int} &\triangleq \mathcal{D}\left\{\frac{1}{jn\omega_0}\right\}_{n\in[-h,h],n\neq 0} \end{aligned}$$

Differentiation FTM Given a harmonic vector $\boldsymbol{U}$ with fundamental angular frequency denoted as ω_0, the derivative of this vector and the corresponding FTM, ($\boldsymbol{\Lambda}_D$) is described as:

$$\begin{aligned} y(t) &= \frac{du(t)}{dt} \\ Y_n &= jn\omega_0 U_n \\ \boldsymbol{\Lambda}_D &\triangleq \mathcal{D}\left\{jn\omega_0\right\}_{n\in[-h,h]} \end{aligned} \tag{3.12}$$

Time Shift FTM Given a harmonic vector $\boldsymbol{U}$, if the fundamental frequency is to be shifted by ϕ radians, and every n^{th} harmonic component is shifted by $n\phi$, then the equivalent time domain signal is time delayed by $\phi\frac{T}{2\pi}$ seconds, where T is the period in seconds of the fundamental frequency component. This operation is implemented as a diagonal FTM ($\boldsymbol{\Lambda}_{\Phi}(\phi)$) as follows:

$$\begin{aligned} Y_n &= e^{jn\phi}U_n \\ \boldsymbol{\Lambda}_{\Phi}(\phi) &\triangleq \mathcal{D}\left\{e^{jn\phi}\right\}_{n\in[-h,h]} \end{aligned} \tag{3.13}$$

FTM for Product of Signals Consider the product of two signals $v(t)$ and $u(t)$; the time domain product of signals is equivalent to the element-wise convolution of their corresponding harmonic vectors $\boldsymbol{V}$ and $\boldsymbol{U}$ which are both truncated up to the h^{th}

harmonic. The FTM implementation of this operation is described as follows:

$$w(t) = v(t)u(t) \tag{3.14}$$

$$\sum_{n=-h}^{h} Wne^{jn\omega_0 t} = \sum_{n=-h}^{h} V_n e^{jn\omega_0 t} \sum_{m=-h}^{h} U_m e^{jm\omega_0 t}$$

$$= \sum_{n-m=-2h}^{2h} V_{n-m} \sum_{m=-h}^{h} U_m e^{jm\omega_0 t} \tag{3.15}$$

which can be written in terms of the modulation vector, $\mathbf{\Gamma}(t)$ and a product of a Toeplitz matrix with a harmonic vector:

$$\mathbf{\Gamma}(t)\boldsymbol{W} = \mathbf{\Gamma}(t)\mathcal{T}\{\boldsymbol{V}\}_{n\in[-2h,2h]}\boldsymbol{U}$$

$$\boldsymbol{W} = \mathcal{T}\{\boldsymbol{V}\}_{n\in[-2h,2h]}\boldsymbol{U} \tag{3.16}$$

Effectively, the Toeplitz transform of the first harmonic vector ($\mathcal{T}\{\boldsymbol{V}\}_{n\in[-2h,2h]}$) is the FTM from the second harmonic vector to the output harmonic vector. This is typically the FTM formed from the harmonic vector of a switching function.

Sampling FTM A special case of the FTM as a signal multiplier is the Sampling FTM. An impulse train also known as Dirac comb, $\delta_T(t)$ is described as a recurring Dirac delta, $\delta(t)$ at $t = nT, n \in \mathbb{Z}$ and as a harmonic series in 3.17.

$$\delta_T(t) \triangleq \sum_{n=-\infty}^{\infty} \delta\left(t - nT\right) \tag{3.17a}$$

$$= \frac{1}{T} \sum_{n=-\infty}^{\infty} e^{-jn\omega_0 t} \tag{3.17b}$$

Multiplying this function with another signal, $u(t)$, effectively samples $u(t)$ at $t = nT$. In the harmonic domain, $\boldsymbol{\delta}(f)_{n\in[-h,h]}$ is a vector containing the set of coefficients from 3.17b, truncated up the h^{th} harmonic. It is a vector whose elements are all equal to $\frac{1}{T}$. The corresponding FTM is generated by taking the Toeplitz transform of $\boldsymbol{\delta}(f)$:

$$\boldsymbol{\Delta} = \mathcal{T}\{\boldsymbol{\delta}(f)\}_{n\in[-2h,2h]} \tag{3.18}$$

which is a square matrix whose elements are all equal to $\frac{1}{T}$.

For a time-shifted sampling function, where $u(t)$ is sampled at $t = nT + n\phi\frac{T}{2\pi}$; ϕ in

radians,

$$\delta_{T_\phi}(t) \triangleq \sum_{n=-\infty}^{\infty} \delta\left(t - nT - n\phi T/2\pi\right) \tag{3.19a}$$

$$= \frac{1}{T} \sum_{n=-\infty}^{\infty} e^{-jn\omega_0 t} e^{-jn\phi t} \tag{3.19b}$$

The corresponding FTM is

$$\boldsymbol{\Delta}_\phi = \frac{1}{T} \mathcal{T}\{e^{-jn\phi}\}_{n\in[-2h,2h]} \tag{3.20}$$

3.4 THREE-PHASE SIGNALS

To extend a single phase signal to a three phase signal expressed as X_ψ[††], a notation ψ that takes the value of $0, 2\pi/3$ and $-2\pi/3$ is used to represent phases A, B and C. In addition, the sequence of each harmonic is defined as r_k, which takes a value of $+1, -1$ or 0 for positive, negative or zero sequence respectively. A general expression for a three phase signal with DC and harmonic components is shown in 3.21.

$$x_\psi(t) = \sum_{k\in\mathbb{Z}} X_k e^{j(k\omega_0 t - r_k\psi)} \tag{3.21}$$

Phase sequence r_0 is assigned to the DC component as well. Although this may seem counter-intuitive, it is important that the DC component is represented consistently with the non-DC components. The DC component is considered as zero-sequence ($r_0 = 0$) while positive and negative sequence DC components sum to zero. Likewise, the DC component, if present in any of the three phases, has to be properly included in the model.

The equivalent harmonic domain expression with harmonic truncation up to the h^{th} harmonic takes the following form:

$$\begin{aligned} \boldsymbol{X}_\psi(\omega) &= [\ \boldsymbol{X}_a \quad \boldsymbol{X}_b \quad \boldsymbol{X}_c\ ]^T \\ &= [\ \boldsymbol{X}_a \quad \boldsymbol{\Lambda}_\Phi(s\tfrac{2\pi}{3})\boldsymbol{X}_a \quad \boldsymbol{\Lambda}_\Phi(-s\tfrac{2\pi}{3})\boldsymbol{X}_a\ ]^T \end{aligned} \tag{3.22}$$

where

$$\boldsymbol{X}_a = \left[\ X_{-h} \quad \ldots \quad X_{-2} \quad X_{-1} \quad X_{DC} \quad X_1 \quad X_2 \quad \ldots \quad X_h\ \right]^T$$

and $\boldsymbol{\Lambda}_\Phi(\pm s\frac{2\pi}{3})$ are phase shift FTMs described in 3.13.

[††]A subscript ψ is placed if there is a combination of single phase and three phase variables in the same expression. Otherwise, this subscript is not necessary as most signals are three phase.

Typically, sequence components is being used to analyse power systems during unbalanced conditions. The most common of which is for fault analysis [7]. The reason mainly is that sequence components provides a framework to analyse an unbalanced condition as a set of balanced condition. In many cases, these sequence components are decoupled from each other such that each sequence component can be analysed independent from the other components. The value of using symmetrical components is anchored on this decoupled behaviour between components. The total effect of the unbalance is solved by summing the effect of these symmetrical components.

Interestingly, previous investigations on HVDC links [38], [75], [31], established that the harmonic interaction across the converter is sequence dependent. That is, positive sequence harmonic distortions are frequency shifted one way while negative-sequence harmonic distortions are frequency shifted the other way. A similar sequence-dependent harmonic interaction is present in FACTS controllers such as the TCR. This also means that the decoupled behaviour between symmetrical components allows the investigator to analyse the harmonic interactions one sequence component at a time. The total harmonic interaction is described by the total effect of the symmetrical components. In this thesis, all three phase models are developed in sequence components.

For many power electronic converters there is no available path for zero-sequence. Specifically, a six-pulse TCR is typically connected in delta. With equidistant firing in all three-phases, zero-sequence is trapped within the delta and no zero-sequence is expected to flow through the line. In the simplest harmonic modeling, the zero-sequence components are eliminated from the model thus reducing the matrix sizes and the computational burden for the analysis. Such positive and negative sequence only model as indicated in 3.23 is the one described in this chapter.

$$\boldsymbol{X}_{\psi} = \begin{bmatrix} \boldsymbol{X}_a & \boldsymbol{X}_b & \boldsymbol{X}_c \end{bmatrix}^T \Leftrightarrow \begin{bmatrix} \boldsymbol{X}_p & \boldsymbol{X}_n & (\boldsymbol{X}_z) \end{bmatrix}^T \tag{3.23}$$

The sequence components are obtained using the standard phase-to-sequence transform matrix detailed in power system analysis texts such as [17]. Except for [4], there is very little publication providing details on the transform from phase components to sequence components (and vice-versa) as applied to harmonic signals. Appendix B presents the use of the transform in harmonic analysis.

3.5 POSITIVE FREQUENCY MODEL

Using the Euler's equation for cosine function as shown in 3.24, a periodic signal such as in 3.3 truncated up to the h^{th} harmonic can be written as in 3.25

$$\cos\theta = \frac{e^{j\theta} + e^{-j\theta}}{2} \tag{3.24}$$

$$x(t) = \sum_{k=0}^{h} \bar{X}_k \cos\left(k\omega_0 t + \theta_k\right) \tag{3.25}$$

where $\bar{X}_k$ in 3.25 is twice X_k in 3.3.

Accordingly, if a variant of the modulation function is defined as $\bar{\mathbf{\Gamma}}(t)$

$$\bar{\mathbf{\Gamma}}(t) = \begin{bmatrix} 1 & \cos(\omega_0 t) & \cos(2\omega_0 t) & \dots & \cos(h\omega_0 t) \end{bmatrix} \tag{3.26}$$

the periodic function in 3.3 can be written as

$$x(t) = \bar{\mathbf{\Gamma}}(t)\bar{\boldsymbol{X}} \tag{3.27}$$

where $\bar{\boldsymbol{X}}$ is a positive frequency only harmonic vector of the periodic signal.

$$\bar{\boldsymbol{X}}(\omega) = \begin{bmatrix} X_{DC} & \bar{X}_1 & \bar{X}_2 & \dots & \bar{X}_h \end{bmatrix}^T$$

FTM for Product of Signals With a positive frequency only harmonic vector, the structure of the FTM for product of signals is correspondingly updated. A systematic procedure for building the FTM for a positive frequency only model was presented in [74] and is briefly presented here.

Consider the product of two functions $v(t)$ and $u(t)$,

$$w(t) = v(t)u(t) \tag{3.28}$$
$$\sum_{l=0}^{h} W_l \cos(l\omega_0 t) = \sum_{l=0}^{h} V_l \cos(l\omega_0 t) \sum_{k=0}^{h} \cos(k\omega_0 t)$$

The product of each pair of harmonic component is a sum and a difference of harmonics using a well-known trigonometric identity,

$$V_l \cos(l\omega_0 t) U_k \cos(k\omega_0 t) = \frac{V_l U_k}{2}[\cos((l+k)\omega_0 t) + \cos((l-k)\omega_0 t)] \tag{3.29}$$

This shows that for each pair of harmonic input, there is always an upward (i.e. $l+k$) and a downward (i.e. $l-k$) frequency shift.

The upward frequency shifts can be implemented as a lower triangular Toeplitz FTM

$$\mathbf{\Lambda}_{up} = \mathcal{T}\{\boldsymbol{V}_n, \emptyset\}_{n\in[0,h]} \tag{3.30}$$

where $\emptyset$ denote an empty set. The downward frequency shifts can be implemented as an upper triangular Toeplitz FTM

$$\mathbf{\Lambda}_{dn1} = \mathcal{T}\{\emptyset, \boldsymbol{V}_n^*\}_{n\in[0,h]} \tag{3.31}$$

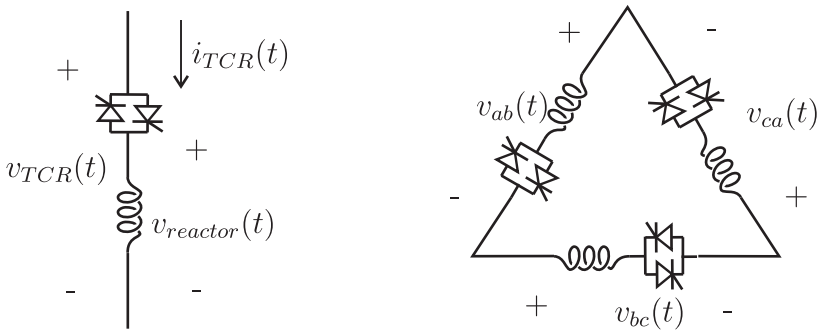

(a) 1-phase TCR (b) 3-phase TCR

Figure 3.1: Thyristor-Controlled Reactor circuit models

and a Hankel FTM

$$\mathbf{\Lambda}_{dn2} = \mathcal{H}\{\boldsymbol{V}_n\}_{n\in[0,2h]} \tag{3.32}$$

The total FTM to capture the harmonic convolution or the product of signals in a positive frequency only model is the sum of these component FTMs.

$$\mathbf{\Lambda} = \mathcal{T}\{\boldsymbol{V}_n, \emptyset\}_{n\in[0,h]} + \mathcal{T}\{\emptyset, \boldsymbol{V}_n^*\}_{n\in[0,h]} + \mathcal{H}\{\boldsymbol{V}_n\}_{n\in[0,2h]} \tag{3.33}$$

A detailed description in deriving this positive frequency FTM from positive-and-negative frequency FTM is presented in Appendix A.

3.6 TCR BASIC OPERATION

IEEE definition [1] for Thyristor-Controlled Reactor (TCR) states,

> *A shunt-connected thyristor-controlled inductor whose effective reactance is varied in a continuous manner by partial conduction control of the thyristor valve.*

The equivalent circuit for a single phase TCR is shown in Fig. 3.1a. Typically, a three phase TCR used in the power system is connected in delta as further shown in Fig. 3.1b

The anti-parallel thyristors are controlled by associated control circuitry. A typical block diagram for a voltage-controlled TCR is shown in Fig. 3.2.

The voltage and current plots of one phase of a TCR are shown in Fig. 3.3 where a distorted voltage (expressed as $V_{TCR} = V_0 + \Delta V$) is applied across the TCR. For the first half-cycle, partial conduction is initiated at $\omega t = \alpha_1$[‡‡].

Conduction proceeds until thyristor current drops to zero, which occurs when the integral of the voltage throughout conduction equates to zero; graphically, area A_1 equals

[‡‡]Throughout this thesis, $\alpha[0, \pi/2]$ is measured from the peak of the fundamental frequency component of the TCR voltage, whereas in most other publications $\alpha[\pi/2, \pi]$ is measured from the TCR voltage zero-crossing.

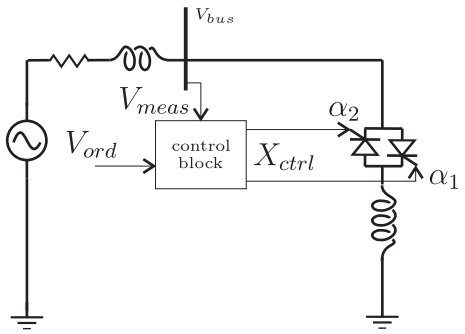

Figure 3.2: Control block in a Voltage-Control TCR

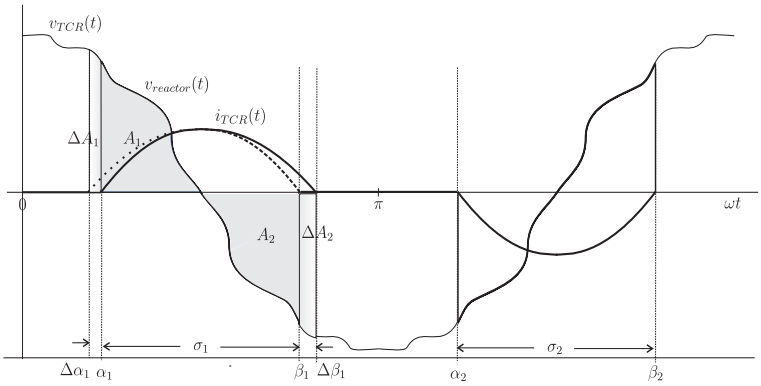

Figure 3.3: Thyristor-Controlled Reactor Voltage and Current plots showing switching instants and conduction period

area A_2 in Fig. 3.3. Without voltage distortion and assuming an ideal reactor, symmetrical switching occurs (i.e. $\beta_1 = \pi - \alpha_1$ and $\sigma_1 = \pi - 2\alpha_1$). However depending on the voltage distortion, conduction ends earlier or later (indicated as $\Delta\beta_1$). This instant is referred in the rest of the model as a switch-off instant variation.

Another Switching Instant Variation (SIV) happens at switch-on ($\Delta\alpha_1$). It typically results from distortion in the timing and control signals. This SIV symmetrically affects both the start and end of conduction which is modeled in detail in the succeeding section. For the rest of the model, equidistant firing where $\alpha_2 = \alpha_1 + \pi$ is assumed and SIV similarly affects the positive and negative half-cycles of conduction.

3.7 SINGLE PHASE TCR MODEL

In modelling a reactor with negligible resistance as shown in Fig. 3.1, the voltage across the reactor results from the switching of the thyristor pair which is a function of the switch-on angle (α) and the switch-off angle (β). The conduction period (σ) is defined as the difference between the switch-off and the switch-on angles. The switch-on angle is controlled by the control circuit but is also susceptible to variation due to error in the timing circuit (e.g. Phase-Locked Loop controller). As mentioned in the preceding

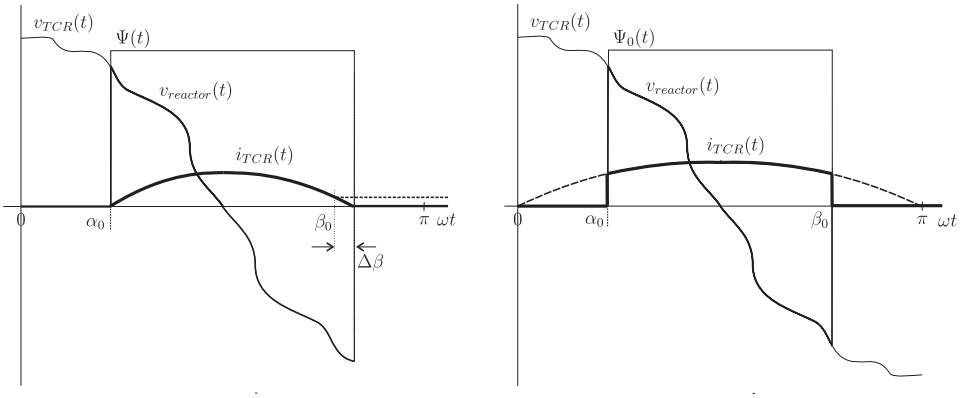

(a) chopped voltage is integrated (b) integrated voltage is chopped

Figure 3.4: Modeling Approaches for Reactor Currents

section, switch-off is a function of switch-on ($\beta = \pi - \alpha$) when the voltage has no distortion. However, with TCR voltage distortion the switch-off varies around the base case value.

There are two approaches for modeling the current flowing through the reactor in a TCR. The first approach is by multiplying the applied voltage (v_{TCR}) by the switching function (Ψ) to obtain a chopped voltage across the reactor ($v_{reactor}$) to be followed by an integration to obtain the TCR current (i_{TCR}). The second method is by integrating the applied voltage to obtain a continuous current before multiplying by the switching function to obtain the TCR current. These procedures are illustrated in Fig. 3.4

The first approach as shown in Fig. 3.4a, is highly suitable if the switch-off instant ($\beta_0 + \Delta\beta$) is accurately known. Otherwise, the limitation is that for an inaccurate switching instant β, a finite reactor current may be present during non-conduction. This approach is used for base case model as presented in Section 3.7.1.

The second approach is highly suitable if the switch-off instant is not known *a-priori* since the the current is forced to zero after conduction. However, the reactor current during switch-on (α_0) may jump from zero to a finite value which renders the rest of the conduction current inaccurate. An additional procedure needs to be done to rectify this problem. This approach is used for modeling the small-signal current due to voltage variation as presented in Section 3.7.2, where the additional procedure is also described.

For both approaches the TCR current is a function of the applied voltage and the switching function which is defined by the switching instants α and β.

$$i_{TCR}(t) = f(v_{TCR}, \alpha, \beta) \tag{3.34}$$

With a small-signal model, a generalised expression for the base case response is

$$i_{TCR_0} = f(v_{TCR_0}, \alpha_0, \beta_0) \tag{3.35}$$

while the small-signal response is obtained using the first term of the Taylor series expansion

$$\Delta i_{TCR}(v_{TCR}, \alpha, \beta) = \frac{\partial i}{\partial v}(\alpha_0, \beta_0)\Delta v + \frac{\partial i}{\partial \alpha}(\beta_0, v_{TCR_0})\Delta\alpha + \frac{\partial i}{\partial \beta}(\alpha_0, v_{TCR_0})\Delta\beta \tag{3.36}$$

The total response is the sum of the base case response and the small-signal response. The model for the base case response is presented in Section 3.7.1. The small-signal response components in 3.36 are presented in Sections 3.7.2 to 3.7.4.

3.7.1 Base Case TCR Current

Typically in a linearised power system model, the base case operating point is the steady-state response when a balanced fundamental frequency-only rated voltage is applied as an input. Such requirement is not technically necessary for a small-signal analysis. Any stable operating point where the input voltage may be unbalanced by a negative-sequence component or containing harmonic components, or both, can be arbitrarily chosen and a small-signal analysis can be performed about it. A comprehensive way of solving the base case harmonic domain response is either through an off-line time-domain simulation followed by an FFT or through an iterative harmonic domain simulation. In this subsection where a transfer function approach is applied to solve for the base case, the switching instants of the thyristors are known *a-priori*; the first approach as shown in Fig. 3.4a is employed. To be practical, the balanced fundamental frequency-only voltage is chosen as the input which results in symmetrical switching. Equidistant firing is assumed in all phases. In the time domain, the base case response is

$$\begin{aligned} v_{reactor,0}(t) &= \Psi_0(t) v_{TCR,0}(t) \\ i_{TCR,0}(t) &= \frac{1}{L}\int v_{reactor,0}(t)\, dt \\ &= \frac{1}{L}\int \Psi_0(t) v_{TCR,0}(t)\, dt \end{aligned} \tag{3.37}$$

where $\Psi_0(t)$ is described as a function of fixed switching angles α_0 and β_0 as:

$$\Psi_0(t) = \frac{\beta_0 - \alpha_0}{\pi} + \sum_{n=-\infty}^{\infty} \frac{1}{n\pi}(a_n + jb_n)e^{jn\omega t} \tag{3.38}$$

with

$$a_n = \sin(n\beta_0) - \sin(n\alpha_0)$$
$$b_n = \cos(n\alpha_0) - \cos(n\beta_0)$$

where n is even and not zero. The corresponding harmonic domain expression is

$$\boldsymbol{I}_{TCR} = \left[\frac{1}{L}\boldsymbol{\Lambda}_f \boldsymbol{\Psi}(\alpha_0, \beta_0)\right] \boldsymbol{V}_{TCR,0} \tag{3.39}$$

where the effective base case admittance FTM for a TCR is

$$\boldsymbol{Y}_{TCR,0} = \frac{1}{L}\boldsymbol{\Lambda}_f \boldsymbol{\Psi}(\alpha_0, \beta_0) \tag{3.40}$$

The next subsections describe the analytical procedure to model the small-signal currents from various input distortion. The procedure taken is inspired by Hume's analytical model for HVDC converters [31] wherein the device's total response to an input is analysed as the sum of the steady-state and the transient responses. For a power electronic switching device, the response is analysed only during the conduction period. For every period, there could be a number of noncontinuous short conduction periods. For each of these short conduction periods, a partial steady-state (PSS) response and a partial transient (PT) response is analytically modelled. The following discussions describes the application of such procedure to a TCR circuit. These models are uniquely derived from Hume's since the TCR behaviour is different from that of an HVDC.

3.7.2 Small-Signal Currents from Input Voltage Variation

In modeling the small-signal TCR current due to input voltage variation an important requirement is that the current is zero during non-conduction; hence the second approach to calculate the reactor current model as shown in Fig. 3.4b is employed. For a switched inductive circuit, the total inductor current due to voltage variation is the sum of the steady-state and the transient responses confined to the conduction period, which when combined ensures that the current upon switch-on initiates at zero. Component responses are illustrated in Fig. 3.5 where a third harmonic voltage distortion is introduced. In this figure, the PSS component (dotted) is summed with the PT component (dashed) to give the actual small signal current. The PSS current is the steady-state current component through the reactor due to the applied voltage variation, sampled during the conduction period; this is the time-domain product of the current and the switching signal. In the harmonic domain, it is the convolution of the current and the switching function — the product between switching FTM at the base

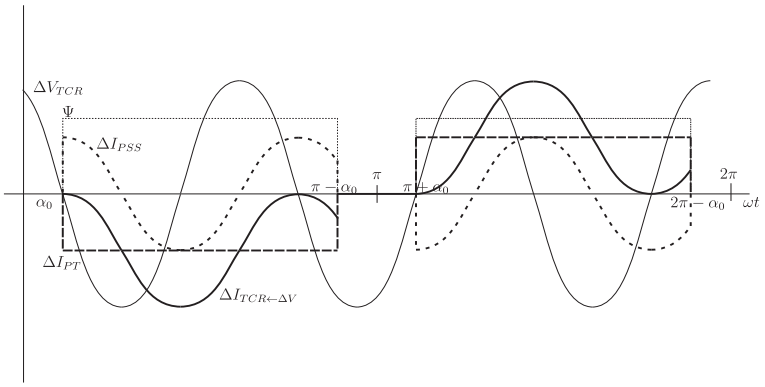

Figure 3.5: Analytical diagram of small-signal current due to voltage variation

case, the harmonic admittance and the input voltage vector.

$$\Delta \boldsymbol{I}_{\Delta V,PSS} = \left[\boldsymbol{\Psi}_0(\alpha_0, \beta_0) \frac{1}{L} \boldsymbol{\Lambda}_{\int} \right] \Delta \boldsymbol{V}_{TCR} \tag{3.41}$$

The PT response for a highly inductive circuit exhibits an exponential decay (i.e. $I_0 e^{-\frac{R}{L}t}$) which is approximated as a constant across the short conduction period. Analytically, it can be shown that this steady signal has a value equal in magnitude but opposite in sign to the PSS at the switching instant, α. For all time, it appears as a modulated series of pulses. In the frequency domain, this pulse train is described by a Pulse Amplitude Modulation (PAM) spectrum modulated by the steady-state component of the inductor current where the PAM spectrum is derived by convolving the impulse train spectrum with a fixed-width rectangular pulse. Details of the analytic derivation of the PAM spectrum and PAM FTM ($\boldsymbol{\Lambda}_{PAM}$) is presented in Appendix D.

$$\Delta \boldsymbol{I}_{\Delta V,PT} = \left[-\boldsymbol{\Lambda}_{PAM}(\alpha_0, \beta_0) \frac{1}{L} \boldsymbol{\Lambda}_{\int} \right] \Delta \boldsymbol{V}_{TCR} \tag{3.42}$$

Therefore the first term in 3.36 which is the small-signal admittance FTM is

$$\begin{aligned} \boldsymbol{Y} &= \boldsymbol{\Psi}_0(\alpha_0, \beta_0) \frac{1}{L} \boldsymbol{\Lambda}_{\int} - \boldsymbol{\Lambda}_{PAM}(\alpha_0, \beta_0) \frac{1}{L} \boldsymbol{\Lambda}_{\int} \\ \boldsymbol{Y} &= \left[\boldsymbol{\Psi}_0(\alpha_0, \beta_0) - \boldsymbol{\Lambda}_{PAM}(\alpha_0, \beta_0) \right] \frac{1}{L} \boldsymbol{\Lambda}_{\int} \end{aligned} \tag{3.43}$$

This approach gives a linearised description of the inductor current due to voltage variation except that it does not take into account the variation in switch-off instant. Under this constraint, the thyristors turn-off at $\pi - \alpha_0$ and $2\pi - \alpha_0$ for the first and second half-cycles, respectively. Thyristors turn-off when the current gets to zero-value where the exact zero-crossing can be computed as a non-linear function of the voltage variation using an iterative solution, but this is not included in this linearised model.

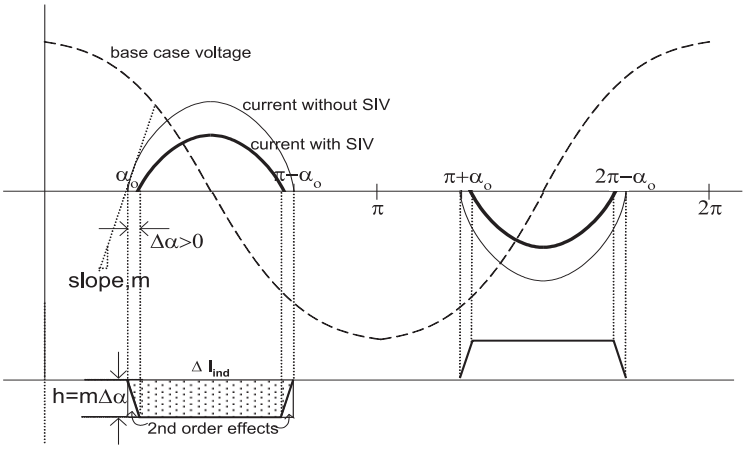

Figure 3.6: Analytical model showing the effects of an SIV delay to the reactor phase current.

3.7.3 Small Signal Currents from Controlled Switching Instant Variation

Any variation in the controlled switching instant, α as described in 3.6 has both linear and non-linear small-signal effects on the inductor current. Fig. 3.6 illustrates the effect of SIV on the phase current. A switching instant delay, $\Delta\alpha > 0$ (or advance, $\Delta\alpha < 0$) is equivalent to a trapezoidal pulse being subtracted from (or added to) the base case current. As a first-order approximation, this can be described by a rectangular pulse with pulse height equal to $m\Delta\alpha$ and pulse duration equal to the base case conduction period. The slope, m is the change in the base case reactor current with respect to angle at the switching instant, and is derived as the ratio between the reactor voltage at the switching instant and the constant reactance (expressed as $\frac{1}{L}\boldsymbol{V}_{TCR,0}$). The triangular areas that comprise the difference between the rectangular approximation to the trapezoidal pulse has an individual area equal to $[m \cdot \Delta\alpha][\Delta\alpha]$ which is second-order dependent on the modulating signal, $\Delta\alpha$; as such is excluded in this model. In the frequency domain, this rectangular pulse train is described by another PAM spectrum with pulses within the conduction regions, (α_0, β_0) and $(\pi+\alpha_0, \pi+\beta_0)$ being modulated by the product of m and $\Delta\alpha$.

$$\Delta\boldsymbol{I}_{\Delta\alpha} = [\boldsymbol{\Lambda}_{PAM}(\alpha_0, \beta_0)] \left[\frac{1}{L}\boldsymbol{V}_{TCR,0}\right] \Delta\boldsymbol{\alpha} \tag{3.44}$$

Such that the FTM for the second term in 3.36 is

$$\boldsymbol{\Lambda}_{\Delta\alpha} = \boldsymbol{\Lambda}_{PAM}(\alpha_0, \beta_0)\frac{1}{L}\boldsymbol{V}_{TCR,0} \tag{3.45}$$

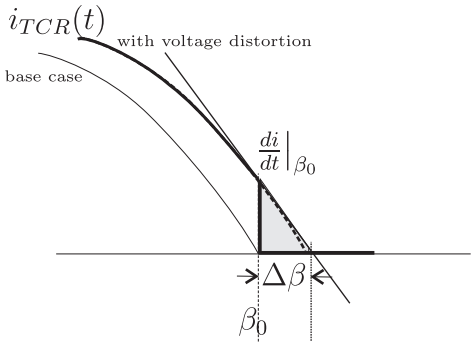

Figure 3.7: Analytical model showing the effects of an SIV-off delay to the reactor phase current.

3.7.4 Small Signal Currents from Uncontrolled Switching Instant Variation

Variation in switching instants occurring at β may be due to two separate input variations. The first type is that any variation in switch-on, $\Delta\alpha$, has a corresponding effect on switch-off at β. Its effect on the TCR current has been covered in the preceding subsection. The second type is the switch-off variation due to small-signal variation in applied voltage which was neglected in Section 3.7.2. A further analysis is presented here as shown in Fig. 3.7. The heavy line shows the resulting reactor current based on the model in Section 3.7.2. It clearly shows the abrupt drop in current at $\omega t = \beta_0$, associated with the linearised model. The dashed line indicates the correct trajectory of the current that ends at $\omega t = \beta_0 + \Delta\beta$. The magnitude of the error is

$$A_{error} = \frac{1}{2}\left.\frac{di}{dt}\right|_{\beta_0} (\Delta\beta)^2 \tag{3.46}$$

As the error is a second order function of the switching instant variation, $\Delta\beta$, this component can be dropped from the small-signal model.

The same conclusion was reached by Lima, Semlyen and Iravani [39] when they analysed the sensitivity of the harmonic current to the switch-off (i.e. Δt_{off} in their publication).

3.8 THREE PHASE TCR MODEL

The single phase model is extended to a three phase model implemented in Matlab®. The single phase variables are extended to three phase by appending phases b and c as described in 3.22 followed by a transform to symmetrical components (3.23). Every FTM in the single phase model is extended to three phase symmetrical components using the procedure described in Appendix B.

To validate the three phase model, an equivalent system is built in EMTDC™/PSCAD® using discrete components for time-domain simulation with solution step of 10μs for at least 25 cycles of the fundamental frequency. Time-domain data which is at least eight

samples per period at the highest frequency of interest (i.e. 50th harmonic or 2500 Hz) is converted to frequency domain using FFT for direct comparison with the frequency domain results of the model.

3.8.1 Base Case

The power system consists of an 11kV, 50Hz three phase voltage source directly supplying power to a delta-connected TCR. Each leg has a 3.85 mH inductance. The thyristor firing angle is set to 135°. The time-domain plot of line A current (Fig. 3.8a) shows a match between the time-domain simulation result and the predicted response based on the linearised harmonic domain model. The other two phases look similar, hence are not shown. The harmonic spectra of the two signals in sequence components likewise agree well (Fig. 3.8b).

In the next subsections, two cases are presented to demonstrate the performance of the FTM-based models in predicting the results of a time-domain simulation. Even as these demonstrations are not exhaustive, the cases that were chosen illustrate the accomplishments and the limitations of the models.

3.8.2 Input Voltage Variation

To illustrate the capability of the model under distorted source conditions, a 5%, 2nd harmonic, negative sequence voltage source distortion was introduced. Time-domain plots of phase A line current comparing the time-domain simulation result (i.e. using EMTDC/PSCAD) and the predicted response from the FTM-based model (i.e. implemented as a Matlab code) are shown in Fig. 3.9a. The predicted response was able to track most of the signal except during switch-off of the phase currents as highlighted. As discussed in the previous section this difference is due to the fact that the linearised model is not able to accurately predict the TCR phase current switch-off instants—as this is second order dependent on voltage variation. Fig. 3.9b shows the harmonic domain plots showing the positive and negative sequence components of the resulting current, presented as percentage of the fundamental components. Similarly, the error due to incorrect model of switching instants presents as significant errors in the magnitudes of the harmonic components. 5% voltage distortion is unrealistically large for this device, and the disagreement shown is consistent with the linearisation that was made.

3.8.3 Switching Instant Variation

To illustrate the validity of the model for controlled switching instant variation, a 3° (0.05236 rad) 2nd harmonic signal is introduced as an SIV on top of the 135° base case

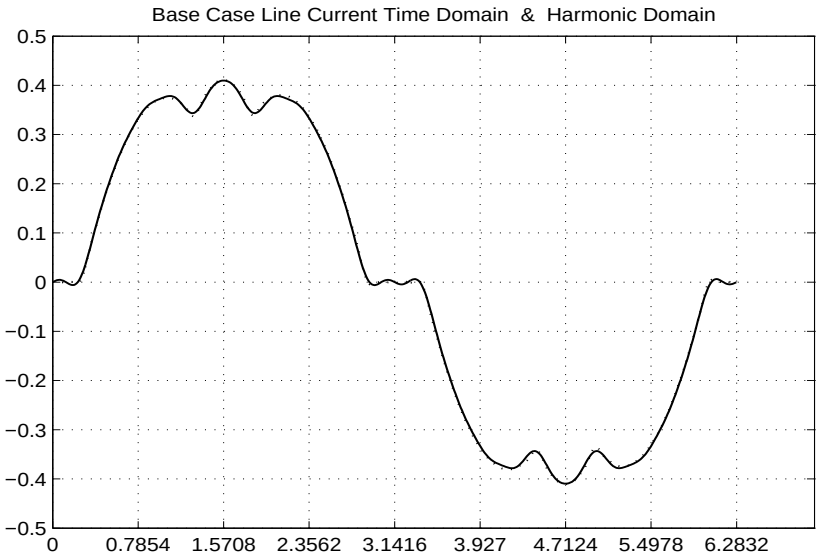

(a) Time Domain plots of base case TCR line currents

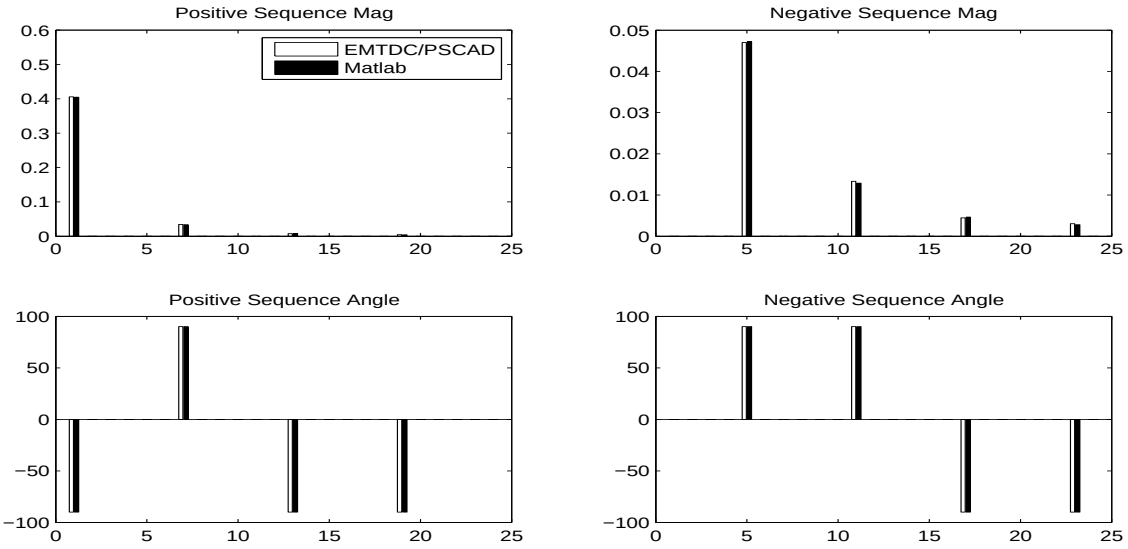

(b) Harmonic Domain Plots of Base Case TCR Currents

Figure 3.8: Base Case Validation Results

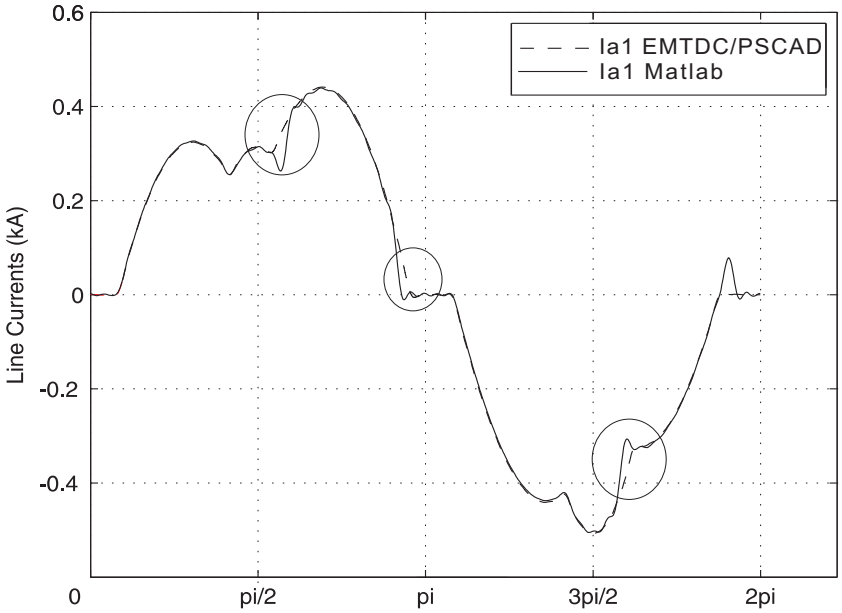

(a) Time-domain plots of TCR line currents with source voltage variation, highlighting the error around the switch-off instant of the phase currents

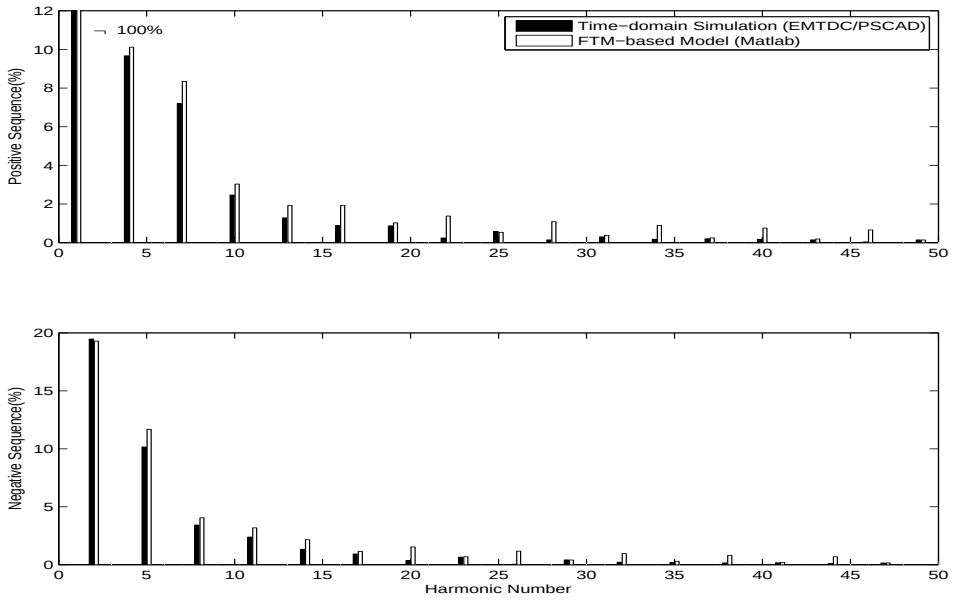

(b) Harmonic-domain plots of TCR line currents with source voltage variation. Presented as magnitudes of sequence components and in percentage of the fundamental frequency

Figure 3.9: Effect of Voltage Variation Validation Results

firing angle. Time-domain plots for the three-phases (Fig. 3.10a) and the frequency-domain plots for positive and negative sequences (Fig. 3.10b) show reasonable match between time-domain simulation and linearised harmonic domain response. Careful inspection of the harmonic plots show that for a number of harmonics, the results of the FTM-based model overestimated the values obtained from the EMTDC solution. This is expected since the linearised model approximated the trapezoidal area (representing the change in current due to switching instant variation) as a rectangular area as described in Sec. 3.7.3.

3.9 ANALYSIS AND CONCLUSION

This chapter presented a linearised harmonic domain model implemented as a set of Frequency Transfer Matrices that were analytically developed. It was shown that this formulation effectively models the harmonic effects of small-signal input voltage variation on the TCR small-signal current. However, switching instant variation as a non-linear effect of voltage variation could and should not be included in a linearised model. The other type of switching instant variation which is caused by timing and signalling error and affects the switch-on of the thyristors has also been modeled.

The analytical technique employed in the development of this model will be beneficial as we proceed to develop a Harmonic State-space model of the TCR. However, the linearised transfer function approach to model the harmonic interaction in a TCR also highlights a few limitations in this procedure. As the model is steady-state, the dynamics of the harmonics are not captured at all. For the purpose of investigating harmonic instability, it is important to be able to observe the time-varying interactions as well.

The model for the effect of switching instant variation on the reactor current (3.7.3) provides a powerful tool to incorporate control procedures into the model as was previously done on an HVDC converter [75]. Control signals can be posed as switching instant modulators to produce a desired effect on the TCR current and reactive power. In the succeeding chapters, the same principle will be applied with the linearised model written in a state-space formulation where control models are incorporated.

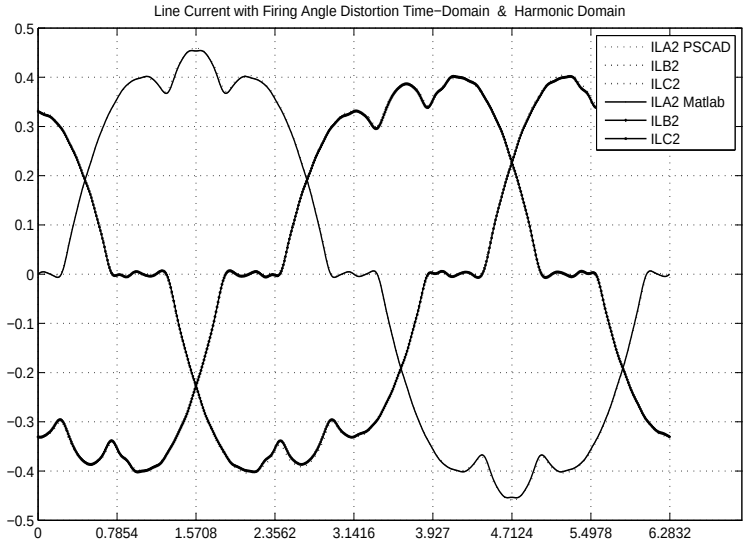

(a) Time-domain plots of TCR line currents with modulated switching instant variation currents

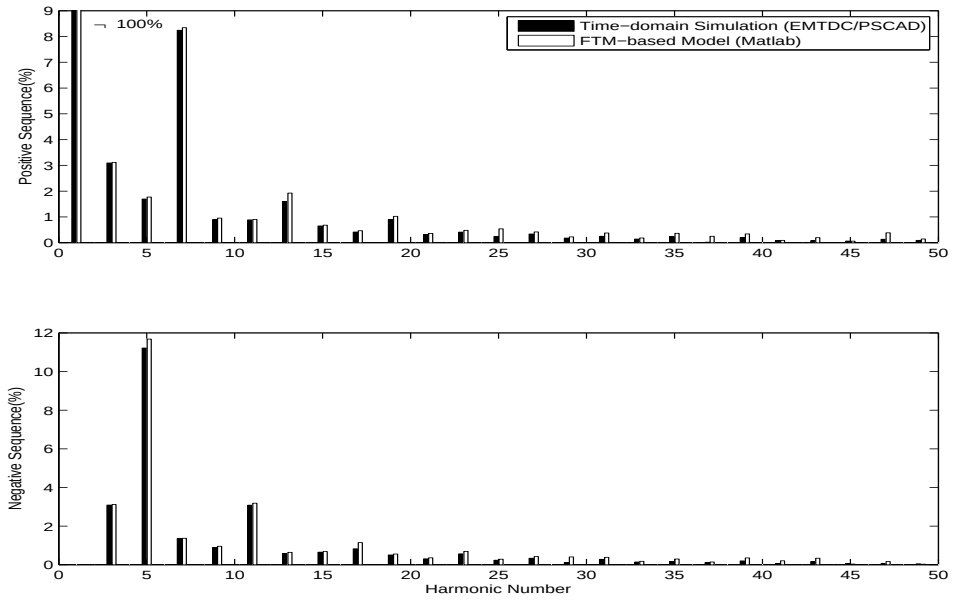

(b) Harmonic-domain plots of TCR line currents with switching instant variation, presented as magnitudes of sequence components and in percentage of the fundamental frequency

Figure 3.10: Effect of Switching Instant Variation Validation Results

Chapter 4

UNCONTROLLED TCR HARMONIC STATE SPACE MODEL

4.1 INTRODUCTION

Chapter 3 presents a model that captures the small-signal steady-state harmonic interaction across a Thyristor Controlled Reactor (TCR). However, there was no attempt to model the dynamics of the harmonics. By defining the state variable harmonics as additional state variables and incorporating the harmonic interaction using the frequency transfer matrix across the TCR in a state-space equation, it is possible to capture both the steady-state and the dynamics of individual harmonics.

Harmonic Domain analysis is traditionally involved in describing the steady-state harmonics in the power system. However with the increasing demand for power quality and reliability in the system, and increasing threat of harmonic instability caused by the proliferation of devices and controllers that affect and are affected by harmonics, the issue is slowly shifting to include not only the steady-state condition but transients as well. Specifically, instabilities that were caused by harmonic interaction have been reported in train in Europe [46], in large photovoltaic installations in the Netherlands [20], and in HVDC-FACTS installations in North America [26], [27]. These cases are expected to increase with more complex installations of power electronics controllers in the system.

Wereley [72] in his seminal work introduced the Harmonic State Space (HSS) and extended the classic state-space to explicitly include the harmonics as additional state variables. In doing so, he was able to extend Linear Time Invariant (LTI) modeling and analysis techniques to Linear Time Periodic (LTP) systems. More importantly for the purpose of this thesis, a power system that includes FACTS controllers as an LTP system can be modeled using LTI techniques that incorporates both the controller model and the harmonic interaction across the power electronic device. The TCR, however, is a nonlinear device since thyristor switching is affected by voltage distortion. This chapter presents a procedure to model this nonlinear effect in an HSS to achieve a time invariant state space model.

Recently there have been similar attempts to model the dynamics of individual harmon-

ics, termed as Extended Harmonic Domain (EHD) [58] or Dynamic Harmonic Domain (DHD) [57], [15]. These formulations produce a description identical to HSS. It is to be noted that as this modeling technique is fundamentally about applying state-space concepts in the harmonic domain model, this thesis is keeping the term Harmonic State Space (HSS). This chapter presents the development of an HSS model for a TCR without an implementation of active control, that accurately captures the dynamics and steady-state of individual harmonics. This model improves on similar models previously published firstly by incorporating the effect of switching instant variation and secondly by proposing a harmonic selection procedure to reduce the size of the HSS model.

4.2 EXPONENTIALLY MODULATED PERIODIC SIGNAL AND FREQUENCY TRANSFER MATRIX

In this section, the Harmonic State Space (HSS) set of equations is presented. It starts with the Exponentially Modulated Periodic (EMP) function as the basis signal before the discussion on the usage of the HSS equation for Linear Time Periodic (LTP) systems. Although the concepts are based on Wereley's derivation using harmonic balance [72] the discussion that follows is a general treatment of Madrigal and Rico's operational matrices [41] which is a logical extension of the harmonic domain presented in the previous chapter.

4.2.1 Exponentially Modulated Periodic Signal

The basis function in this formulation is an Exponentially Modulated Periodic (EMP) signal described in 4.1.

$$z(t) = \sum_{k\in\mathbb{Z}} Z_k e^{s_k t} \tag{4.1}$$

As $s_k = s + jk\omega_0$, we have

$$z(t) = e^{st} \sum_{k\in\mathbb{Z}} Z_k e^{jk\omega_0 t} \tag{4.2}$$

With $s \in \mathbb{C} = \sigma + j\omega_n$, each harmonic is modulated according to an exponential $e^{\sigma t}$ and a natural frequency, ω_n. This EMP signal is a generalised description of the periodic signal described in 3.3, where an $s = 0$ degenerates to the steady-state periodic signal. As an extension to 3.6, an EMP signal can be alternately described in terms of the modulator vector, $\mathbf{\Gamma}(t)$ as:

$$z(t) = e^{st}\mathbf{\Gamma}(t)\boldsymbol{Z} \tag{4.3}$$

Since Chapter 3 deals with steady-state description, each X_k in 3.3 is limited to constant values while $e^{st}Z_k$ in 4.2, can be an exponentially modulated sinusoidal signal.

4.2.2 Product of EMP signals

Consistent with the discussion in Subsection 3.3.2 where the product of two time-domain periodic signals is equivalent to the discrete convolution of the harmonic components, it is implemented as a product between a Toeplitz-form FTM and a harmonic domain vector. The product between an EMP signal, $x(t)$ and a time periodic signal $A(t)$ which has constant harmonic coefficients, is described as:

$$\begin{aligned} y(t) &= A(t)z(t) \\ e^{st}\mathbf{\Gamma}(t)\boldsymbol{Y} &= e^{st}\mathbf{\Gamma}(t)\mathcal{T}\{\boldsymbol{A}\}\boldsymbol{Z} \end{aligned} \tag{4.4}$$

or

$$\boldsymbol{Y} = \boldsymbol{A}_{\mathcal{T}}\boldsymbol{Z} \tag{4.5}$$

where $\boldsymbol{A}_{\mathcal{T}}$ indicates the Toeplitz transform of the harmonic vector $\boldsymbol{A}$ as defined in 3.8.

For the special case where $A(t)$ is a constant A and not a function of the harmonic frequency,

$$\boldsymbol{A}_{\mathcal{T}} = A\boldsymbol{\mathcal{I}} \tag{4.6}$$

where $\boldsymbol{\mathcal{I}}$ is the identity matrix.

4.2.3 Derivative of EMP signals

To describe the dynamics of the harmonic vector, the derivative of the modulation vector is expressed as:

$$\dot{\mathbf{\Gamma}}(t) = \mathbf{\Gamma}(t)\boldsymbol{N} \tag{4.7}$$

where $\boldsymbol{N}$ is the same Derivative FTM introduced in 3.12 with a diagonal structure illustrated in 3.7.

The derivative of the time-varying signal in 4.3 is expressed as

$$\dot{z}(t) = e^{st}\mathbf{\Gamma}(t)s\boldsymbol{Z} + e^{st}\mathbf{\Gamma}(t)\boldsymbol{N}\boldsymbol{Z} \tag{4.8}$$

4.3 HARMONIC STATE SPACE EQUATIONS

A Linear Time Periodic (LTP) system is described as follows

$$\dot{x}(t) = A(t)x(t) + B(t)u(t) \tag{4.9a}$$

$$y(t) = C(t)x(t) + D(t)u(t) \tag{4.9b}$$

where $A(t)$, $B(t)$,$C(t)$, and $D(t)$ are time-periodic functions. Based on 4.4 and 4.8, the dynamic equation (4.9a) of an LTP system is

$$\begin{aligned} e^{st}\boldsymbol{\Gamma}(t)s\boldsymbol{X} + e^{st}\boldsymbol{\Gamma}(t)\boldsymbol{N}\boldsymbol{X} &= e^{st}\boldsymbol{\Gamma}(t)\boldsymbol{A}_{\mathcal{T}}\boldsymbol{X} + e^{st}\boldsymbol{\Gamma}(t)\boldsymbol{B}_{\mathcal{T}}\boldsymbol{U} \\ s\boldsymbol{X} + \boldsymbol{N}\boldsymbol{X} &= \boldsymbol{A}_{\mathcal{T}}\boldsymbol{X} + \boldsymbol{B}_{\mathcal{T}}\boldsymbol{U} \\ s\boldsymbol{X} &= (\boldsymbol{A}_{\mathcal{T}} - \boldsymbol{N})\boldsymbol{X} + \boldsymbol{B}_{\mathcal{T}}\boldsymbol{U} \end{aligned} \tag{4.10}$$

In the same manner, 4.9b is written as

$$\begin{aligned} e^{st}\boldsymbol{\Gamma}(t)\boldsymbol{Y} &= e^{st}\boldsymbol{\Gamma}(t)\boldsymbol{C}_{\mathcal{T}}\boldsymbol{X} + e^{st}\boldsymbol{\Gamma}(t)\boldsymbol{D}_{\mathcal{T}}\boldsymbol{U} \\ \boldsymbol{Y} &= \boldsymbol{C}_{\mathcal{T}}\boldsymbol{X} + \boldsymbol{D}_{\mathcal{T}}\boldsymbol{U} \end{aligned} \tag{4.11}$$

A similar method of deriving the Harmonic State Space (HSS) based on harmonic balance previously presented by Wereley in [72] is presented in Appendix E. In [72] it was also pointed that although the coefficient matrices $\boldsymbol{B}_{\mathcal{T}}$, $\boldsymbol{C}_{\mathcal{T}}$ and $\boldsymbol{D}_{\mathcal{T}}$ are Toeplitz blocks, $\boldsymbol{A}_{\mathcal{T}} - \boldsymbol{N}$ is quasi-Toeplitz at best hence standard Toeplitz matrix analyses such as those presented in [12] do not apply. On the other hand, since these complex coefficient matrices can be alternately expressed as real elements in tensor form [63], such LTP systems are analysed using standard LTI techniques.

For the power system with a TCR (or with any FACTS controller which has switching circuits), the linear characteristic is kept as long as the switching instants are fixed. Hence, the HSS model is easily applicable. However, the reality is that the thyristor' switching instants vary with voltage distortion and control inputs. In which case, the coefficients, $\boldsymbol{B}_{\mathcal{T}}$, and $\boldsymbol{D}_{\mathcal{T}}$ can not be expressed as constant matrices but as functions of the input signal making the system nonlinear. In this model, a novel procedure is introduced to model this nonlinearity in the HSS.

4.3.1 Frames of Reference

The dynamic equation of an LTP system is presented in 4.10. However, even an LTI system which is connected to an LTP system has to be described using the same HSS formulation. Consider a single-input, single-output LTI subsystem, with a lone state variable, the dynamic equation is as follows:

$$\dot{x}(t) = \boldsymbol{A}x(t) + \boldsymbol{B}u(t) \tag{4.12}$$

where $\boldsymbol{A}$ and $\boldsymbol{B}$ are both single-element constant matrices. If this subsystem is to be connected to an LTP subsystem that is described with n harmonics, the HSS equation for the LTI subsystem expands to the form in 4.10 where $\boldsymbol{X}$, $\boldsymbol{U}$ are vectors of length $2n + 1$.

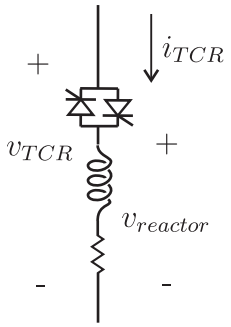

Figure 4.1: Single-phase Thyristor-Controlled Reactor circuit

The new state matrix, $\bar{\boldsymbol{A}}$ which is equal to $\boldsymbol{A}_{\mathcal{T}} - \boldsymbol{N}$ is an expanded version of the original single-element state matrix, $\boldsymbol{A}$. However, the eigenvalues of the new state matrix, $\bar{\boldsymbol{A}}$ includes all of $A - jn\omega$ for $n \in \{-h, \ldots, -2, -1, 0, 1, 2, \ldots, h\}$ for up to the h^{th} harmonic where the $n = 0$ term is the same as the lone eigenvalue of the original state matrix. This implies that the HSS-formulated LTI system provides a facility to observe the same LTI system simultaneously from a number of frames of reference, specifically from all the harmonic frequencies. With frames of reference anchored on individual harmonic frequencies, each harmonic signal with both transients and steady-state, is observed on its own frame of reference.

This does not mean that interharmonic signals can not be observed. Interharmonic signals can be observed as modulated versions of the harmonic frequency. For example, an interharmonic signal whose frequency is d times the fundamental frequency, can be observed as a signal varying at a rate of $d - n$ times the fundamental frequency when observed at the n^{th} harmonic frame of reference.

$$\begin{aligned} x(t) &= Xe^{jd\omega_0 t} \\ &= X_d e^{j(d-n)\omega_0 t} e^{jn\omega_0 t} \end{aligned} \tag{4.13}$$

$$\bar{x}_n(t) = X_d e^{j(d-n)\omega_0 t} \tag{4.14}$$

where $n \in \mathbb{Z}$ while $d \notin \mathbb{Z}$ and $\bar{x}_n(t)$ is the observed signal at the n^{th} harmonic frame of reference.

4.4 SINGLE PHASE TCR HARMONIC STATE SPACE MODEL

Prior to developing an HSS model for a three phase TCR, a model for a single phase TCR is presented in this section. This elementary model highlights a number of principles that will be extended to the three phase model. The HSS modelling procedure is applied to a TCR where the reactor is modeled as a large inductance (L) with a small series resistance (R) as shown in Fig. 4.1.

4.4.1 Model with Fixed Switching Instants

The state-space equation for the voltage loop is written as

$$\frac{di_{TCR}(t)}{dt} = \frac{-R}{L} i_{TCR}(t) + \frac{1}{L}\Psi(t) v_{TCR}(t) \tag{4.15}$$

where $\Psi(t)$ for a fixed switching instant model is the same as 3.38.

In reality however, $\Psi(t)$ in a thyristor-based Controller is affected by the applied voltage, $v_{TCR}(t)$, which makes 4.15 nonlinear. As a first approximation, an HSS model with fixed switching instants is presented here.

Applying the HSS formulation in Section 4.3 with the state-variable, $i_{TCR}(t)$ chosen as the output when $v_{TCR}(t)$ is applied across the TCR

$$s\boldsymbol{I}_{TCR} = (\boldsymbol{A}_{\mathcal{T}} - \boldsymbol{N})\boldsymbol{I}_{TCR} + \boldsymbol{B}_{\mathcal{T}}\boldsymbol{V}_{TCR} \tag{4.16a}$$

$$\boldsymbol{I}_{TCR} = \boldsymbol{C}_{\mathcal{T}}\boldsymbol{I}_{TCR} \tag{4.16b}$$

where

$$\begin{aligned}
\boldsymbol{A}_{\mathcal{T}} &= \frac{-R}{L}\boldsymbol{\mathcal{I}} \\
\boldsymbol{B}_{\mathcal{T}} &= \frac{1}{L}\boldsymbol{S}_{\mathcal{T}} = \frac{1}{L}\mathcal{T}\{\boldsymbol{\Psi}_0\} \\
\boldsymbol{C}_{\mathcal{T}} &= \boldsymbol{\mathcal{I}}
\end{aligned}$$

Model Application This model was applied to a TCR circuit with a reactor impedance of $0.1 + j12.095\Omega$ at 50 Hz with equidistant firing at $\alpha = 40°$ measured from the voltage peak. An 11kV fundamental frequency voltage with 5% of 5th harmonic distortion was applied across the TCR. The result as shown in Fig. 4.2 has been considered acceptable in the past as similar results have been presented in publications such as [69]. However upon careful inspection, the current during non-conduction is non-zero as highlighted in Fig. 4.3. The current error is due to switching instant variation (SIV) during switch-off ($\omega t = \beta$ and $\pi + \beta$) brought about by the voltage variation across the TCR. A fixed switch-off (β_0) model results in a residual current during non-conduction if the actual switch-off varies about the fixed switch-off. This significant error in the model is addressed in Section 4.4.2 by incorporating the effect of the switching instant variation.

4.4.2 Model with Switching Instant Variation

The phenomenon of voltage variation resulting in Switching Instant Variation (SIV) was mentioned in Section 3.7.2. However due to its nonlinear characteristic, it was not addressed in the linearised harmonic domain model. The HSS model on the other hand is capable of capturing the dynamics of the harmonics of the state variables which in this

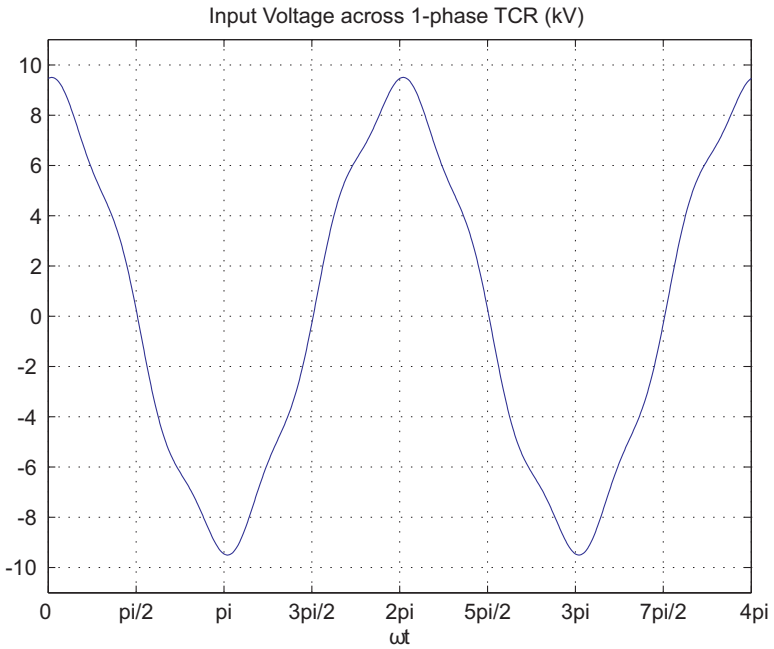

(a) Voltage across the TCR

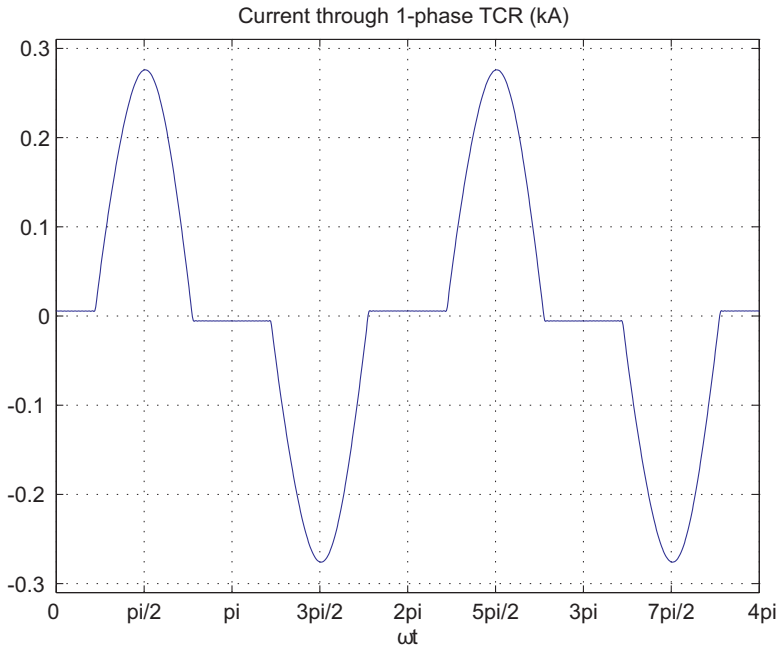

(b) Current through the TCR

Figure 4.2: Single phase Thyristor Controlled Reactor Voltage-Current Response

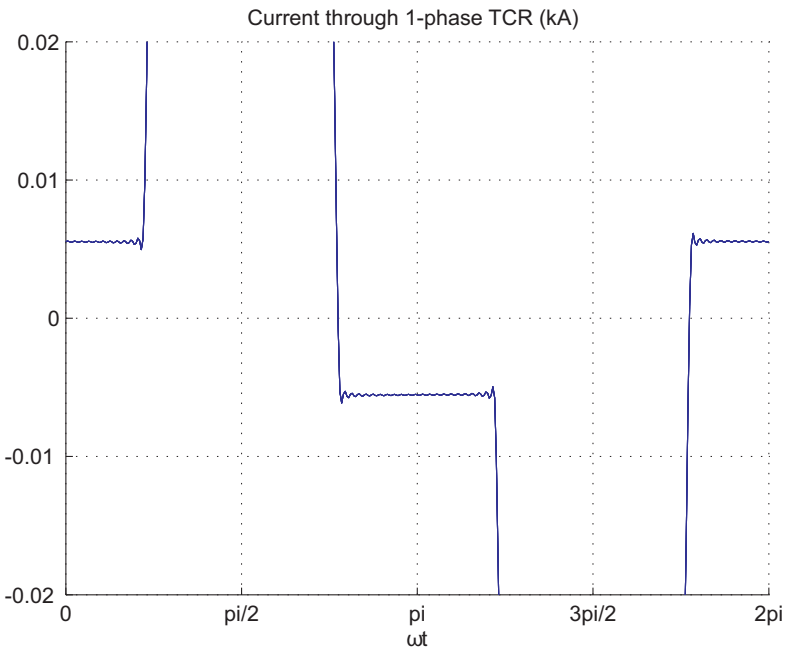

Figure 4.3: TCR current along the zero axis showing current during non-conduction

case is the current through the reactor. Just sampling the reactor current during the conduction period and not sampling it during the non-conduction period is not possible in the HSS formulation. The current has to be set to zero during non-conduction so that it starts from the correct value at the next conduction period. As was presented in the preceding result, an incorrect value for the switching instant results in an incorrect state variable formulation.

The effect of SIV has been described before by Wood [75] and Hume [31] as they described the harmonic interactions in HVDC links, and by Love [40] in his generalised small-signal model for power electronic converters. Mollerstedt [46] did not specifically identify this phenomenon, but his description for the effect of voltage distortion on zero-crossing change is a modulated impulse function. However, none of these previous publications incorporated this SIV effect in an HSS model.

Fig. 4.4a illustrates the trajectory of reactor current from conduction to non-conduction with a fixed switching instant model. Case I refers to a switch-off from a positive value while Case II is from a negative value. In both cases fine lines indicate base case operation while heavy lines indicate resulting cases with small-signal voltage variations. For Case I, the small-signal variation in the reactor voltage produced a reactor current larger than the base case current; this results in a delay in switching instant ($\Delta\beta > 0$). With a fixed switching instant model at β_0, the incorrect result is a positive current during non-conduction whose value is equal to the reactor current at the base case switching instant, $i_{reactor}(\omega t = \beta_0)$. On the other hand if the small-signal voltage variation produces a smaller reactor current, this results in an advance in switching

instant ($\Delta\beta < 0$) which if not correctly captured in the model gives a negative current during non-conduction.

Case II follows a similar interpretation however this time, an advance in switching instant ($\Delta\beta < 0$) results in a positive current during non-conduction, while a delay in switching instant ($\Delta\beta > 0$) results in a negative current during non-conduction.

Based on these, the TCR model is improved by introducing voltage impulses at $\omega t = \beta_0$ and $\omega t = \pi + \beta_0$ that are modulated by the TCR current, i_{TCR}. The area modulated impulse train of voltages when applied across the reactor results in a step current change sufficient to offset the incorrect current during non-conduction. It is to be noted that a pair of impulses π radians apart as shown in Fig. 4.4b is introduced in every period which is consistent with the assumption of equidistant firing for the anti-parallel thyristor pair.

The signal block diagram in Fig. 4.4c shows how the analytical model is implemented. The dynamic equation in 4.15 is updated to 4.17 to include the modulated voltage impulses required to correct the non-conduction current.

$$\begin{aligned} S(t)v_{TCR}(t) + K_d\delta_T(t)i_{TCR}(t) &= L\frac{di_{TCR}(t)}{dt} + Ri_{TCR}(t) \\ \frac{di_{TCR}(t)}{dt} &= \left[\frac{-R}{L} + \frac{K_d}{L}\delta_T(t)\right] i_{TCR}(t) + S(t)v_{TCR}(t) \end{aligned} \tag{4.17}$$

The term $K_d\delta_T(t)$ in 4.17 is a periodic impulse function where scaled impulses occur at every base case switch-off instant. The Dirac comb, $\delta_T(t)$ introduced in 3.17 is modified to suit this model requirement. That is, an impulse occurs every half-cycle and each impulse is delayed to occur during the base case switch-off (at $\omega t = \beta_0$ and $\pi + \beta_0$). It has to be negative-valued, as the purpose of the impulses is to reset a positive reactor current down to zero (or a negative reactor current up to zero).

These impulses are characterised by a harmonic spectrum that does not roll-off where truncation of higher harmonics theoretically results in loss of accuracy in the model. However, each impulse is immediately integrated by the TCR inductor rendering the higher harmonics less relevant. Investigations in this particular model confirmed this. With two impulses for every period, only even harmonic coefficients are present. The scaling factor K_d ensures that the strength of the voltage impulse is sufficient to produce a step current that offsets the sampled current i_{TCR}.

Scaling Factor The sampling property of the unit impulse [50] expresses that when a function, $x(t)$ is multiplied by a scaled impulse, $A\delta(t - t_0)$, the result is an impulse at $t = t_0$ with a scaled strength equal to $x(t_0)$.

$$x(t)A\delta(t - t_0) = Ax(t_0)\delta(t - t_0) \tag{4.18}$$

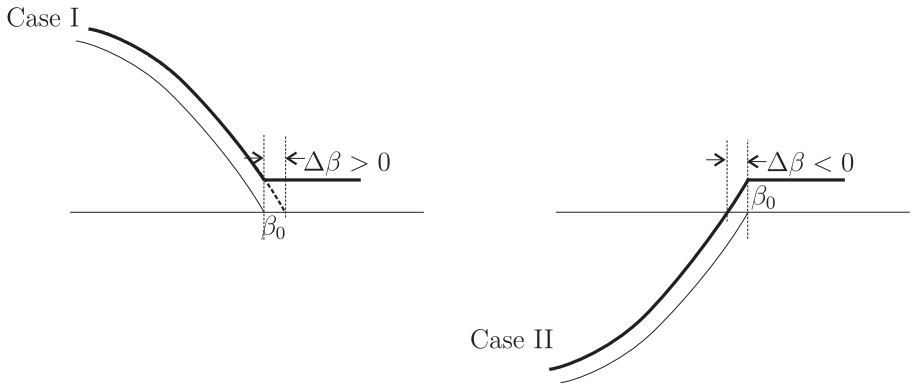

(a) Analysis of switching instant variation and current at non-conduction

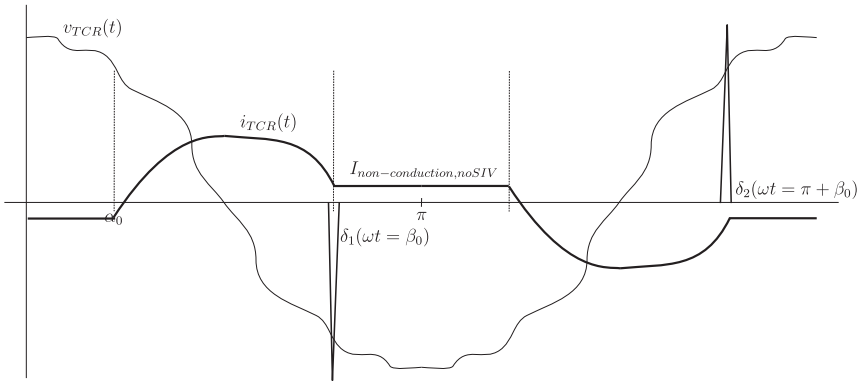

(b) Analytical illustration of switching instant variation model

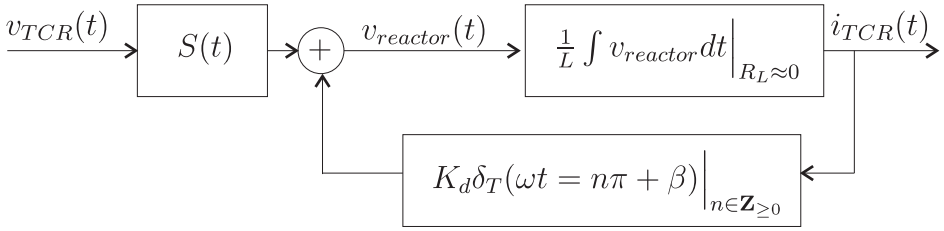

(c) Block diagram model of TCR with Switching Instant Variation

Figure 4.4: Diagrams for Modeling Switching Instant Variation

In this case, i_{TCR} is multiplied to a scaled impulse, $K_d\delta(\omega_0 t = \beta_0)$ which results in a modulated impulse at the switching instant.

$$i_{TCR}(\omega_0 t)K_d\delta(\omega_0 t - \beta_0) = K_d i_{TCR}(\beta)\delta(\omega_0 t - \beta_0) \tag{4.19}$$

The succeeding paragraphs describes the procedure to determine K_d.

The reactor current, i_{TCR}, is the sum of the currents from the voltage output of the thyristor, $i_{V_{thyristor}}$, and from the voltage impulse, $i_{V_{impulse}}$.

$$i_{TCR} = i_{V_{thyristor}} + i_{V_{impulse}} \tag{4.20}$$

As the voltage impulse is infinitely large and infinitely short, the effect of the voltage drop across the resistance from the resultant rise in current is negligibly small. Thus all of the voltage impulse effectively appears across the inductance.

An impulse voltage across the inductance results in a step current of the form $K\mu(\omega_0 t - \beta_0)$.

$$\begin{aligned} v_\delta(\omega_0 t) &= -K_d\delta(\omega_0 t - \beta_0)i_{TCR}(\omega_0 t) \\ &= -K_d i_{TCR}(\beta_0)\delta(\omega_0 t - \beta_0) \end{aligned} \tag{4.21}$$

$$\begin{aligned} i_{V_{impulse}}(\omega_0 t) &= \frac{-1}{\omega_0 L}\int K_d i_{TCR}(\beta_0)\delta(\omega_0 t - \beta_0)d\omega_0 t \\ &= \frac{-K_d i_{TCR}(\beta_0)}{\omega_0 L}\mu(\omega_0 t - \beta_0) \end{aligned} \tag{4.22}$$

where $i_{V_{impulse}}$ steps from 0 to $\frac{-K_d i_{TCR}(\beta_0)}{\omega_0 L}$. Technically at the switching instant ($\omega t = \beta_0$), the step current is undefined (i.e. between zero and the step height). However, a step function represented by truncated harmonics is defined everywhere as shown in Fig. 4.5 for the case where $i_{V_{thyristor}}(\beta_0) > 0$ and $i_{V_{impulse}}(\beta_0^+) < 0$. The value at the switching instant is midway between the initial and final values.

$$\begin{aligned} i_{V_{impulse}}(\beta_0) &= \frac{-K_d i_{TCR}(\beta_0)}{2\omega_0 L} \\ K_d &= -2\omega_0 L\frac{i_{V_{impulse}}(\beta_0)}{i_{TCR}(\beta_0)} \\ &= 2\omega_0 L \end{aligned} \tag{4.23}$$

since the ratio between $i_{V_{impulse}}(\beta_0)$ and $i_{TCR}(\beta_0)$ is -1.

Modulated Impulse FTM The corresponding FTM is as introduced in 3.20 and is updated here for a pair of impulses in every period.

$$\mathbf{\Delta}_\beta = \frac{2\omega_0}{T}\left[\mathcal{T}\{e^{-jn\beta}\} + \mathcal{T}\{e^{-jn(\pi+\beta)}\}\right]_{n\in[-2h,2h]} \tag{4.24}$$

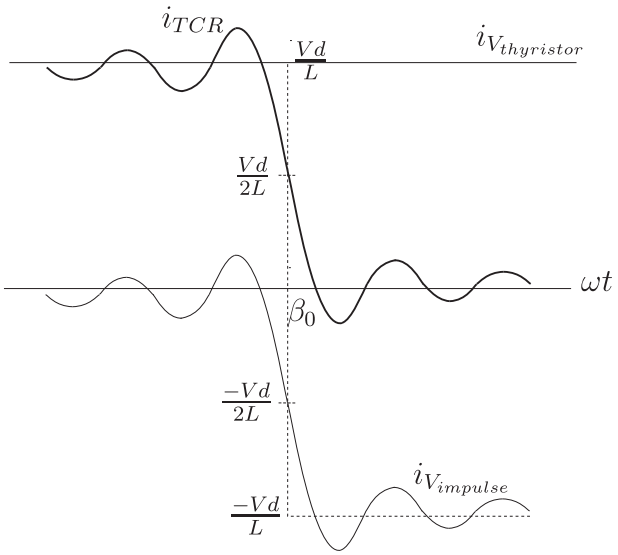

Figure 4.5: Step Current i_{TCR} and its components, $i_{V_{thyristor}}$ and $i_{V_{impulse}}$; with harmonic truncation

The HSS model for a single phase TCR with SIV model improves from 4.16 to

$$s\boldsymbol{I}_{TCR} = (\boldsymbol{A}_{\mathcal{T}} + \boldsymbol{\Delta}_{\beta} - \boldsymbol{N})\boldsymbol{I}_{TCR} + \boldsymbol{B}_{\mathcal{T}}\boldsymbol{V}_{TCR} \tag{4.25a}$$

$$\boldsymbol{I}_{TCR} = \boldsymbol{C}_{\mathcal{T}}\boldsymbol{I}_{TCR} \tag{4.25b}$$

For the same test system described earlier in this section, the resulting current for this improved model is shown in Fig. 4.6

4.5 MODEL REDUCTION

This modelling procedure requires a separate state variable for every inductor and capacitor for every harmonic modelled. For even relatively simple systems, the state-space becomes unreasonably large, and any method of reducing the size of the state-space is of great computational value. A reduced model translates to a more efficient calculation and facilitates analysis of more complex systems. This is done by selecting the harmonics to be included in the model resulting in a smaller set of simultaneous equations (i.e. smaller matrix dimensions).

The switching functions of a six-pulse TCR modulate the fundamental frequency ($\pm 1\omega_0$), to a range of frequencies known as the characteristic harmonics. These are harmonics $6n+1$ in positive sequence and $6n-1$ in negative sequence. In fact, any applied frequency is always modulated up or down by $6n\omega_0$. To completely capture the frequency coupling characteristics of the TCR system, it is necessary to provide an HSS representation of the AC system at frequencies separated by $6n\omega_0$. Any set of frequencies, separated by $6n\omega_0$ will be sufficient, although it makes sense to choose the character-

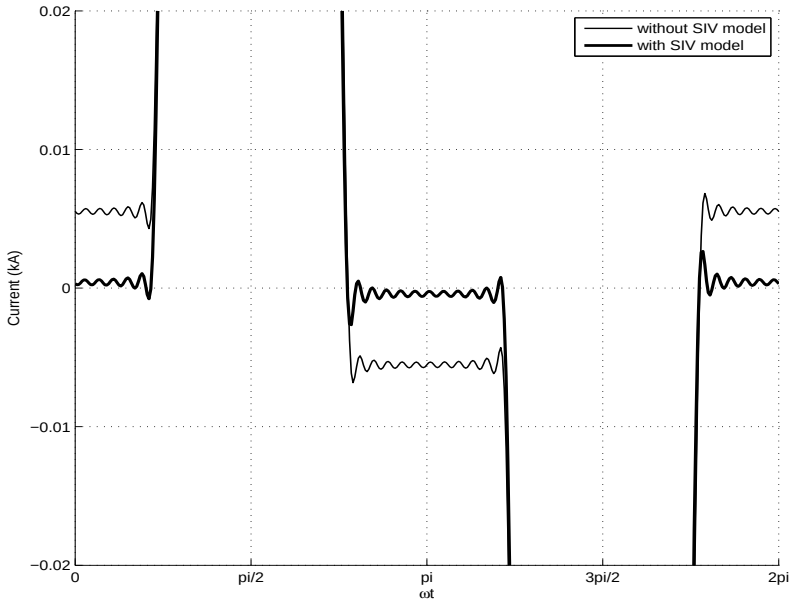

Figure 4.6: TCR current along the zero axis showing current during non-conduction

istic harmonics as a suitable set. In general, the characteristic harmonics of a p-pulse converter is described as follows [8]:

$$H_c = np \pm 1 \qquad n \in \mathbb{Z} \tag{4.26}$$

where $n \geq 0$ including the fundamental frequency when $n = 0$. If an input signal with a non-characteristic frequency exists, it can be implemented in a reduced HSS simulation by modulating one of the inputs at an appropriate frequency[†]. For example, if a second harmonic $e^{j2\omega_0 t}$ is required, it can be injected by modulating the fundamental frequency input by $e^{j\omega_0 t}$. As a rule, an m^{th} harmonic signal can be injected by modulating an n^{th} harmonic by $e^{j(m-n)\omega_0 t}$, where $n \in H_c$.

$$x_m(t) = X_m e^{st} e^{jm\omega t} \tag{4.27}$$

$$\Leftarrow X_m e^{st} e^{j(m-n)\omega t} e^{jn\omega t} \tag{4.28}$$

where this type of harmonic transformation is not biunivocal, as indicated by the left arrow. This is the key that facilitates the selection of harmonic equations that are included in the HSS formulation. The list of characteristic harmonics for the converter determines both the minimum set of independent equations, and the harmonic numbers

[†]This formulation is similar to the one described in Sec. 4.3.1 but is repeated here since this one refers to the generation of an input signal while the previous one refers to interpreting an output signal. In addition, the context here is with respect to non-characteristic frequencies, while the previous one is with respect to interharmonic frequencies.

that will represent any signal in the system. By properly arranging the independent equations and the harmonic numbers of the signals, the Toeplitz-type character of the A, B, C, and D matrices are kept.

The same procedure for model reduction can be applied in a single phase TCR model although the benefit is not as significant as in a three phase TCR. The switching function of the thyristor pair includes the DC component and all even harmonics which indicates that signals across the converter is harmonically coupled either with the same harmonic or $\pm 2n, n \in \mathbb{Z}$ harmonics away, which makes it a 2-pulse converter. Starting with a fundamental frequency base case signal, it is expected that the complete response can be captured even if the model is reduced to only include odd harmonics ($h = 2n \pm 1, n \in \mathbb{Z}$). Similarly, this does not mean that only odd harmonics are captured in the response, but any other frequency can be expressed as an exponentially modulated version of an odd-harmonic signal.

For the rest of the thesis, no distinction is made between a full model with all harmonics and a reduced model with selected harmonics; both up to the highest harmonic of interest. However, all models that were used in the validation were reduced models. At this stage, the primary reason for using reduced models is to be able to model systems with more components. Even though expected, quicker calculation is not part of the scope of this model development and will not be investigated in the produced model.

4.6 THREE PHASE TCR HARMONIC STATE SPACE MODEL

Unlike the single phase HSS model in the previous section where a closed-form dynamic equation is written and a transform to HSS is systematically employed, building the three phase model is done by analytically developing HSS models for individual LTP subsystems and then connecting them to form a more complex LTP system. This method's scalability is more practical and is consistent with other techniques applied in building power system models. Similar to the three phase linearised model in Chapter 3, this HSS model is described in sequence components.

In this model, voltage and current variables are in symmetrical components represented as truncated harmonic vectors with harmonic reduction. The procedure for harmonic reduction was presented in Section 4.5 while the corresponding structure for symmetrical components is presented in Appendix C. With voltage and currents as input and output signals, the power system in Fig. 4.7a is equivalent to the block diagram model in Fig. 4.7b including the effect of SIV where subsystems are defined by the broken line boundaries.

HSS models are then developed for each subsystem as follows: thyristor switches, system impedance, reactor bank and the modulated voltage impulse function. It was described in Chap.3 that positive and negative sequence components are sufficient to describe the terminal (i.e. bus voltages and line currents) characteristics of a linearised

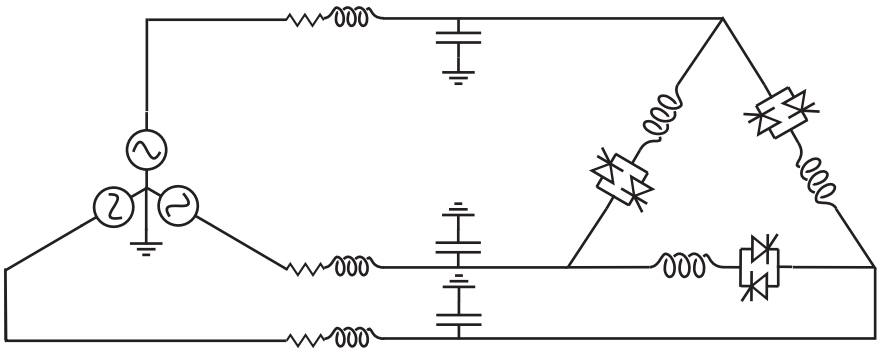

(a) 3-phase TCR Circuit Diagram

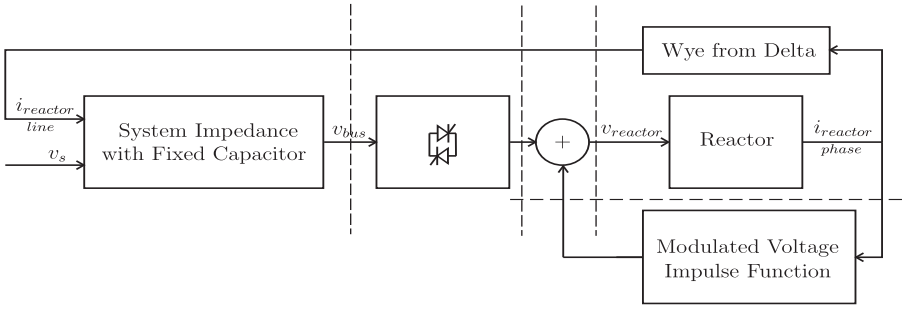

(b) Equivalent block model of the TCR Circuit

Figure 4.7: 3-phase TCR Circuit and Block Diagrams

harmonic domain model of a three phase TCR. However for the HSS model, it is important to completely describe all the state-variables, not just the terminal variables. The reactor current, as one of the state-variables, has to be described adequately with the inclusion of the zero sequence component. This is the case irrespective of whether the reactors are connected in delta or in wye. Hence, for each component model presented below, the HSS model is written in the positive, negative and zero sequence components.

4.6.1 Thyristor Switches PNZ model

The switching function ($S(t)$) for thyristor pair with fixed switching instants for single phase circuit in 3.38 is extended to three phase and is transformed to symmetrical components. Appendix B presents the details for extending a single phase FTM to a three phase FTM in symmetrical components and is succinctly presented here as:

$$\boldsymbol{V}_{reactor,PNZ} = \boldsymbol{S}_{PNZ}\boldsymbol{V}_{TCR,PNZ} \tag{4.29}$$

4.6.2 RLC Circuits PNZ model

The state-space equations for passive circuits containing resistors, inductors and capacitors (RLC) are obtained from the differential equations using circuit laws. These

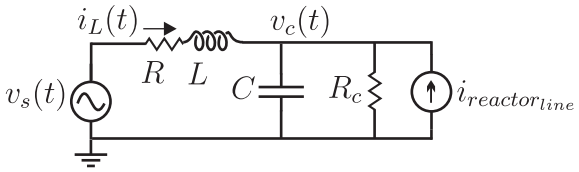

Figure 4.8: TCR supply side impedance circuit

equations are systematically extended to the HSS using the procedure described in Section 4.3.

Reactor Circuit The reactor circuit is modelled as a large reactance in series with a small resistance. For the three phases, there is no significant coupling between the phases hence the phase circuits are modeled independently. With the reactor currents as the state variables, the dynamic equations in symmetrical components are identical to the dynamic equations in phase components.

$$\frac{di_{reactor}(t)}{dt} = \frac{-R}{L} i_{reactor}(t) + \frac{1}{L} v_{reactor}(t) \tag{4.30}$$

For the measurement equations, both line and phase currents for the delta connected reactor circuits are written as outputs. Phase currents are just the reactor current state variables, resulting in an identity $\boldsymbol{C}$ matrix. The expressions for the line currents as a function of the state variables are as follows:

$$i_{reactor_{line}p}(t) = -\sqrt{3} e^{j\frac{-\pi}{6}} i_{reactor_{ph}p}(t) \tag{4.31a}$$

$$i_{reactor_{line}n}(t) = -\sqrt{3} e^{j\frac{\pi}{6}} i_{reactor_{ph}n}(t) \tag{4.31b}$$

Zero sequence current is trapped within the delta such that no zero sequence flows through the line.

Supply side Circuit The AC system at the supply consists of the Thevenin impedance at the substation busbar. The FACTS controller transformer may be modeled separately or incorporated into the series impedance. At the bus where the TCR is connected, a fixed capacitor with small resistive admittance is connected for reactive power supply. For the supply side impedance circuit, the per phase effective circuit showing the passive components is shown in Fig. 4.8

With the inductor current and the capacitor voltage as state variables, the set of dynamic equations is

$$\begin{bmatrix} \frac{dv_C}{dt} \\ \frac{di_L}{dt} \end{bmatrix} = \begin{bmatrix} \frac{-1}{R_C C} & \frac{1}{C} \\ \frac{-1}{L} & \frac{-R}{L} \end{bmatrix} \begin{bmatrix} v_C \\ i_L \end{bmatrix} + \begin{bmatrix} & \frac{1}{C} \\ \frac{1}{L} & \end{bmatrix} \begin{bmatrix} v_s \\ i_{reactor_{line}} \end{bmatrix} \tag{4.32}$$

For the measurement equations, bus voltage and line currents are taken as outputs. The bus voltage is the equivalent line-to-line capacitor voltage while the line current is equal to the inductor current. The measurement equations in symmetrical components are as follows:

$$\begin{bmatrix} v_{bus_{LL}p} \\ i_{line,p} \end{bmatrix} = \begin{bmatrix} \sqrt{3}e^{j\frac{\pi}{6}} & \\ & 1 \end{bmatrix} \begin{bmatrix} v_{C_{ph}p} \\ i_{L,p} \end{bmatrix} \tag{4.33a}$$

$$\begin{bmatrix} v_{bus_{LL}n} \\ i_{line,n} \end{bmatrix} = \begin{bmatrix} \sqrt{3}e^{j\frac{-\pi}{6}} & \\ & 1 \end{bmatrix} \begin{bmatrix} v_{C_{ph},n} \\ i_{L,n} \end{bmatrix} \tag{4.33b}$$

Zero sequence component of bus voltage is zero. Likewise, without any path from the voltage source neutral to ground, there is no zero sequence component in the line current.

4.6.3 Impulse Train PNZ model

The effect of Switching Instant Variation (SIV) is incorporated into the model by adding modulated impulses to the reactor voltage. The principle for a single phase model is presented in Section 4.4.2 which is extended here for a three phase model. The current through the reactor is sampled to detect the effect of SIV. For delta-connected TCR which traps zero sequence components within the delta, most other models leave out zero sequence components. However it should not be done in this model because of the significance of this variable. Firstly, because the reactor current is a state-variable whose accuracy is paramount to an HSS model. Secondly, the reactor current is used to modulate the voltage impulses to compensate the effect of switching instants in the thyristor.

The FTM for the modulated impulse in a single phase model is presented in 4.24. This FTM is extended to three phases and transformed to sequence components. Procedure and standard equations are described in Appendix B.

4.6.4 Base Case Model

In a linearised model, any system operating condition can be modeled as a small-signal variation about a base case operation. A critical concern is identifying a suitable base case. In this TCR, base case operation is chosen where a balanced three phase purely fundamental frequency voltage is applied at the substation supply side. Even with this choice, the bus voltages at the thyristor connection generally contain harmonic frequencies. Hence if one of our objectives is to control this bus voltage, the base case model shall likewise include such harmonic components.

$$Vbus = Vbus_{base} + \Delta Vbus \tag{4.34}$$

Table 4.1: Impedances used for the Test System

Components	Values
System Impedance	3.1mΩ and 0.1mH in series
Reactor (delta connected, per phase)	38.5mH with 0.1Ω series resistance
Shunt Capacitor (bus-to-ground, per phase)	500 uF with 10kΩ shunt resistor

where $Vbus_{base}$ may include harmonics and unbalance.

An operating point is defined by the supply voltage, v_s, (see Fig. 4.7) a controlled switch-on instant, α_0, synchronised with the supply voltage and a known switch-off instant, β_0. The switch-on, α_0, is fixed by the controller and in this case is measured from the peak of the fundamental frequency component of the supply voltage. However because of the switching behaviour of the thyristor, the switch-off instant, β cannot be easily predicted. Firstly, because of voltage distortion at the bus voltage where the TCR is connected which is due to the distorted current flowing through the supply impedance. Secondly because of the small resistance in the reactor model, the current drawn by the reactor is not exactly equal to the integral of the voltage. In this research, the switch-off, β_0 was arrived at using a Newton-Raphson type iterative technique. The objective function is that the phase current has to be zero during non-conduction, while the gradient describes the change in phase current with a change in switch-off angle (β). As an alternative, base case operating point can be obtained by performing a purely time-domain, EMTDC-type simulation.

With v_s, α_0 and β_0 defined in the system, the base case bus voltage, $Vbus_{base}$, together with the base case line current, $Iline_{base}$ is computed.

4.6.5 Small-signal model

As a small-signal model, the HSS model is expected to accurately describe the response of the system to a small-signal input such as voltage source distortion. In the succeeding section, the small-signal response is generated by applying a small-signal distortion as an input to the the model.

4.7 RESULTS AND VALIDATION

To validate the above procedure, a reduced HSS model for a 3-phase TCR was built in MATLAB and the result was compared to a purely time-domain simulation using PSCAD-EMTDC. A test system similar to the circuit shown in 4.7a was used. System parameters are provided in Table 4.1 for an 11kV system. A preliminary analysis was performed to observe the worst harmonic distortion as a function of switch-on angle, hence representative results below were done at $\alpha = 20°$.

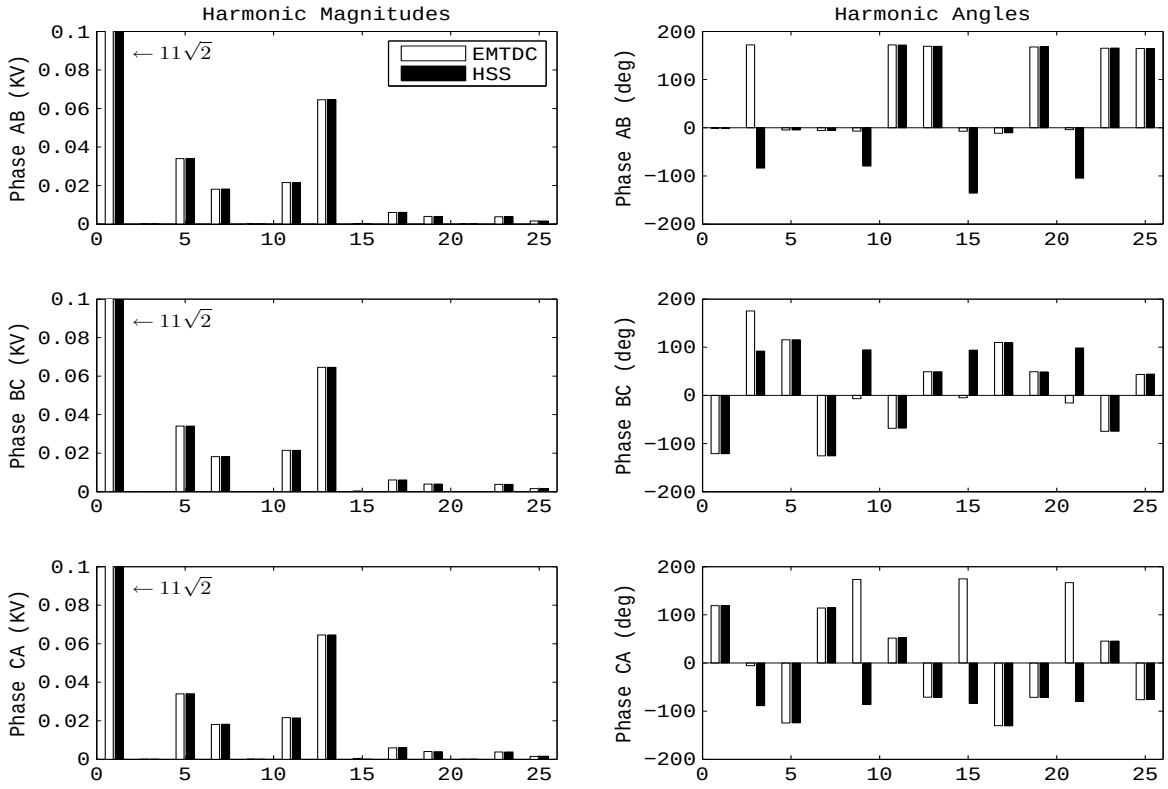

Figure 4.9: Base Case Bus Voltage Harmonic Plots for Phases AB, BC, CA for time-domain(EMTDC) simulation and HSS model.

4.7.1 Base Case Results

For the base case operation, an 11kV positive-sequence was supplied to the TCR system. The thyristor was set to switch-on at $\omega t = 20^\circ$ while an iterative solution as described in Section 4.6.4 was performed to arrive at the correct switch-off instant, which in this case turned out to be 159.472°. If the bus[‡] voltage was free of any distortion and the reactor is ideal without any resistance, a perfectly symmetrical switching (i.e. $\beta_0 = 160^\circ$) would be expected. However with a finite system impedance included in the test system, the bus voltage is slightly distorted compared to the supply, hence the slightly different switch-off instant.

With known switching instants, the reduced HSS model was built using the procedures presented in the preceding sections. Results for the base case steady-state harmonics in the bus line-to-line voltage validated with the EMTDC solution is shown in Fig. 4.9

With a voltage input (V_s) that is purely fundamental frequency, the bus voltage is expected to contain only the characteristic harmonics (i.e. $6n \pm 1, n \in \mathbb{Z}_{\geq 0}$). Figure 4.9 shows that this is precisely the case. This harmonic plot compares the results for both time-domain (in white bars) and the reduced HSS (in black bars). The magnitude plots on the left column shows match between the two methods of analysis. The angle

[‡]For this section on results, the *bus* refers to the connection point between the TCR and the fixed shunt capacitor.

plots on the right column shows a number of seeming discrepancies at the following harmonics: 3^{rd}, 9^{th}, 15^{th}, and 21^{st}. These are all triplen harmonics and since the magnitudes at these harmonics are all nil, any discrepancy in the angle is immaterial.

4.7.2 Supply with Distortion Results

Having established a sound base case, the small-signal result of this HSS model was validated by observing both the bus voltages and the line[††] currents. To analyse the reduced HSS model's small-signal performance on an unbalanced input, a 5% 2^{nd} harmonic distortion was introduced in-phase with the 11kV nominal voltage. The HSS result was generated by applying this signal distortion as input to the small-signal HSS model. On the other hand, the EMTDC result was generated by separately applying two sets of signals to the circuit model. The first set of signal is the base case input described earlier, while the second set of input is the base case input plus the distortion. The small-signal result presented in the succeeding validation plots is the difference between the results in these two ETMDC simulations.

With the described voltage input distortion, the reduced HSS model attempted to model the switching instant variation (SIV) at the thyristor switch-off. Figure 4.10 shows the small-signal steady-state currents through each phase of the delta-connected reactors. As indicated by practically zero currents during every non-conduction, the reduced HSS reasonably captured the switch-off SIV. For the HSS results, Gibbs effect is observed as ringing when the current is chopped to zero. This effect is expected with harmonic truncation. Alves, Pilotto and Watanabe [6] proposed a technique to minimise this effect by replacing the step signal with a suitable ramp function. This technique, however was not attempted in this study. Except for the Gibbs effect, the result of the current study for SIV model agrees with the EMTDC simulation results. No other publication has been found that showed this type of detailed comparison between an HSS model and a time-domain simulation.

Figures 4.11a and 4.11b show the new steady-state harmonics for the bus voltage and the small-signal line currents. Fig. 4.11a was zoomed to emphasise good results even at harmonics beyond the fundamental and the 2^{nd} harmonic distortion. An important observation is that non-characteristic harmonics are now present in the output (i.e. as compared to the base case result, Fig. 4.9). Even if they were not included in the model structure, these harmonics were captured by the reduced model. There are however some harmonics such as the 15th in the bus voltage and the 14th and 16th in the line currents that are present in the EMTDC results but are missing in the HSS results. This discrepancy results due to the fact that the impulse function is a linearised model of SIV.

[††]The *line* refers to the supply line to the TCR including the fixed shunt capacitor.

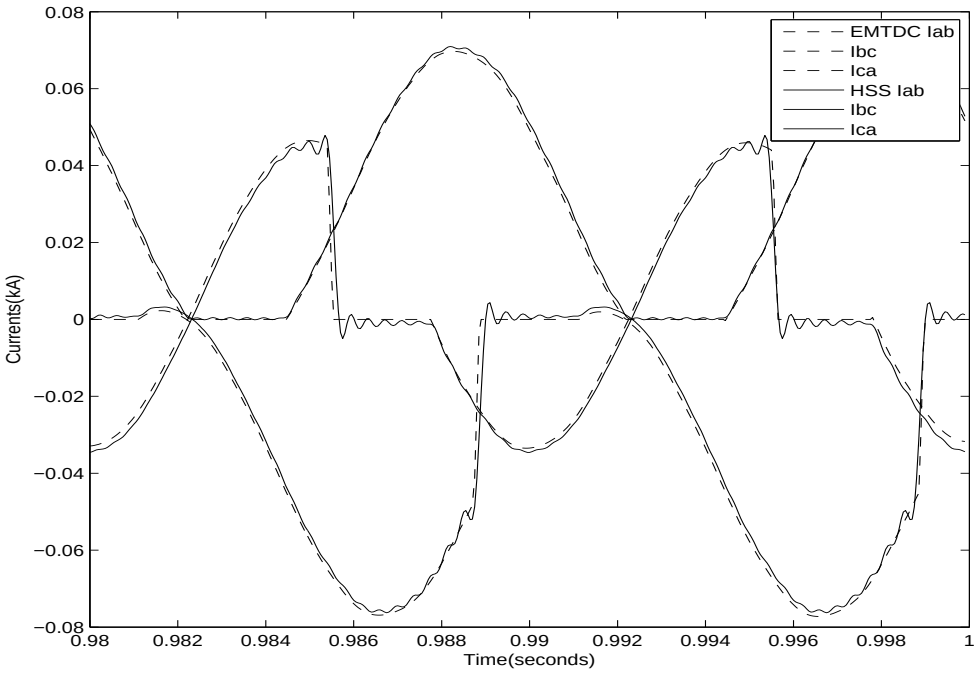

Figure 4.10: Steady-state Reactor Phase Currents Small-signal for time-domain (EMTDC) simulation and HSS model.

The transient response of the HSS model was also analysed. From zero initial condition, the system's transient to steady-state was observed. Since the HSS model naturally produces individual harmonics (while EMTDC produces a true transient of the signal) it is necessary to construct the true transient signal as sum of individual harmonic transients to compare with the EMTDC result. Figures 4.12 and 4.13 are snapshots of the first few cycles of both small-signal bus voltage and small-signal line current for all three phases. In every case, both simulations showed results that were consistent with each other. Previous publications on EHD and DHD would not show this since their emphasis was on harmonic dynamics. However, for this model development, the emphasis is on the actual response of the system to an input change that may cause instability; it is necessary to show that the model properly captures the true transient response.

4.8 CONCLUSION

This chapter presented a reduced HSS model of a three phase TCR. A procedure has been developed to reduce the size of the HSS equations by using the characteristic harmonics of the converter. This was made possible by describing each harmonic as a modulated signal wherein a model with limited number of harmonics can describe

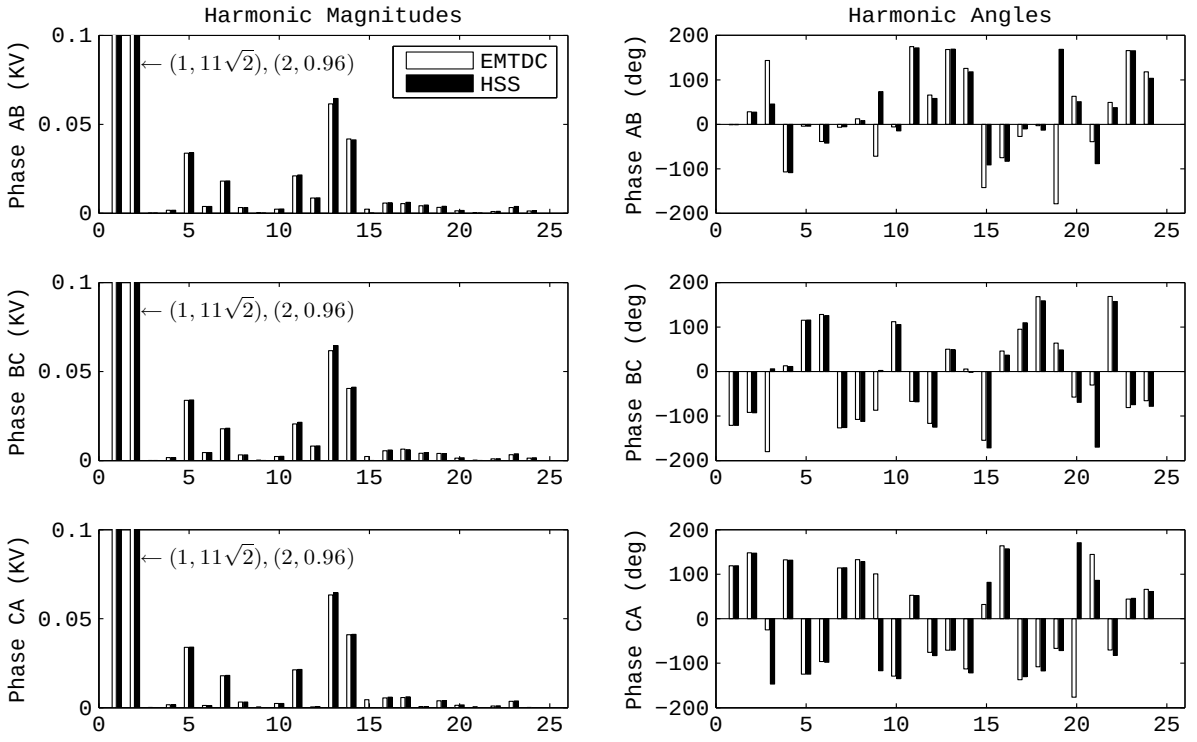

(a) Bus Voltage Harmonic Plots for Phases AB, BC, CA

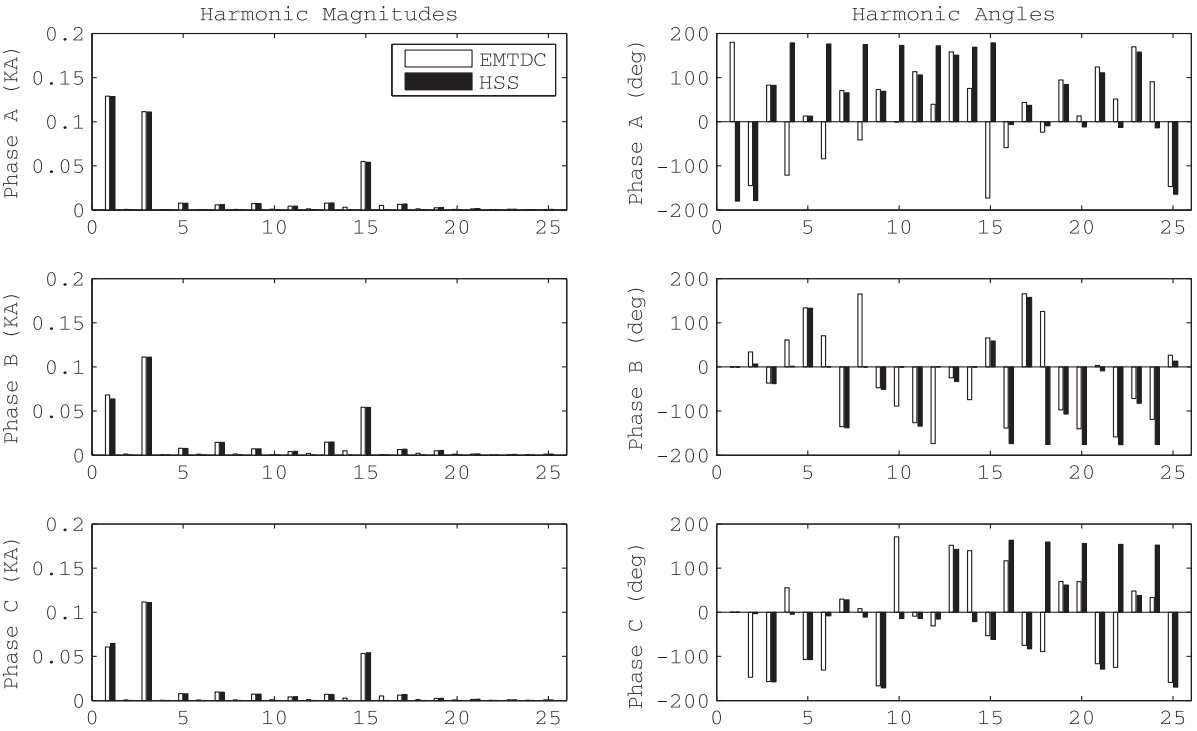

(b) Small-signal Line Current Harmonic Plots for Phases A, B, C

Figure 4.11: Harmonic Plots for Three-Phase Bus Voltage and Line Currents for time-domain (EMTDC) simulation and HSS model

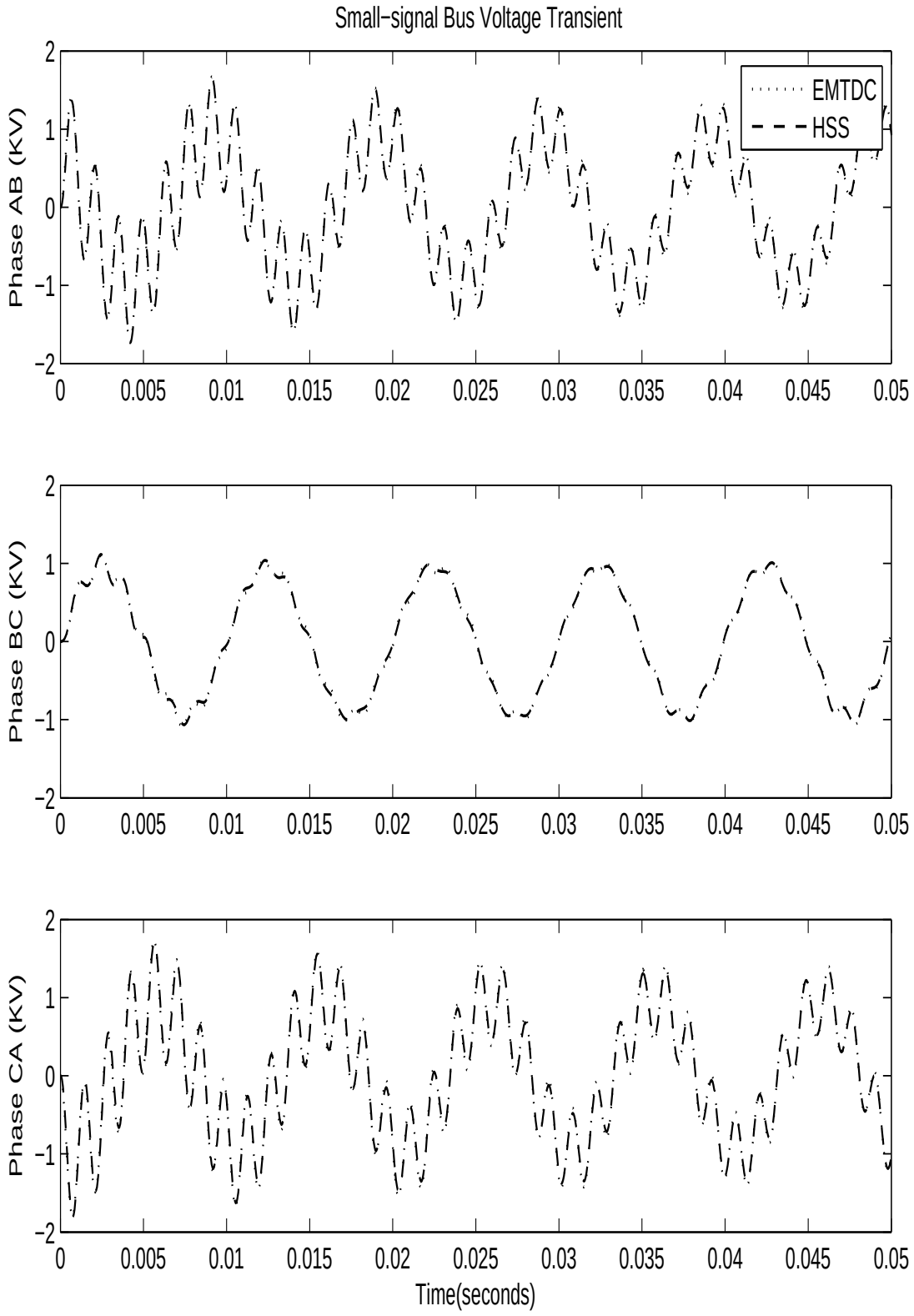

Figure 4.12: Snapshot of Small-signal Bus Voltages during transient for time-domain (EMTDC) simulation and HSS model.

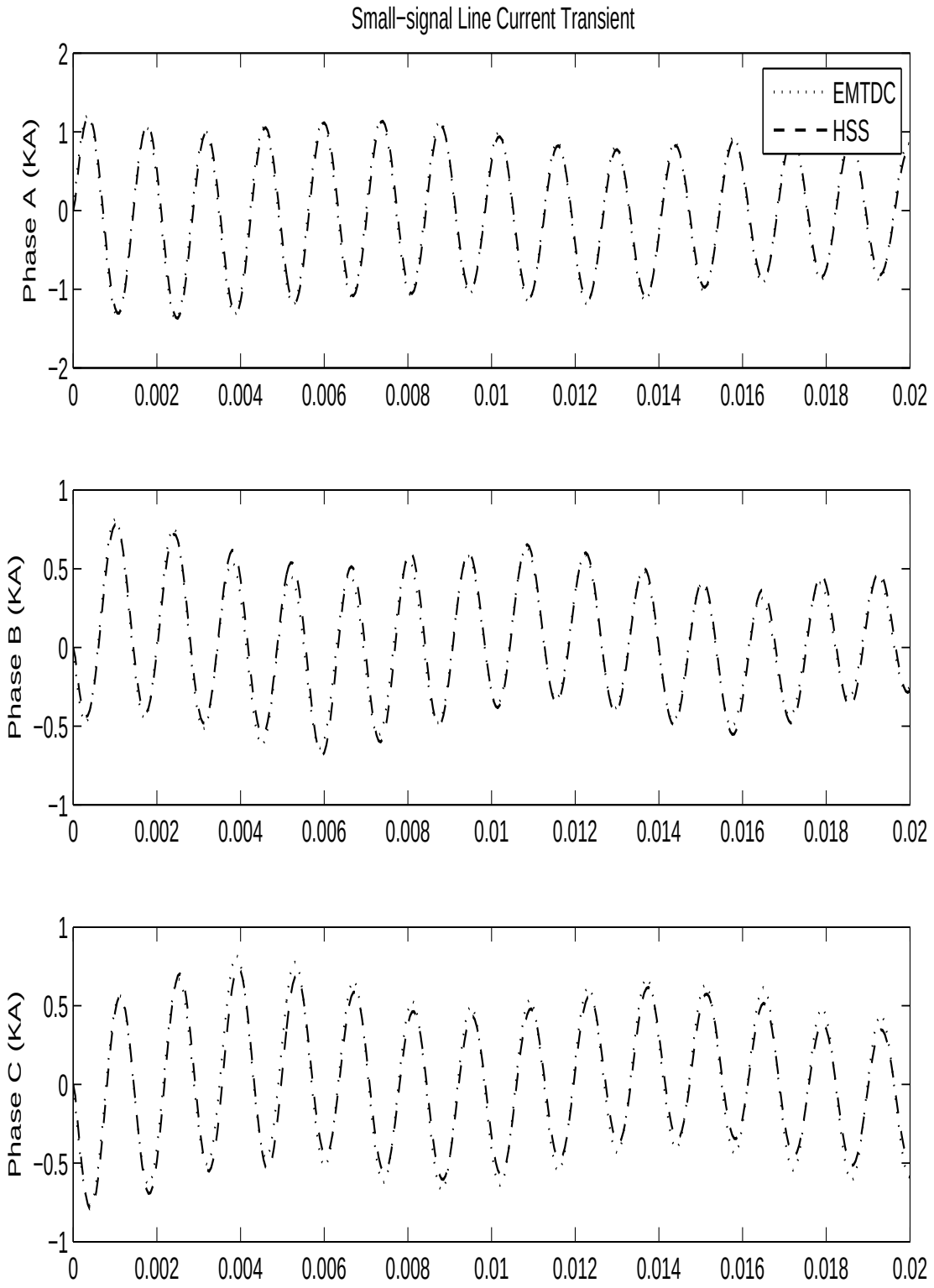

Figure 4.13: Snapshot of Small-signal Line Currents during transient for time-domain (EMTDC) simulation and HSS model.

responses with frequencies that may or may not be in the list. The characteristic harmonics are the minimum list that ensures that the dominant modes of harmonic interaction are still captured by the model.

In building the model, a modular procedure consistent with the principles of LTI system modeling was employed. This accommodated a structured model while working on less complex integro-differential equations. A systematic procedure to extend LTI equations to HSS equations was also presented.

In this model of a FACTS controller, the switching instant variation in the thyristor due to voltage distortion was captured in the model by introducing modulated voltage impulse train.

The result of the HSS model has been validated using a purely time-domain (EMTDC) simulation matching both the steady-state and transients of three phase bus voltages and line currents. In the succeeding chapter, the model for switching instant variation is used to accommodate a voltage control algorithm in the HSS model.

Chapter 5

CONTROLLED TCR HARMONIC STATE SPACE MODEL

Extended Harmonic Domain and Dynamic Harmonic Domain models of FACTS controllers have been presented recently in [58], [48], [69] describing the dynamic transient of individual harmonics. However what is lacking in current literature is the attempt to incorporate controls into these harmonic domain models. Even the most recent publication [69] concluded that control system strategies could be considered for these models but is something that is yet to be done. This chapter addresses that by presenting a Harmonics State Space (HSS) model that includes the TCR model from the previous chapter augmented with the necessary control blocks for a voltage controlled system. The first section briefly describes some characteristics of the TCR in voltage control that are pertinent to describing the models and analysis that follows. Figure 5.1 shows the block diagram of the model that is comparable to an elementary feedback control diagram indicating the major blocks, namely, the controller, the plant, the process, and the sensor. The process block consists of the interaction between the system impedance with fixed capacitor and the reactor connected via the thyristors. This is the scope of the previous chapter where the HSS model is presented in detail. Section 5.2 presents the details of the models for the rest of the components. Section 5.3 describes the model by observing the pole-zero plots, while section 5.4 presents the step response of the model validated with a purely time-domain simulation. The last section illustrates an application of this model for controller design.

5.1 TCR VOLTAGE CONTROL

A TCR is installed in a power system to provide the required reactive power compensation to a specific bus in the system. This achieves a number of related objectives among which are voltage control and improved voltage stability. Figure 5.2a illustrates a schematic representation of bus voltage control in a power system with a TCR. Typical configuration of Static VAR Compensator (SVC) includes shunt capacitor to allow continuous control of bidirectional reactive power within limits.

The voltage-current characteristic of the SVC is shown in Fig. 5.2b. The second quad-

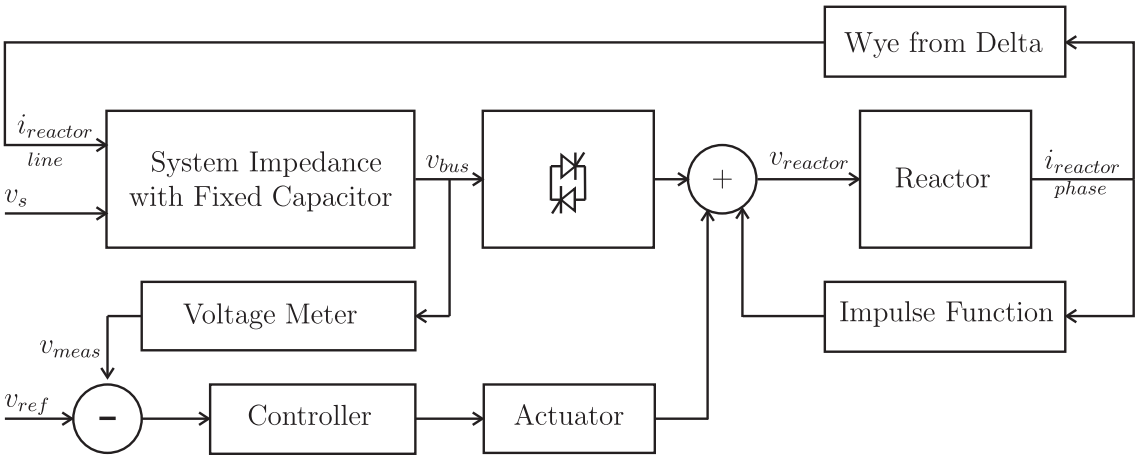

Figure 5.1: Block Diagram of Small-signal Model of Voltage Controlled TCR

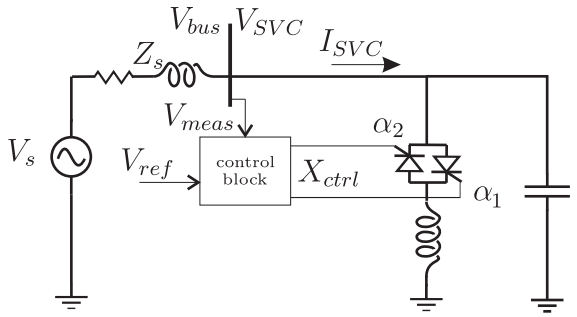

(a) Schematic Diagram

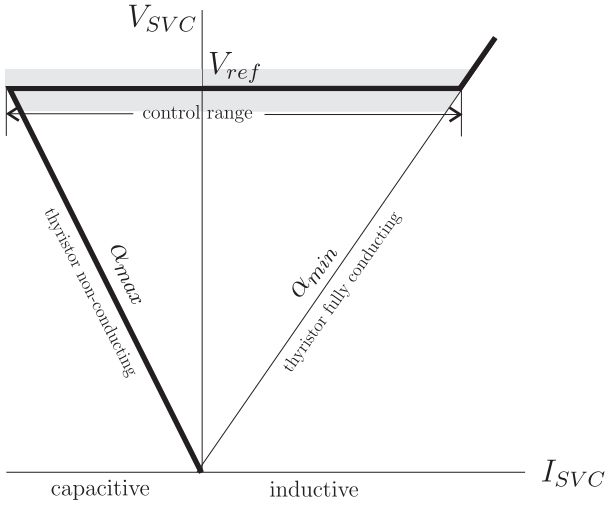

(b) Voltage-Current Characteristic

Figure 5.2: Static VAR Compensator Diagrams

rant limit refers to the condition when the thyristor is non-conducting (switching angle, α is maximum) where the SVC operates as a fixed capacitor. The rest of operating points in the second quadrant indicated as capacitive operation signify that the thyristor is partially-conducting but the resulting reactive power absorbed by the reactor is still less than the reactive power supplied by the capacitor. The first quadrant limit refers to when the thyristor is fully-conducting (α is minimum). Operating points in the first quadrant indicated as inductive signify that net reactive power is absorbed by the TCR.

With voltage control in place, the terminal voltage of the SVC follows V_{ref} for various values of α while within the control range. Hence, an SVC operating point is uniquely defined by the set of parameters, $\{V_{ref}, \alpha, \beta\}$, where β has to be specified since it varies due to SVC voltage distortion. The small-signal TCR model together with the analysis of its dynamics is done about a pre-calculated operating point. It is expected that this SVC configuration with controls is inherently stable. In the succeeding sections, the primary objective is to develop a model that accurately captures this voltage-current characteristic and shows the stable dynamics involved with dynamic control.

In this thesis, a simple voltage control procedure is incorporated such that the terminal voltage of the SVC is flat within the range of allowable current. This basic model is sufficient to illustrate how the controls affect the dynamics of harmonics. Figure 5.2b shows a gray area around the control range which indicates that in SVC installations, the actual shape of the voltage with respect to current can be shaped with proper control procedures. If a step-down transformer is included in this model, then the voltage-current characteristic will have a negative slope governed by the transformer's leakage reactance, X_{trafo}. In more sophisticated voltage regulator designs, a positive voltage-current slope between 1% to 10% (typically around 5%) across the control range is implemented. A positive voltage regulation provides advantages related to SVC sizing, sharing of reactive power across parallel compensators, and excursions about the normal operating point. Details for this are described in [42]. It is also common for the voltage regulator to be designed to operate at a set current I_{set} even with small variations about the reference voltage (e.g. $V_{ref} \in [0.95V_{ref}, 1.05V_{ref}]$. This avoids unnecessary operation during small disturbances and spares the SVC from drifting towards its limits [32]. Again, these advanced voltage-current shapes, although common in TCR installations, are not incorporated in this model.

5.2 COMPONENT MODELS

Based on Fig. 5.1 the SVC model is composed of the process, the controller, the actuator, and the sensor. The process which is composed of the reactor, the power system impedance and the thyristor is completely modelled in detail in Chapter 4. The model development of the remaining components are presented in this section.

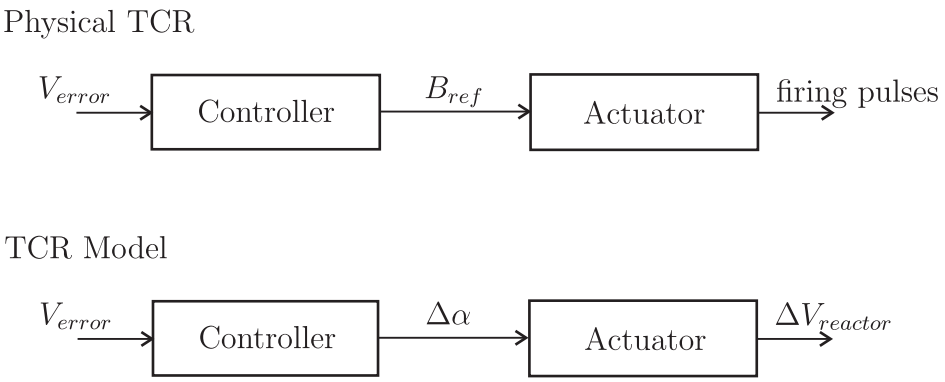

Figure 5.3: Comparing Controller and Actuator between a Physical TCR and a TCR Model

In physical TCR systems, the controller accepts the voltage error signal and produces the corresponding susceptance value which in turn is used by the actuator to generate the firing pulses for the thyristors. In this small-signal TCR model, however, the same voltage error signal is used to produce the switching instant variation (SIV) indicated as $\Delta\alpha$ via the controller before using this to generate the small-signal voltage variation to be introduced to the reactor. These blocks are shown in Fig. 5.3. In physical TCR systems, the first stage in the actuator is a function that calculates the firing angle from the desired susceptance value (i.e. $\alpha = f(B_{ref})$ which is a non-linear function). In this small-signal model, the linear scaling from ΔB to $\Delta\alpha$ can be incorporated into the controller gains; instead of firing pulses, the small-signal actuator model directly produces the effect of SIV which is the small changes to reactor voltage.

5.2.1 Voltage Regulator as Controller Model

The voltage regulator is the controller for this scheme. By operating on the voltage error between the measured voltage and the reference voltage, a control signal is produced based on a desired performance criteria. For the purpose of this model development, it is sufficient to have a controller that accurately corrects a step change in the error signal.

The IEEE provides two basic models for the voltage regulator to be used in SVC models [32]. Both models operate on the voltage error and produce a reference value for the susceptance (B_{ref}) that serves as the control signal for the actuator. The first basic model includes a slope-setting constant and is not employed in this current model. The second basic model as shown in Fig. 5.4 includes a non-windup integrator and a proportional gain with a first-order time constant, T_p. As the time constant may be zero, this regulator is equivalent to the familiar Proportional-Integral (PI) controller.

Instead of producing a susceptance value, with units of $\frac{1}{\Omega}$, this voltage regulator is scaled to produce a value for switching instant variation, with units of degrees or

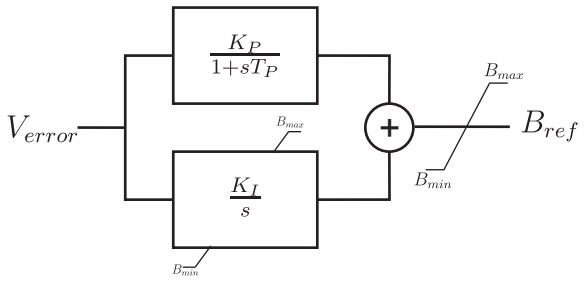

Figure 5.4: IEEE Voltage Regulator model for Basic Model 2

radians. The state-space description of the PI controller is presented in 5.1 with the integrator output as the lone state variable.

$$\begin{aligned} \frac{dx}{dt} &= K_I V_{error}(t) \\ \Delta\alpha(t) &= x(t) + K_P V_{error}(t) \end{aligned} \tag{5.1}$$

where the state-variable $x(t)$ is the integrator output.

5.2.2 Actuator Model

Actuator is a general term for the device that transforms a control signal to another signal that produces a significant effect on the process [22]. To significantly affect the process, the actuator in a physical TCR produces correct firing pulses to initiate thyristor switching. For this small-signal model, there is no direct access to the switching instants, instead the effect of switching instant variation, which is reactor voltage variation, is produced by the actuator.

Impulse Generator as an Actuator

The actuator model consists of a train of impulses at the base case switching instants modulated by the control signal. The principle is that switching instant variation which results in conduction angle variation can be modeled as additional (positive or negative) impulses at the base case switching instants. This occurs during both the switch-on and the switch-off of the thyristors. The impulse strength is modulated by the control signal which in this case is the switching instant variation. There are two approaches to implement this. The first one is by introducing impulses at both the switch-on and switch-off. The first impulse establishes the correct reactor current during the conduction period, and the second impulse returns the current back to zero at the end of the conduction period. The second approach is by introducing a modulated impulse during switch-on only while the end-of-conduction correction is left to be captured by the SIV model on the reactor side as described in Sec. 4.4.2. Either approach is expected

to perform suitably for a small-signal model, but the former was implemented in this model. Aside from the apparent time delay between this pair of impulses, there is also an overall delay associated with the actuator and is discussed in the next paragraphs.

Actuator Time Delay

A number of publications such as [30] and [42] describe a time delay associated with thyristor-based controllers, such as the TCR. This delay primarily results from the fact that the firing signal is not continually sampled but is sampled only as often as the thyristor switching. Sampling is only twice per period in single phase TCR, and six times per period in three phase TCR. For example, the effect of a step change in firing angle can be delayed by up to $\frac{T}{2}$ for a single phase and by up to $\frac{T}{6}$ for a three phase. Typically, a value midway this range has been used and is generalised as $\frac{T}{2p}$ where p is the number of pulses in the controller.

Introducing a time delay to an LTI model is inherently complicated. However, a rational function approximation of which Padé approximation is most commonly used, suits most models. Vajta [68] made observations that Padé approximation whose numerator polynomial is one degree less than the denominator polynomial provides an excellent approximation that avoids the unwanted jump at the origin that is exhibited by rational functions that have the same degree in the numerator and the denominator. A second order rational approximation is shown in 5.2

$$e^{-sT_d} \approx \frac{6 - 2sT_d}{6 + 4sT_d + (sT_d)^2} \tag{5.2}$$

where T_d is the time delay in seconds.

In this model, a delay block implemented as in 5.2 is incorporated into the actuator model. Resulting from rational function approximation of this delay, a Right-Hand-Plane (RHP) zero is introduced at $s = \frac{3}{T_d}$ making it a non-minimum-phase system.

5.2.3 Measurement Block

In a voltage-controlled TCR, the sensor block is a three phase voltage meter that converts a three phase signal to a single continuous signal suitable for active control. The true RMS of a three phase signal is the aggregate RMS described in 5.3.

$$V_{RMS} = \frac{\sqrt{V_A^2 + V_B^2 + V_C^2}}{\sqrt{3}} \tag{5.3}$$

However, the requirement for this model development is a linearised model where the input to the measurement block is a set of three voltage signals which is fundamental

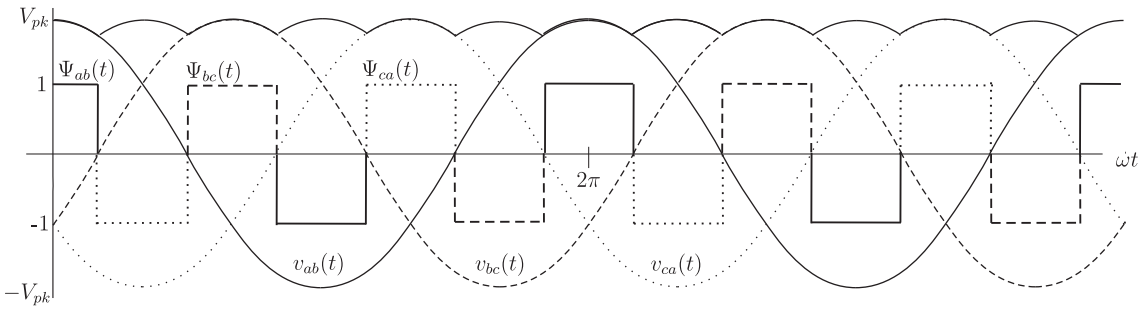

Figure 5.5: Switching Function for a three phase Voltage RMS Meter

frequency with some distortion, and the output is expected to be a time-varying DC signal which is referred to here as the effective value of the bus voltage.

The PSCAD/EMTDC model for meter as described in its documentation refers to it as a root-mean-square (RMS) meter:

$$V_{RMS} = \frac{\pi}{3\sqrt{2}} \left(max(V_A, V_B, V_C) - min(V_A, V_B, V_C) \right) \tag{5.4}$$

It can be observed that the output is an approximation of the true RMS value and may contain error especially for highly distorted voltage signals. In spite of this, as the intention in this model development is to validate the control model in HSS with a time-domain simulation using PSCAD/EMTDC, it is still sensible to build a measurement block model that matches the latter's measurement procedure. This function is equivalent to a rectifier which can be implemented as a linearised switching function with respect to the input voltages. The model presented here is comprised of two stages: the first involves the description for harmonic coupling from input set of signals to the measured signal; the second involves the filtering of higher harmonics out of the measurement.

Sequence Components to Measured Value

To capture the harmonic coupling from the measured signal to a predominantly DC output, a rectifier model is employed. This rectifier transforms a set of three fundamental frequency voltages to a DC signal. The rectifier, however has frequency coupling characteristics that couples harmonics.

Figure 5.5 shows the switching function, $\Psi(t)$ employed in this model and is described mathematically in 5.5.

$$\Psi_{LL,\psi}(t) = \sum_{n \in \mathbb{Z}_{odd}} \frac{-2j}{n\pi} \cos\left(n\frac{\pi}{6}\right) e^{j(n\omega t - n\frac{\pi}{2} - \psi)} \tag{5.5}$$

where $\psi = 0, \frac{2\pi}{3}$ and $\frac{-2\pi}{3}$ for the three phases and in-phase with the peak of the base case line-line bus voltage (V_{bus}) to be measured.

The resulting time-varying signal from the time-domain product of the switching function and the signals being measured is indicated in Fig. 5.5 as $V_{RMS}(t)$ and is characterised by a large DC value and $6n$ harmonics. The FTM from sequence components (PNZ) to the measured value is developed by taking the Toeplitz transform of the necessary coefficients as described in 5.6.

$$\mathbf{\Lambda}_{meas,P} = \mathcal{T}\{S_{6n-1}, S_{-6n-1}\}_{n\in\mathbb{Z}_{\geq 0}} \tag{5.6a}$$

$$\mathbf{\Lambda}_{meas,N} = \mathbf{\Lambda}^*_{meas,P} \tag{5.6b}$$

$$\mathbf{\Lambda}_{meas,Z} = \mathcal{T}\{S_{6n+3}, S_{-6n+3}\}_{n\in\mathbb{Z}_{\geq 0}} \tag{5.6c}$$

where $(\cdot)^*$ indicates conjugate transpose of a matrix.

With the base case signal primarily a fundamental frequency signal, the most important transfer is from the fundamental frequency to DC. From the switching function presented in 5.5, the transfer from a fundamental frequency voltage, $V^1_{bus,pk}$ to DC is described in 5.7.

$$\begin{aligned} V^{DC}_{meas} &= k\frac{-2j}{\pi}\cos\left(\frac{\pi}{3}\right)e^{j(\omega t-\psi)}V^1_{bus,pk} \\ |V^{DC}_{meas}| &= k\frac{1}{\pi}|V^1_{bus,pk}| \end{aligned} \tag{5.7}$$

where k is a scaling factor which is computed for the case where a balanced sinusoidal signal of amplitude V_{pk} will result to an RMS value of $\frac{V_{pk}}{\sqrt{2}}$:

$$k = \frac{\pi}{\sqrt{2}} \tag{5.8}$$

If the voltages to be measured include any distortion, the switching instants of the switching function are expected to vary with the distortion. Various cases are analysed to model if such SIV has to be included in the small-signal model. Figure 5.6 shows the effect of voltage distortion on the resulting trajectories and the switching instants.

Cases I and II show the resulting larger value (i.e. $max(t)$) between a pair of intersecting voltage signals, while Cases III and IV show the resulting lower value (i.e. $min(t)$) between another pair of signals.

For Case I, small voltage distortion is introduced to the v_{ab} while $v_{bc,0}$ remains undistorted. To capture the larger value, $max(t)$ between v_{ab} and $v_{bc,0}$, the switching instant gets delayed from γ_0 to γ_a. However, with a fixed switching instant model (i.e. fixed at γ_0), the trajectory of the maxima is shown in bold lines and has an error equal to the area of the shaded triangle. The area of this triangle is approximated as $\frac{\Delta v_{ab}\Delta\gamma}{2}$, where Δv_{ab} is measured at $\omega t = \gamma_0$. For a linearised model, this area is insignificant and is dropped from the model.

Case II shows the trajectory of the larger value, $max(t)$ when $v_{ab,0}$ is maintained at its

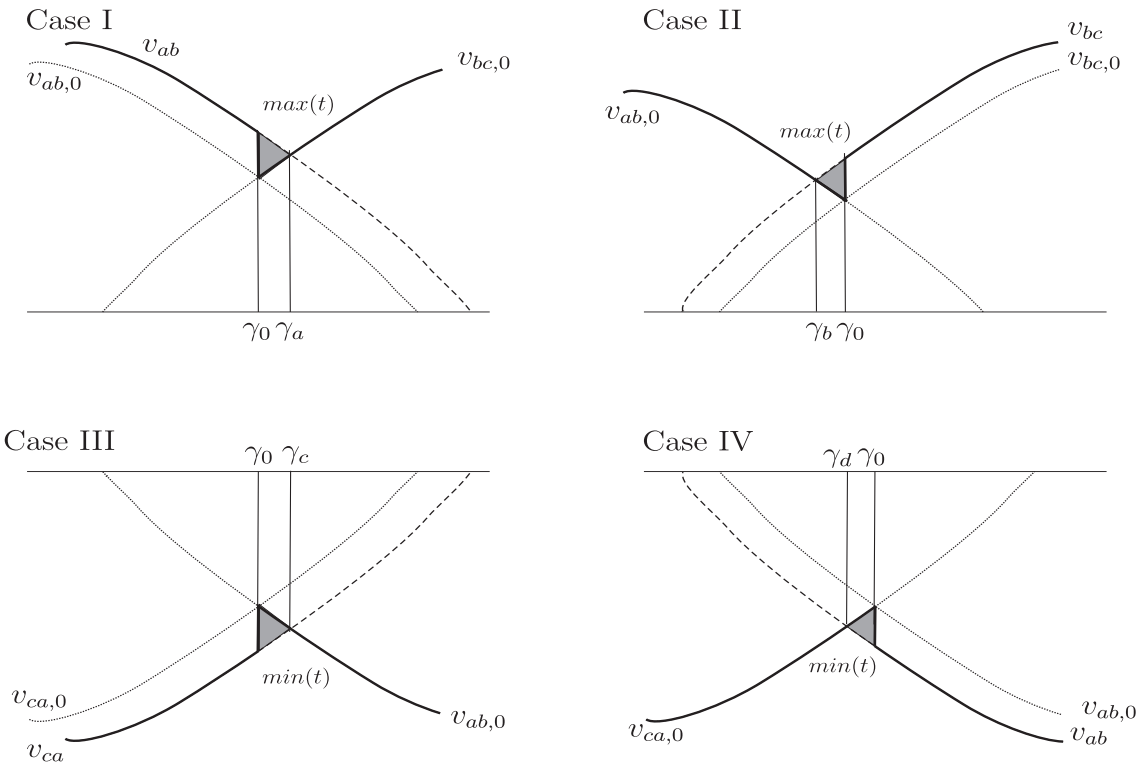

Figure 5.6: Small-signal analysis of Switching instant variation for RMS meter

base case while a small voltage distortion is introduced to v_{bc}. Again for a linearised model with fixed switching instant, the error is very small. Cases III and IV show analogous cases for the trajectories of the lower value, $min(t)$.

First-order lag filter for the Measurement Block

In typical time-domain models such as the one implemented in PSCAD/EMTDC, the analog meter includes a first-order lag filter to eliminate the higher harmonics from the meter output. In the frequency domain, this results in magnitude attenuation and phase lag at higher frequencies. In the time domain, an input step change results in an exponential rise according to the filter time constant. In this HSS model, the switching function based RMS voltage meter only delivers DC signal and suppresses all harmonics. However a lag filter is still included in the model to capture the DC signal's exponential rise. In addition, the pole introduced by the meter's lag filter affects the overall controller performance. The LTI model of a first order lag filter is described as

$$\begin{aligned} T\frac{dx}{dt} &= -x(t) + u(t) \\ y(t) &= x(t) \end{aligned} \tag{5.9}$$

These individual components together with the HSS model of the process described in the previous chapter are connected according to Fig. 5.1 to constitute the small-signal HSS model for the TCR in a voltage control procedure.

5.3 POLE ZERO PLOTS

Introducing the harmonics as additional state variables adds complexity to the high-order model that is not easy to interpret especially as more components are added into the system. It is beneficial at this stage to draw insights into the characteristic of the HSS model by observing the poles and zeros of the model. The set of poles as the eigenvalues of the state matrix describes the dynamics of the system. On the other hand, the set of transmission zeros is subject to change with the input-output set. In this case, the closed-loop model shown in Fig. 5.1 is used, where V_{ref} is the input and the measured voltage, V_{bus_meas} is the output.

Figure 5.7a describes the major components of the plant model including the system impedance with fixed capacitance, the reactor circuit and the set of thyristors that connects them. This basic model excludes the effect of switching instant variation and control. The pole-zero plot is shown in Fig. 5.7b for the case where only fundamental frequency is included in the model, which is equivalent to a dynamic phasor model. The plot also shows the movement of the poles as the TCR operating point traverses from non-conduction to full conduction.

As this model includes the fundamental frequency, the view available to the observer is referred to the fundamental frequency frame of reference[†]. The pole-pair closer to the imaginary axis corresponds to the reactor (i.e. an RL circuit with large inductor in series with small resistor). In the DC frame of reference, an RL circuit has only one pole at $s = -\frac{R_L}{L}$. However, in the fundamental frequency frame of reference, this is equivalent to a pole-pair, whose real component is still $-\frac{R_L}{L}$ with imaginary components equal to $\pm\omega_0$ in units of rad/s.

The set of pole-pairs farther from the imaginary axis correspond to the RLC circuit of the system impedance - fixed capacitor combination. In the DC frame of reference, a series RL in series with a shunt RC is observed as a pole-pair, whose real component is $\frac{-1}{2CR_C} + \frac{-R_L}{2L}$ with imaginary components equal to the undamped natural frequency ω_n of the LC combination (i.e. $\omega_n = \frac{1}{\sqrt{LC}}$). However, in the fundamental frequency frame of reference, the same system is observed as two pole-pairs with each pair centered at ω_n. The imaginary components are then $\omega_n \pm \omega_0$ and $-\omega_n \pm \omega_0$.

Figure 5.7b also indicates movement of poles as the the firing angle is delayed from thyristor non-conduction to full-conduction. As it proceeds, the system impedance and

[†]Frames of reference is introduced in Sec. 4.3.1

the reactor impedance couples together and the natural frequency at the source side increases with the conduction angle as shown in the trajectory of poles.

When harmonics of the state variables are included into the model new poles will arise which do not signify new eigenvalues in the system. Instead the original eigenvalues are replicated as new poles seen in the new frames of reference. Figure 5.8a shows the new pole-zero plot when odd harmonics up to the 9th ($h = [1, 3, 5, 7, 9]$) are included in the model at a specific thyristor conduction angle. As expected new poles are located at $\pm h\omega_0$ and at $\pm\omega_n \pm h\omega_0$. As the reactor is delta-connected, triple-n harmonics do not behave as the characteristic harmonics. The additional harmonics at this stage do not yet have a significant effect on the dynamics of the model. The dominant poles are still those related to the reactor circuit and not from the RLC circuit which is incorrect since the effect of SIV has not been incorporated into the model.

As presented in Chap. 4 the HSS model for the TCR takes into account the SIV. Figure 5.8b shows that the poles shift when the effects of SIV is incorporated into the model. The reactor poles significantly shifts to the left which effectively removes them from the TCR dynamics. This supports the idea that an accurate SIV model reflects the inherent stability of the TCR system. The inclusion of the SIV in the model makes the RLC poles the dominant poles, which is an accurate representation of the system.

In a voltage controlled circuit, models for a controller and an actuator that affect the thyristor switching instants are included. To close the loop, a voltage meter to measure the three phase bus voltages is connected in the plant, as shown in Fig. 5.1

As described earlier, the measurement block includes a first-order lag filter with a time constant, T of 0.02 seconds which corresponds to the fundamental frequency period. Hence, an unconnected meter introduces a pole located at $s = -\frac{1}{T}$. An unconnected PI controller introduces a pole at $s = 0$ and a zero at $s = -\frac{K_I}{K_P}$ where K_I is the integrator constant and K_P is the proportional constant. Upon connection to the rest of the HSS model, the poles shift as shown in Fig. 5.9a where the pole at the origin shifts to the left which is a more likely representation of the stable TCR system. These control poles have strong interaction with other poles closer to them, which in this case is the pole-pair related to the RLC circuit viewed from the 5^{th} harmonic reference frame.

In typical power systems, the resonant frequency of the system impedance with the shunt capacitor can occur around one of the characteristic harmonics, h_c. In the example used here, the resonant frequency is close to the 5^{th} harmonic (i.e. $h_c = 5$). The poles for this resonant frequency can be observed from the h_c^{th} frame of reference as low frequency poles whose reflected frequency is $\omega_p = \pm\omega_n \mp h_c\omega_0$ which may fall within the controller's bandwidth.

The controller, on the other hand, acts on the fundamental frequency signal. If there is strong coupling between the fundamental frequency and the characteristic frequency, h_c, either through the TCR switching FTM or through the meter FTM, then the

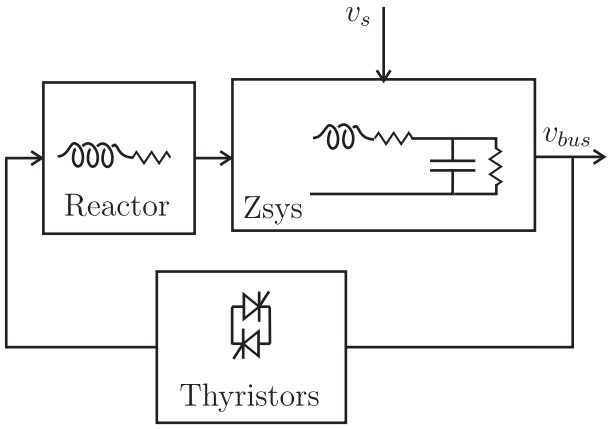

(a) Block Diagram

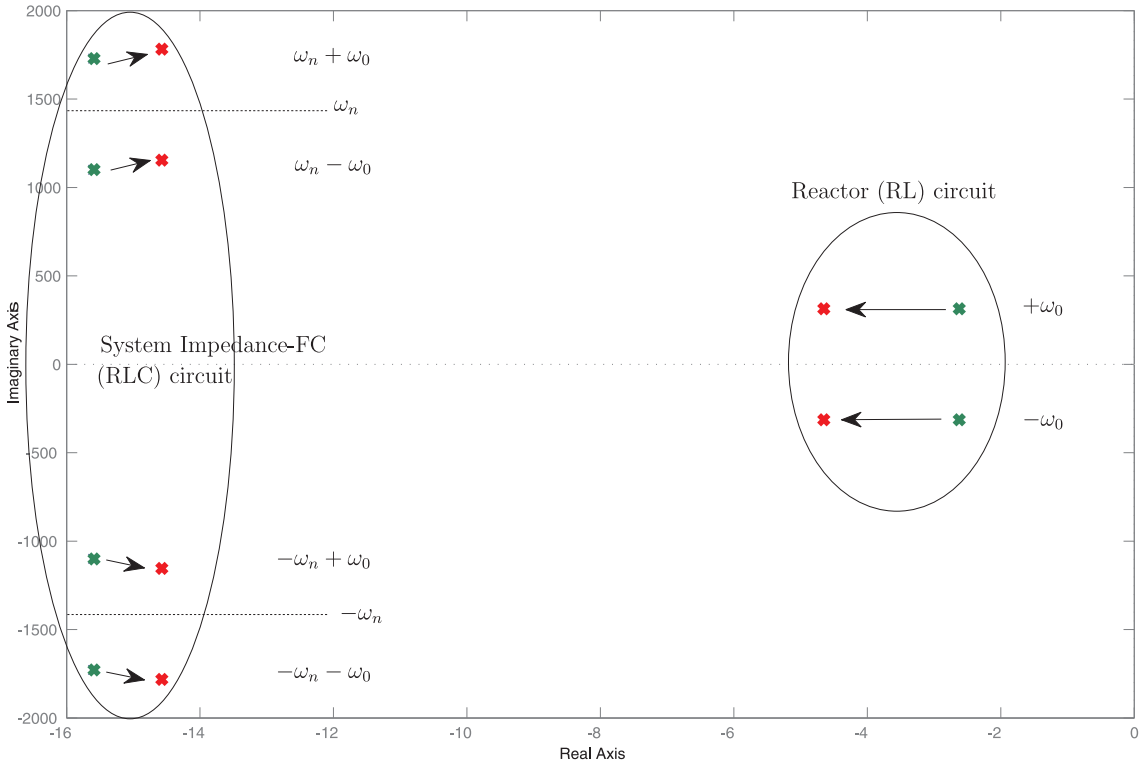

(b) System Poles

Figure 5.7: Process Model Without Correctly Modelling Switching Instant Variation, Fundamental Frequency Frame of Reference Only

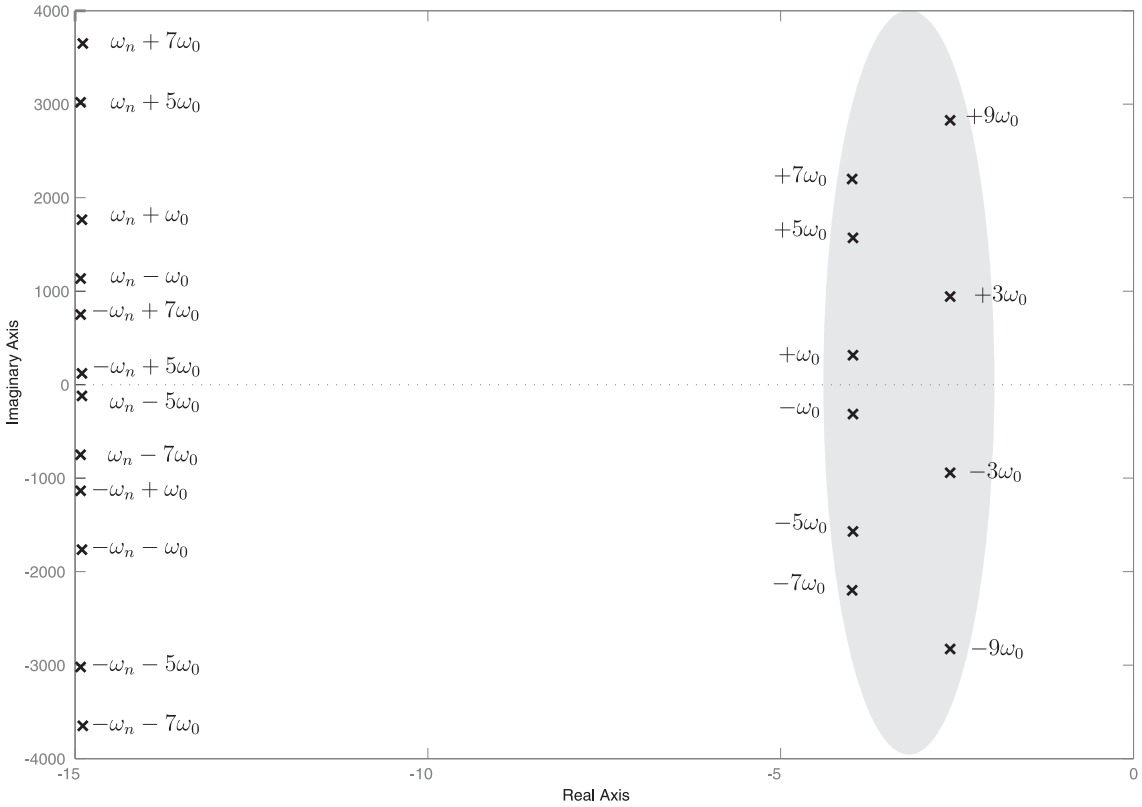

(a) Without SIV effect in the model

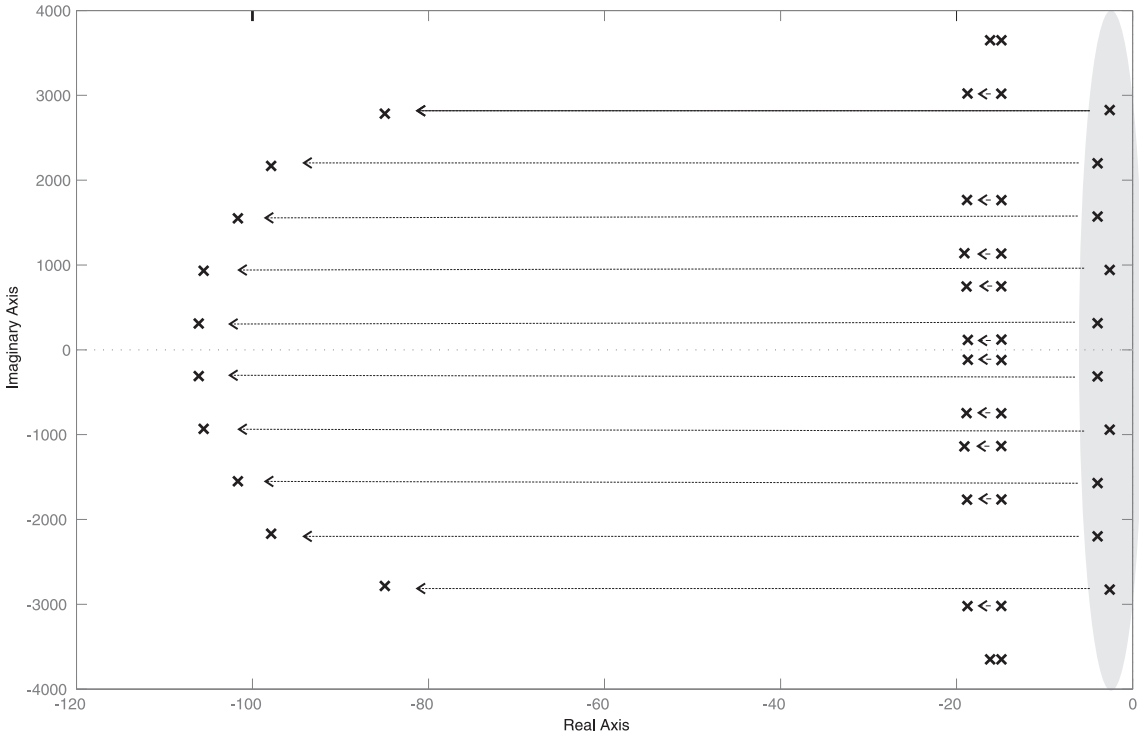

(b) Poles Shift when SIV effect is incorporated into the model

Figure 5.8: Pole Zero Plots for the HSS model of the Process up to the 9th Harmonics

controller gain contributes to the pole's reduced damping. In general, low values of ω_p which are reflections from lower order characteristic harmonics are most likely to be less damped. In this example, since there is strong coupling between the fundamental frequency and the 5^{th} harmonic in the TCR, the low frequency pole-pair at ω_p which are associated with the 5^{th} harmonic turned out to be the least damped poles.

The insight from the ongoing discussion is that the damping of poles close to a particular characteristic harmonic may be affected by the controller gain if there is strong coupling between that characteristic harmonic and the fundamental frequency.

As a final pole-zero plot for model, Fig. 5.10 shows the RHP zero due to the delay, T_d introduced into the model as described in Sec. 5.2.2.

5.4 VALIDATION WITH A STEP RESPONSE

The system's response to a step input provides significant insights into the system's behaviour. Strictly speaking, a step change in input, such as in V_{ref}, rarely happens in the power system. However it is important to observe the system's quick response to such an instantaneous change in the input which makes this highly suitable for validating any proposed model. As related to frequency response, Kuo [37] observed that the step function, due to the jump discontinuity, in principle has a spectrum composed of a wide band of frequencies. Hence a step input can be interpreted as applying various frequency signals. Prior to conducting a small-signal test on the HSS model, a proper base case operating point has to be established. The succeeding subsection will present the procedure to obtain such operating point. Subsequent subsections will show the results of the small-signal analysis.

Base Case Solution

Similar with the procedure for described in Chap. 4 the base case operating point is solved using a Newton-Raphson iterative solution. For a given supply voltage (V_s) and a fixed reference voltage (V_{ref}), the exact switching instants are solved iteratively. Figure 5.11 shows the algorithm with pseudocode describing a procedure to arrive at the base case operating solution. There are two iterative procedures: the first solves for the switch-on angle (α) while the second solves for the switch-off angle (β). The condition for the first procedure is that for a pre-set supply voltage (V_S) and reference voltage (V_{ref}) a correct value of α is obtained. For the second procedure, the condition is that the reactor phase current is zero during non-conduction at a correct value of β. This second procedure is identical to the iterative procedure described in Chap. 4. A more efficient algorithm is to nest the two procedures (i.e. complete iteration to β within every iteration of α). However a simpler algorithm that produces the same result is to cascade these two procedures as indicated in the figure.

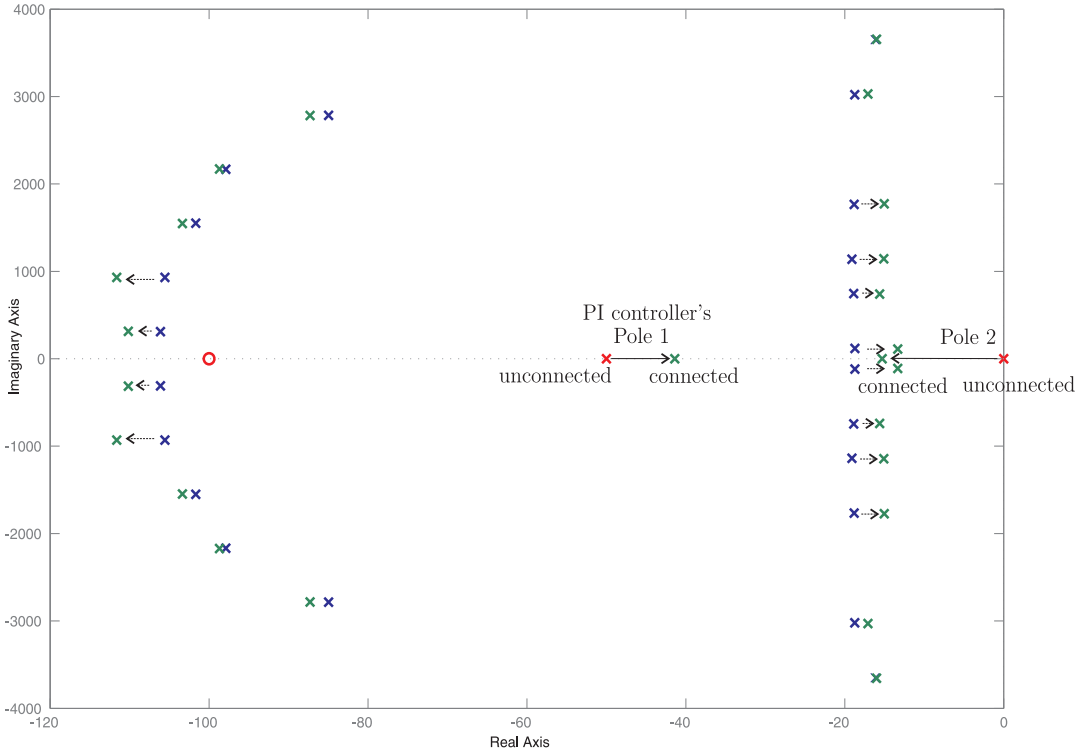

(a) Interaction with Control Poles

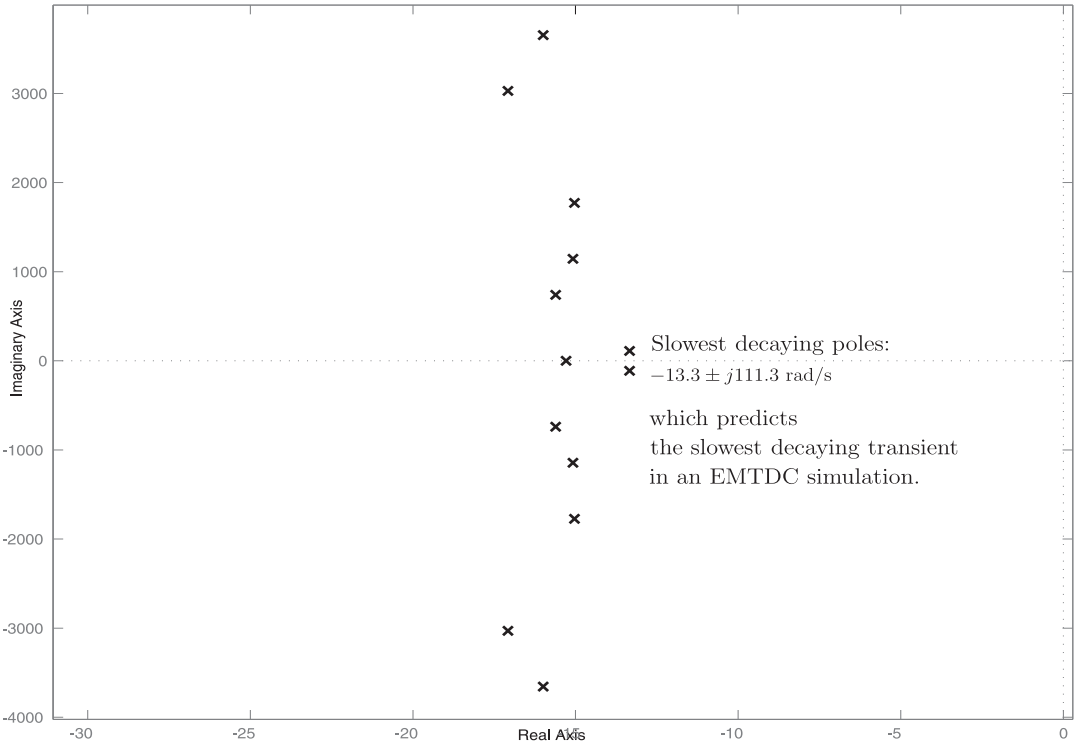

(b) System Poles Highlighting the Dominant Poles

Figure 5.9: Pole Zero plots HSS model of the TCR in Voltage Control up to the 9th Harmonic

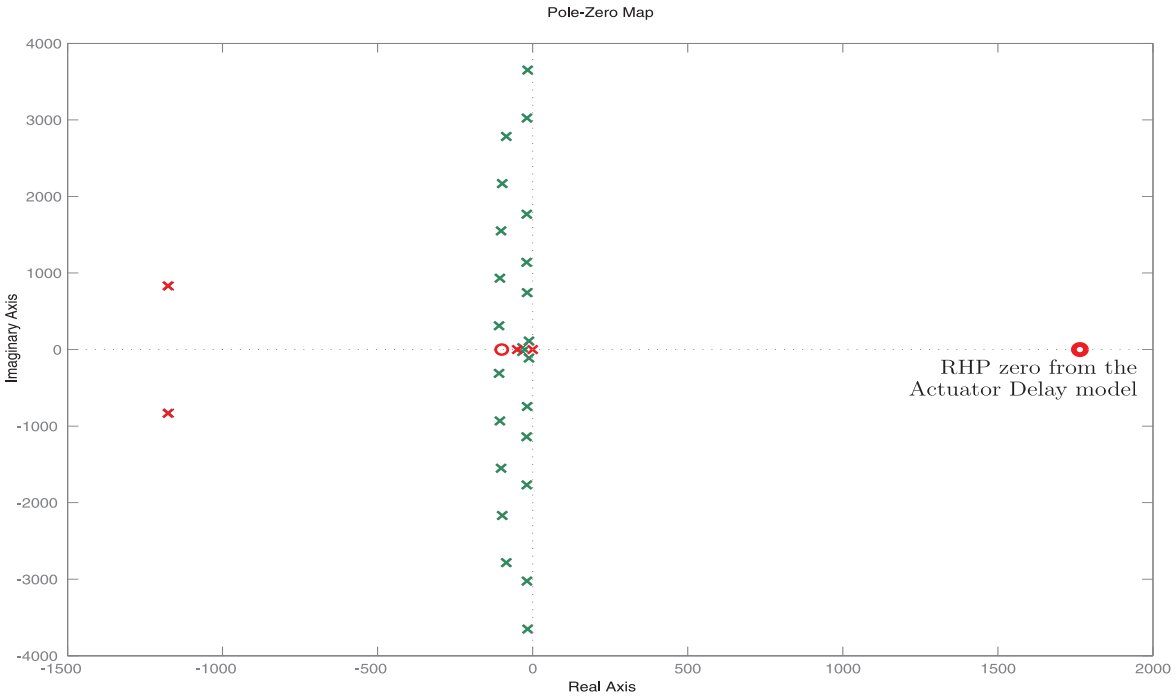

Figure 5.10: Showing the Right-Hand-Plane Zero from the Delay model

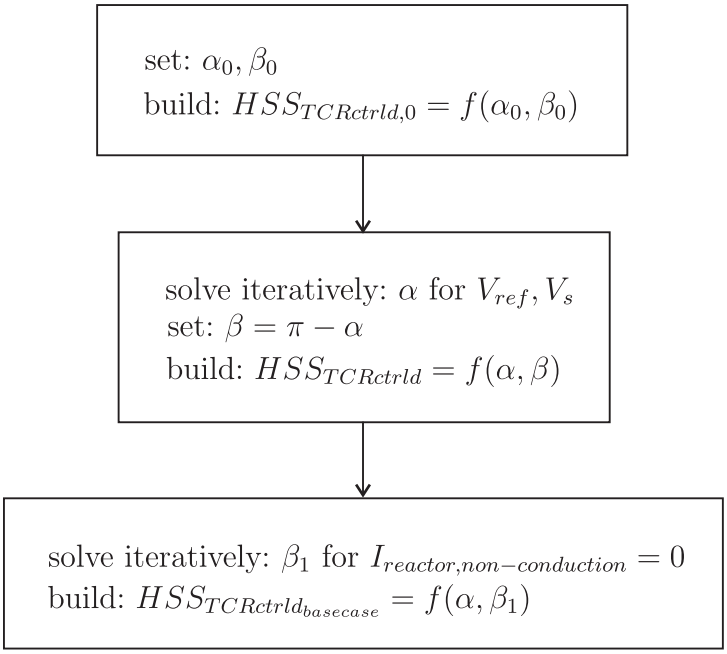

Figure 5.11: Algorithm for solving base case operating point for TCR with Voltage Control

Step Response

To validate the small-signal HSS model of the TCR, the step response is obtained and compared with the results of a purely time-domain solution done in PSCAD/EMTDC.

From Fig. 5.1, the system is analysed for two small-signal inputs, namely V_{ref} and *disturbance* introduced to v_s, and one output, V_{meas}. The step response for a small-signal step change to the reference voltage is shown in Fig. 5.12a. With this input-output pair, the observed actuator time delay confirms the on-minimum-phase characteristic of the system. The transient response of the model agrees with the purely time-domain simulation results. The slowest decaying transient which is consistent in both the time-domain simulation and the HSS model result is estimated to have a period of 0.054 seconds which corresponds to an angular frequency of 116 rad/s. This is consistent with the frequency of the dominant pole which was calculated at 111.3 rad/s. In addition to the prominent dynamics of the response, the time-domain simulation (i.e. EMTDC) shows a persistent 6th harmonic oscillations. This $6n$ harmonics are inherent in the rectifier-based measurement that is implemented in PSCAD/EMTDC. For the HSS model, only the DC value of the measurement block is delivered as output and was used for the control, while all other harmonics are dropped.

Figure 5.12b shows the dynamics of individual harmonics of the bus voltage. This type of output is what is typically produced by all DHD and EHD models. This information is being used to generate dynamic electrical indices, which are time-varying measures of power, voltage and current. For the small-signal bus voltage, the 5^{th} harmonic voltage is the largest, which is even larger than the fundamental frequency. This is expected since the resonant frequency of the system impedance is very close to the 5^{th} harmonic. The 5^{th} harmonic line current is not necessarily large.

For a fundamental frequency step change in the *disturbance*, the measured voltage goes back to the ordered voltage according to the transient response shown in Fig. 5.13a. Again, the HSS model result, particularly the main dynamics agrees with the PSCAD/EMTDC results. This time, the amount of $6n$ harmonics in the EMTDC result is more severe. However, these were not captured by the limited HSS meter model. An improved meter model should be able to capture the $6n$ harmonics. The transient of individual harmonics is shown in Fig. 5.13b.

5.5 APPLICATION

One basic application of this model is in the design of SVC voltage regulator where the eigenvalues (i.e. poles) of the system shifts with varying controller constants which is sometimes referred to as a parametric anlysis [55]. With the proportional constant (K_P) set to $\frac{10^\circ}{kV}$, the integrator constant (K_I) is varied from $\frac{-0.1^\circ}{kV-s}$ to $\frac{6000^\circ}{kV-s}$. It can be observed from Fig. 5.14a that at this value of K_P the poles crossed the imaginary

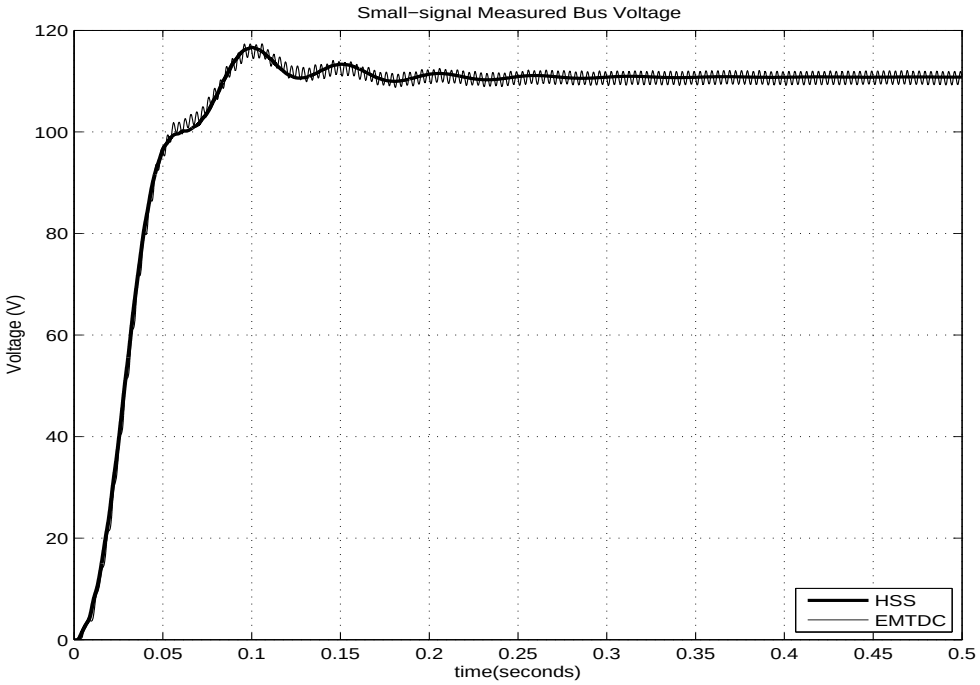

(a) Response to Step V_{ref}

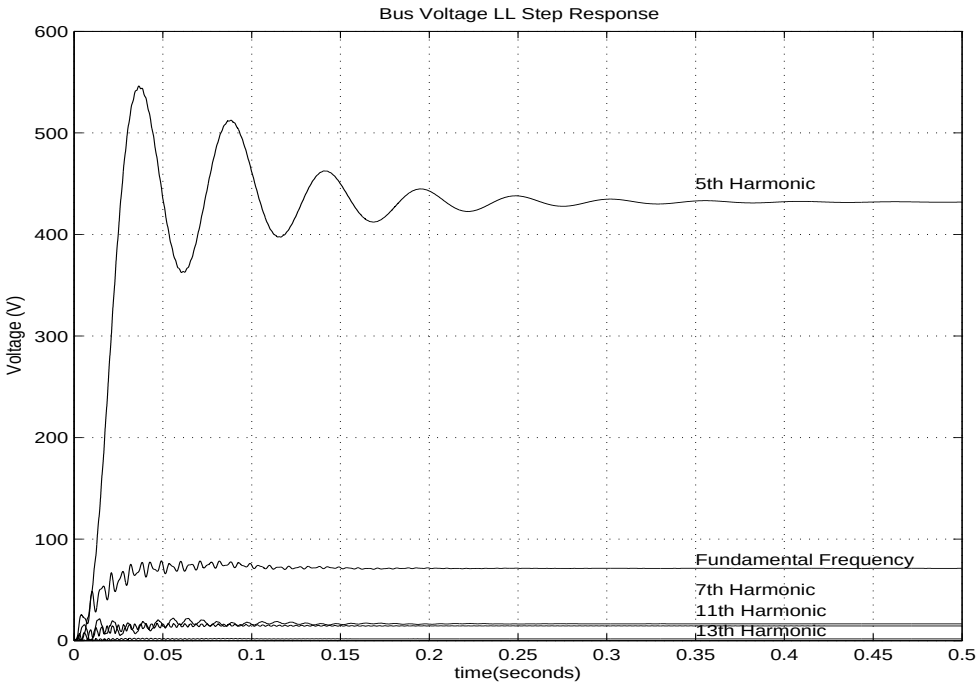

(b) Individual Harmonics

Figure 5.12: Small-signal Response to a Step V_{ref}

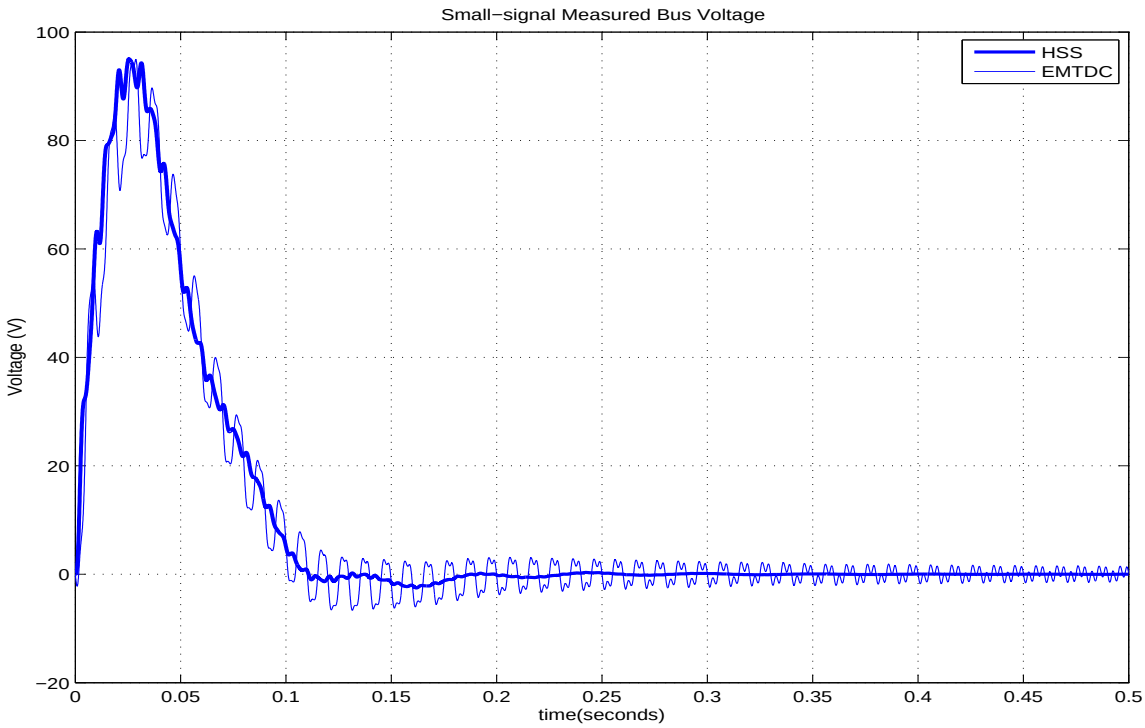

(a) Response Step *disturbance*

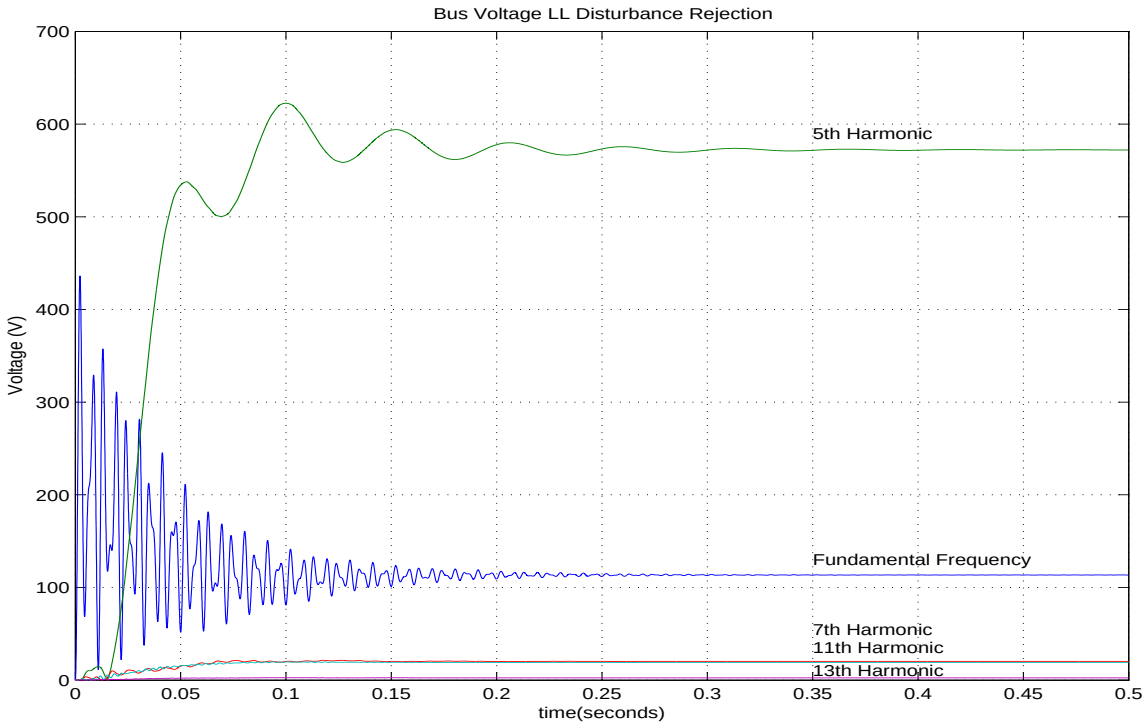

(b) Individual Harmonics

Figure 5.13: Small-signal Response to a Step Disturbance

axis at K_I between 3000 and 4000. These are the dominant poles identified in Sec. 5.3 and is associated to $s_{imag} = \pm|\omega_n - 5\omega_0|$. The system is expected to be stable when $K_I < 4000$.

When $K_I = 1000$, K_P is varied from -30 to 40. It can be observed from Fig. 5.14b that the dominant poles associated with $s_{imag} = \pm|\omega_n - 5\omega_0|$ crossed the imaginary axis at K_P between 30 and 40. On the other hand the poles associated with the controls cross the imaginary axis at K_P between -20 and -30. The system is expected to be stable when $-20 < K_P < 30$.

Typically, these eigenvalue studies are validated using hardware simulation [42]. Even in the absence of any validation, this section illustrates a type of system study that can be performed with this model.

5.6 CONCLUSIONS

This chapter presented a Harmonic State Space (HSS) model of a three phase TCR under voltage control. The development of models for individual components, namely, the controller, the actuator and the sensor have been presented in detail. The resulting model was analysed in terms of pole-zero plots and the step response was validated using a purely time domain simulation in PSCAD/EMTDC.

Based on the pole-zero plots, the inclusion of the switching instant variation (SIV) and the harmonics as additional state variables in the model produced a significant improvement in modelling the dynamics of the model.

An important insight gained from the model in this chapter is that the pole damping can be affected by the controller gain, and the harmonic interaction between the fundamental frequency and the characteristic harmonic closest to natural frequency. Illustrated by a typical power system with a resonant frequency that is close to the 5^{th} harmonic, the 5^{th} harmonic is shown to be very important in analysing the dynamics of the system. In cases where the system resonant frequencies are higher than the 5^{th}, then higher harmonics must be included in the model. In more common cases where the system resonant frequencies are not easily ascertained because of complex harmonic interaction among devices, the HSS formulation provides a general procedure to perform analysis to include the dynamics of harmonics. This was observed when the controller gains were varied to predict the limits prior to stability. Again, the modes related to the resonant frequency and the harmonics in the model, were the first to indicate the possibility of instability.

The purpose of the models developed at this stage is for design and analysis of TCR in a power system, hence the choice of components that were included in the TCR model. It is not yet intended for real-time control or adaptive switching strategies where other components such as delays has to be emphasised and quick calculations would be a

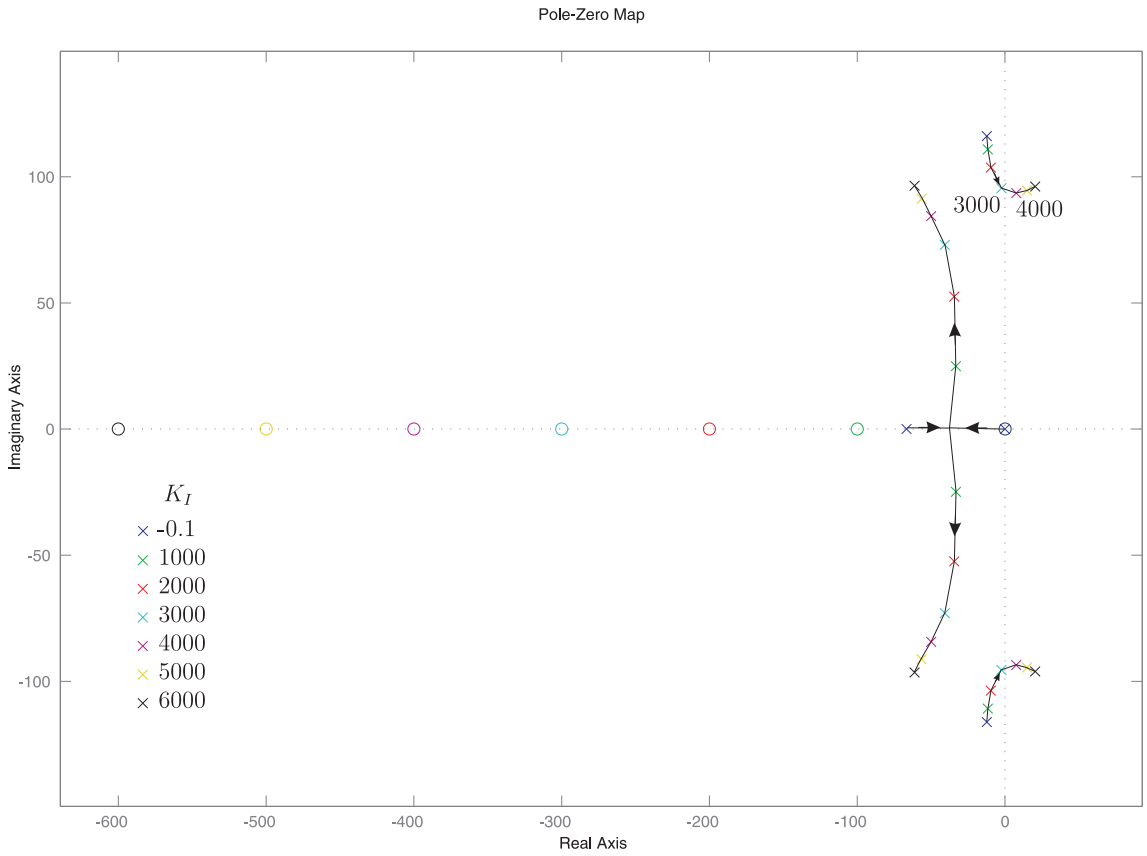

(a) Varying Integral Constant

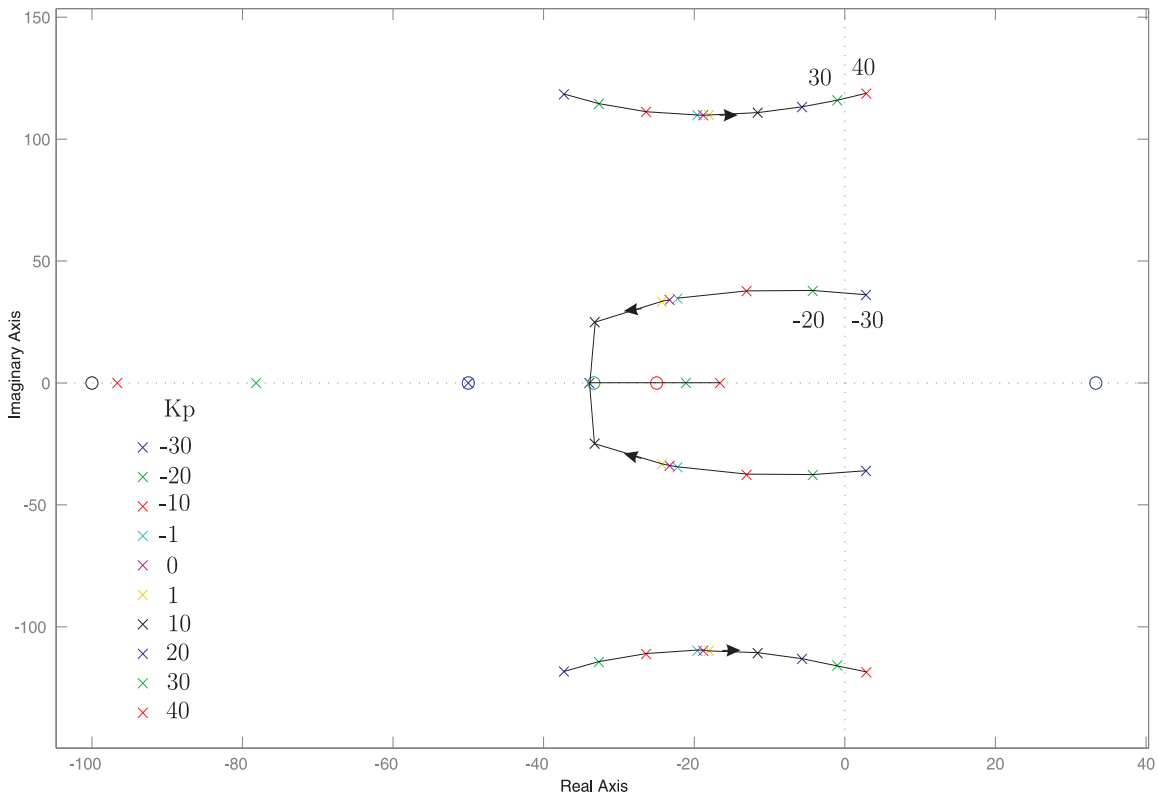

(b) Varying Proportional Constant

Figure 5.14: Voltage Regulator Design

requirement.

The final section of this chapter illustrated an eigenvalue analysis by observing if any RHP pole results from varying the controller gains. This exemplifies a possible contribution of this model to voltage regulator design.

Chapter 6

CONCLUSIONS AND FUTURE WORK

This final chapter summarises the highlights of this thesis and the insights gained in the process of developing the models. It finishes by describing a number of research directions that can be derived from this current work.

6.1 CONCLUSIONS

Harmonic Interactions Presented in this thesis is the development of a Harmonic State Space (HSS) model of a three phase Thyristor Controlled Reactor (TCR). In the process of developing this model, a linearised harmonic domain model was developed which gives insights into the harmonic interactions in a TCR. It also served as a precedent to determine a suitable structure that can accommodate the description for the steady-state and dynamic descriptions of individual harmonics.

Model Reduction With a sound grasp of the harmonic interactions in the TCR, a procedure was proposed to reduce the size of the HSS model. It was demonstrated that the harmonic interactions can be sufficiently described as frequency upshifts and downshifts in multiples of the converter's pulse number. Correspondingly, the harmonic vectors for voltages and currents can be sufficiently described with the coefficients of their characteristic harmonics only. This significant reduction in the size of vectors and matrices in the model facilitates the modelling of power systems with more components.

Model for Switching Instant Variation A procedure was developed to incorporate the nonlinear relationship between voltage distortion and Switching Instant Variation (SIV) into a linearised model. This procedure effectively reduces a Nonlinear Time Variant system to Linear Time Variant model as required by the HSS. Firstly, this was applied to model the effect of TCR voltage distortion on the thyristor switch-off. A voltage impulse is applied at the base case switch-off instant which reduces the TCR's current magnitude to zero when the thyristor is not conducting. Secondly, this is applied to model the effect of incremental change in thyristor conduction angles to

control the TCR bus voltage. A pair of voltage impulses is applied at the base case switch-on and switch-off to represent the effect of changes in thyristor conduction. The strength of the impulses was modulated by the control signal that represents the target change in thyristor firing angles.

Linear State Space Representation The model is in the form of a linear state space system. Eigenvalue analysis, Bode plots, Nyquist analysis and pole-zero plots can all be applied to the system, including the effects of all the TCR frequency coupling. This allows systematic building of models, efficient computation, and powerful system analysis.

System Poles The system poles provided a number of insights into the system dynamic interactions. It was observed that the dynamics of the system is better captured when the effect of SIV is included in the model. Without the voltage impulses to model the SIV, an incorrect set of system poles misrepresents the dominant poles of the system.

In the simple system modelled in this thesis which is comprised of a voltage controlled power system with TCR, it was observed that the pole-pair with least damping was most closely associated with the 5^{th} harmonic. This implies that the dominant mode of the model is significantly affected by the harmonic interactions related to the 5^{th} harmonic and its coupling to the fundamental frequency. For any practical harmonic domain model, it is necessary to truncate up to a reasonably high harmonic number. The dominant poles together with the harmonic number associated to them provide an indicator of the harmonics to be included in the model. Truncation below this will result in an inaccurate dynamic model, while models that include beyond this harmonic do not necessarily result in a significantly better dynamic model.

The use of parametric analysis by observing the system poles while varying the controller gains was shown to illustrate an application of this model for controller design.

Model Validity The linearised harmonic domain model and the HSS models were validated with a purely time-domain simulation in PSCAD/EMTDC. Even with the HSS model for the TCR without the controller, no other publication available has shown this detailed validation where results for both steady-state harmonics and transient signals agree very well in both methods of simulation.

The final HSS model presented is that of a three phase TCR that performs voltage control. The response of the measured voltage to a step change in the reference voltage and a step voltage supply disturbance were presented and validated using PSCAD/EMTDC. The dynamics of the output for both cases agree reasonably well with the purely time-domain simulation. In addition, the dynamics of individual harmonics of the step response were observed and analysed.

The results of this thesis demonstrated that correct HSS model captures the effects of harmonic interactions to the dynamics of the system that includes a TCR. It is reasonable to expect that other FACTS Controllers behave similarly making it very useful to include this type of model in the design of future installations or in the analysis of existing ones.

Finally, the model that has been developed can be applied to analyse harmonic interactions and their effects to the dynamics of a system with two or more power electronic controllers that are electrically close to each other.

6.2 FUTURE WORK

Model Improvements The HSS model for a TCR presented in this thesis demonstrates that the dynamics of the system is affected by the harmonic interactions in the converter. However, if this modelling technique is to be applied to analyse real systems, there are still a number of model improvements that can be investigated.

As previously mentioned, a TCR's voltage regulator introduces a droop to the voltage-current characteristic within the control range. For a full-scale model of TCR for design and analysis, this characteristic has to be included.

Due to the speed of controllers, they are usually affected by oscillations in the range below the fundamental frequency. Hence, most controller designs are limited to only analyse the effects within this range. However the model presented in this thesis opens the possibility to extend analysis beyond this range. This involves extending the measurement block to deliver higher frequency signals aside from the DC signal, and for the controller to be designed to respond to higher frequency error signals.

Alves, Pilotto and Watanabe [6] developed a linearised actuator model by introducing the transient unbalance effect which describes the phenomenon they observed when the TCR shifts from one firing angle to another. It will be worth investigating their actuator model in relation to the one presented in this thesis. In the same paper, they also proposed a technique to introduce a suitable ramp function, replacing a step signal to minimise the Gibbs effect. It will also be worthwhile to investigate the same.

Another component that was not included in this model but may affect the dynamics of the system is the mechanism for synchronizing thyristor switching with the supply side voltage. Any error in synchronisation results to errors or modulation in the thyristor's ordered firing angle. The harmonic interaction between a modulated firing angle and the resulting TCR current was described in the linearised harmonic domain model in Chapter 3. Wood and Osauskas [74] described a linearised PLL model for the synchronisation function. In the HSS model presented in this thesis, the switching angle signal is ideally assumed to be synchronised with the supply voltage and free from any modulation.

State Variable Analysis In using state variable analysis for large power systems, concerns have been raised regarding the possibility of inductors connected in a radial configuration or capacitors in a loop [71]. Although not easily perceptible because of other circuit elements, this happens quite regularly. In both cases, the n^{th} state variable is actually dependent on the other state variables. To circumvent this limitation, alternative procedures have been proposed. The most common is the dependent source model which is described in many network analysis texts, such as [70], where the n^{th} inductor (or capacitor) is replaced with a dependent source. Other techniques are briefly decribed in [71]. These procedures should be seriously considered if the HSS modelling is to be extended to larger power systems. In fact the solution of the HSS model could be implemented using Dommel's technique [19], using specially developed components for inductors and capacitors viewed from different reference frames. While []

A number of documents such as [16] argue that unless the inductor is flux-controlled or the capacitor is charge-controlled, which is the case in the FACTS Controllers that is being modelled here, then the inductor flux (instead of current) and the capacitor charge (instead of voltage) has to be chosen as the state variable. A practical example of this is that if the transformer saturation is to be included in the model where the transformer flux has to be used as a state variable.

Model Extensions The modelling principles presented in this thesis serve as bases to develop HSS models for other FACTS Controllers. The author is personally aware that HSS models for HVDC [51] and STATCOM are currently underway. With the HSS description, harmonic interactions including dynamics are better analysed in power systems with multiple Controllers and HVDC.

Another direct extension of the HSS model is to model interharmonics. In this case, signal vectors are described in terms of coefficients of subintegral multiples of the fundamental frequency and frequency interactions are described as interharmonic upshifts and downshifts. Chavez [18] and Ramirez [56] in separate publications introduced this as Modified Dynamic Harmonic Domain (MDHD), although in both cases there were no reference to controller models.

Appendix A

FREQUENCY TRANSFER MATRIX FOR POSITIVE FREQUENCY-ONLY HARMONIC DOMAIN MODEL

For most of this thesis, harmonic vectors are represented using positive and negative frequency components. This includes the description of special Frequency Transfer Matrices (FTM) in Chapter 3. However, in building the linearised harmonic domain model in the same chapter, all signal vectors and FTMs are represented in positive frequency-only descriptions. This appendix presents the details in describing the signal and developing the FTM for a harmonic domain model whose variables are represented in positive frequency only vector.

Positive Frequency-only Harmonic Vectors A periodic signal $x(t)$ is described as a sum of exponential signal with both positive and negative frequencies which is truncated up to the h^{th} harmonic:

$$x(t) = \sum_{k=-h}^{h} X_k e^{jk\omega_0 t} \tag{A.1}$$

The corresponding description in the harmonic domain is a vector containing the $2h+1$ coefficients:

$$\boldsymbol{X}_{\pm}(\omega) = \begin{bmatrix} X_{-h} & \dots & X_{-2} & X_{-1} & X_{DC} & X_1 & X_2 & \dots & X_h \end{bmatrix}^T \tag{A.2}$$

Using Euler's equation for cosine function, A.3,

$$\cos\theta = \frac{e^{j\theta} + e^{-j\theta}}{2} \tag{A.3}$$

Equation A.1 can be written as:

$$x(t) = \sum_{k=0}^{h} \bar{X}_k \cos\left(k\omega_0 t\right) \tag{A.4}$$

The corresponding description in the harmonic domain is a vector containing the $h+1$

coefficients:

$$\boldsymbol{X}_+(\omega) = \begin{bmatrix} X_{DC} & \bar{X}_1 & \bar{X}_2 & \dots & \bar{X}_h \end{bmatrix}^T$$

where $\bar{X}_k$ is twice X_k in A.1.

Positive Frequency-only FTM Suppose an FTM, $\boldsymbol{\Lambda}$ describes the harmonic transfer from input vector, $\boldsymbol{U}$ to output vector, $\boldsymbol{Y}$:

$$\boldsymbol{Y}_\pm = \boldsymbol{\Lambda}_\pm \boldsymbol{U}_\pm \tag{A.5}$$

$$\boldsymbol{Y}_+ = \boldsymbol{\Lambda}_+ \boldsymbol{U}_+ \tag{A.6}$$

For a model that is truncated up the h^{th} harmonic, $\boldsymbol{\Lambda}_\pm$ is a square matrix with rank $2h+1$ while $\boldsymbol{\Lambda}_+$ is a square matrix with rank $h+1$. The next few paragraphs describe the procedure for building $\boldsymbol{\Lambda}_+$ from $\boldsymbol{\Lambda}_\pm$.

In A.5, the FTM for a harmonic model whose variables are represented in both positive and negative frequencies is as follows:

$$\boldsymbol{\Lambda}_\pm = \mathcal{T}\{\boldsymbol{\Lambda}_l, \boldsymbol{\Lambda}_{-l}\}_{l\in[0,-2h]} \tag{A.7}$$

$$= \begin{bmatrix}
\Lambda_0 & \Lambda_{-1} & \cdots & \Lambda_{-h+1} & \Lambda_{-h} & \Lambda_{-h-1} & \cdots & \Lambda_{-2h+1} & \Lambda_{-2h} \\
\Lambda_1 & \Lambda_0 & \Lambda_{-1} & \cdots & \Lambda_{-h+1} & \Lambda_{-h} & \Lambda_{-h-1} & \cdots & \Lambda_{-2h+1} \\
\vdots & \Lambda_1 & \Lambda_0 & \Lambda_{-1} & \cdots & \Lambda_{-h+1} & \Lambda_{-h} & \Lambda_{-h-1} & \cdots \\
\Lambda_{h-1} & \vdots & \Lambda_1 & \Lambda_0 & \Lambda_{-1} & \cdots & \Lambda_{-h+1} & \Lambda_{-h} & \Lambda_{-h-1} \\
\Lambda_h & \Lambda_{h-1} & \vdots & \Lambda_1 & \Lambda_0 & \Lambda_{-1} & \cdots & \Lambda_{-h+1} & \Lambda_{-h} \\
\Lambda_{h+1} & \Lambda_h & \Lambda_{h-1} & \vdots & \Lambda_1 & \Lambda_0 & \Lambda_{-1} & \cdots & \Lambda_{-h+1} \\
\vdots & \Lambda_{h+1} & \Lambda_h & \Lambda_{h-1} & \vdots & \Lambda_1 & \Lambda_0 & \Lambda_{-1} & \cdots \\
\Lambda_{2h-1} & \vdots & \Lambda_{h+1} & \Lambda_h & \Lambda_{h-1} & \vdots & \Lambda_1 & \Lambda_0 & \Lambda_{-1} \\
\Lambda_{2h} & \Lambda_{2h-1} & \vdots & \Lambda_{h+1} & \Lambda_h & \Lambda_{h-1} & \vdots & \Lambda_1 & \Lambda_0
\end{bmatrix}$$

This FTM can be divided into eight sections as shown in Fig. A.1a. Note that sections a and c overlap at $\boldsymbol{\Lambda}_\pm(h+1, h+1)$.

Using the notation $\boldsymbol{\Lambda}_\pm(m,n)$ to identify each element of this FTM, the range of coordinates, (m,n) for each section is shown in Table A.1

For the positive frequency-only model, the FTM takes the following form:

$$\boldsymbol{\Lambda}_+ = \begin{bmatrix}
\lambda(1,1) & \lambda(1,2) & \cdots & \lambda(1,h) & \lambda(1,h+1) \\
\lambda(2,1) & \lambda(2,2) & \cdots & \lambda(2,h) & \lambda(2,h+1) \\
\vdots & \vdots & \ddots & \vdots & \vdots \\
\lambda(h,1) & \lambda(h,2) & \cdots & \lambda(h,h) & \lambda(h,h+1) \\
\lambda(h+1,1) & \lambda(h+1,2) & \cdots & \lambda(h+1,h) & \lambda(h+1,h+1)
\end{bmatrix}$$

Table A.1: $\mathbf{\Lambda}_{\pm}$ Sections to $\mathbf{\Lambda}_{+}$ Components

$\mathbf{\Lambda}_{\pm}$ Section	Row (m)	Column (n)	Harmonic Coefficients (k)	$\mathbf{\Lambda}_{+}$ Components
a	[h+1,2h+1]	[h+1,2h+1]	[0,h]	I
b	[h+1,2h]	[h+2,2h+1]	[-h,-1]	II
c	[1,h+1]	[1,h+1]	[-h,0]	I
d	[2,h+1]	[1,h]	[1,h]	II
e	[h+2,2h+1]	[1,h]	[2,h+1]	III
f	[h+3,2h+1]	[1,h-1]	[h+2,2h]	IV
g	[1,h]	[h+2,2h+1]	[-(h+1),-2]	III
h	[1,h-1]	[h+3,2h+1]	[-(h+2),-2h]	IV

Wood and Osauskas [74] described that building the positive frequency-only FTM consists of four distinct components, as follows:

(I) bottom-left diagonals including the main diagonal

(II) top-right diagonals

(III) top-left antidiagonals including the main antidiagonal

(IV) bottom-right antidiagonals

The positive frequency-only FTM, Λ_{+}, is built in four steps from elements in various sections of $\Lambda_{\pm}$. This is done by systematically *folding* the eight triangular sections of $\Lambda_{\pm}$ into the four triangular matrix components of Λ_{+}. Firstly $\boldsymbol{I}$ is populated using the elements from sections $\boldsymbol{a}$ and $\boldsymbol{c}$. Secondly, component $\boldsymbol{II}$ is populated using sections $\boldsymbol{b}$ and $\boldsymbol{d}$. Thirdly, component $\boldsymbol{III}$ from sections $\boldsymbol{e}$ and $\boldsymbol{g}$. Finally, component $\boldsymbol{IV}$ from sections $\boldsymbol{f}$ and $\boldsymbol{h}$.

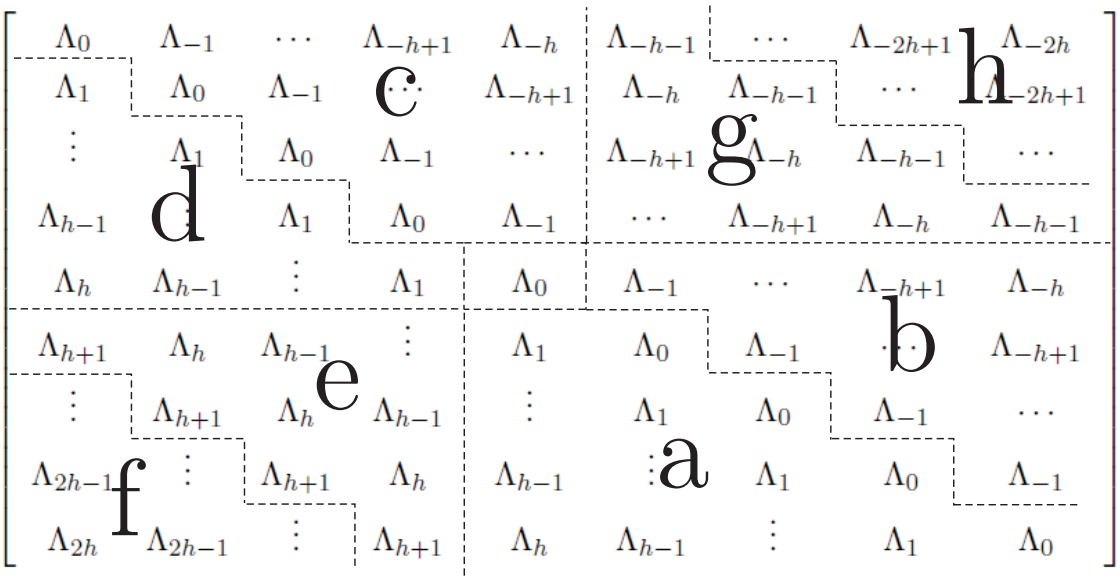

(a) Frequency Transfer Matrix, $\mathbf{\Lambda}_{\pm}$ sections

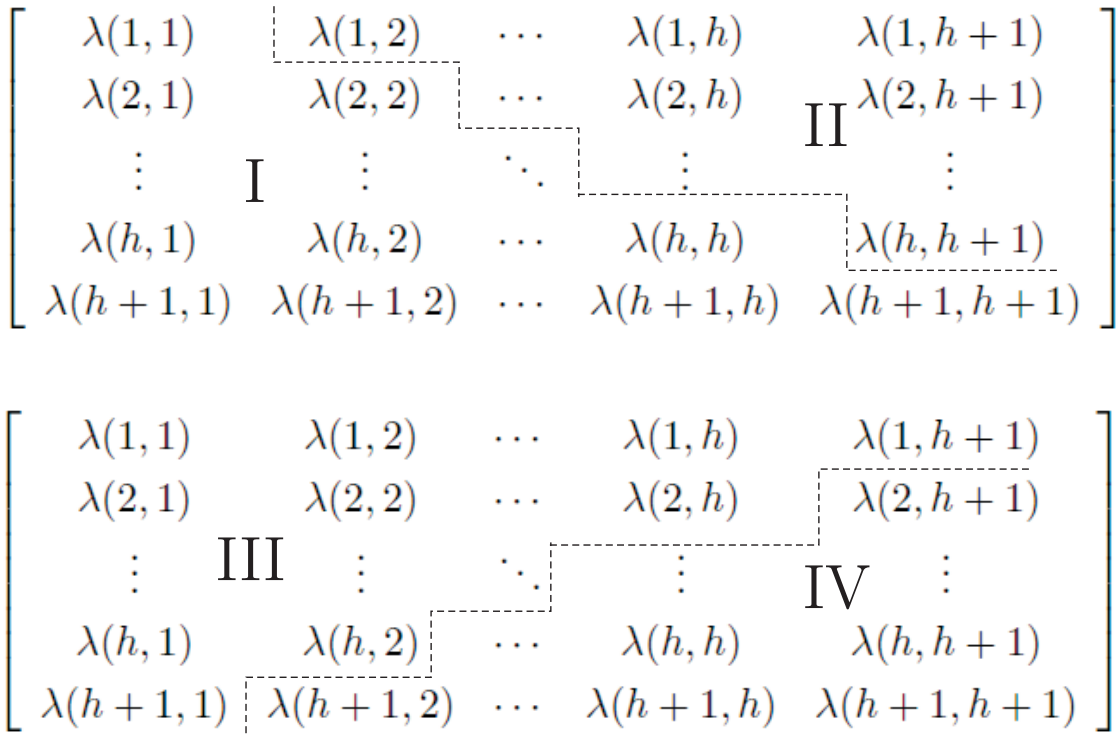

(b) Frequency Transfer Matrix positive frequency-only, $\mathbf{\Lambda}_{+}$ components

Figure A.1: $\mathbf{\Lambda}_{\pm}$ Sections and $\mathbf{\Lambda}_{+}$ Components

Appendix B

FREQUENCY TRANSFER MATRIX IN SYMMETRICAL COMPONENTS

This appendix describes the development of Frequency Transfer Matrices (FTMs) in symmetrical components (i.e. also known as pnz). Although FTMs have been well described in various publications, a detailed description of how it is developed from switching function is still useful. There are two approaches presented in this appendix. The first one starts from an FTM in abc components which is transformed to pnz components. The second approach is by harmonic selection from a direct symmetrical components description.

B.1 ABC TO PNZ FREQUENCY TRANSFER MATRIX

Suppose phase a of the switching function is described by its harmonic coefficients as:

$$s_a(t) = \sum_{m\in\mathbb{Z}} S_m e^{jm\omega_0 t} \tag{B.1}$$

where $S_m \in \mathbb{C}$ and $\boldsymbol{S}_m \forall m$ is the set of harmonic coefficients to form the harmonic vector $\boldsymbol{S}_a$. The FTM associated with this switching function is described by the Toeplitz transform of the harmonic vector S_m

$$\boldsymbol{S}_{a\mathcal{T}} = \mathcal{T}\{\boldsymbol{S}_a\} \tag{B.2}$$

If the switching functions for phases b and c are phase-shifted version of that of phase a by $\frac{-2\pi}{3}$ and $\frac{2\pi}{3}$, respectively as is generally the case then the switching functions are accordingly described as

$$\begin{aligned} s_b(t) &= \sum_{m\in\mathbb{Z}} S_m e^{jm\omega_0 t} e^{jm\frac{-2\pi}{3}} \\ s_c(t) &= \sum_{m\in\mathbb{Z}} S_m e^{jm\omega_0 t} e^{jm\frac{2\pi}{3}} \end{aligned} \tag{B.3}$$

In similar manner, the corresponding FTMs for these switching functions are

$$\begin{aligned} \boldsymbol{S}_{b\mathcal{T}} &= \boldsymbol{\Lambda}_{\Phi}(\tfrac{-2\pi}{3})\boldsymbol{S}_{a\mathcal{T}} \\ \boldsymbol{S}_{c\mathcal{T}} &= \boldsymbol{\Lambda}_{\Phi}(\tfrac{2\pi}{3})\boldsymbol{S}_{a\mathcal{T}} \end{aligned} \tag{B.4}$$

where $\boldsymbol{\Lambda}_{\Phi}(\cdot)$ is as described in 3.13

Taken together, the three-phase FTM in abc components is

$$\boldsymbol{Y}_{abc} = \begin{bmatrix} \boldsymbol{S}_{a\mathcal{T}} & & \\ & \boldsymbol{S}_{b\mathcal{T}} & \\ & & \boldsymbol{S}_{c\mathcal{T}} \end{bmatrix} \boldsymbol{U}_{abc} \tag{B.5}$$

To transform this FTM in abc components ($\boldsymbol{H}_{abc}$) to an FTM in pnz components ($\boldsymbol{H}_{pnz}$), the standard transform presented in typical symmetrical components discussion such as [4] is used

$$\boldsymbol{H}_{pnz} = \boldsymbol{A}_{pnz}^{-1}\boldsymbol{H}_{abc}\boldsymbol{A}_{pnz} \tag{B.6}$$

where

$$\boldsymbol{A}_{pnz} = \begin{bmatrix} 1 & 1 & 1 \\ \vec{a}^2 & \vec{a} & 1 \\ \vec{a} & \vec{a}^2 & 1 \end{bmatrix} \tag{B.7}$$

$$\boldsymbol{A}_{pnz}^{-1} = \frac{1}{3}\begin{bmatrix} 1 & \vec{a} & \vec{a}^2 \\ 1 & \vec{a}^2 & \vec{a} \\ 1 & 1 & 1 \end{bmatrix} \tag{B.8}$$

and $\vec{a} = -0.5 + j\frac{\sqrt{3}}{2}$

For the harmonic domain with a structure that is consistent with the EMP in B.1, $\vec{a}$, $\vec{a}^2$ and 1 in B.7 and B.8 are updated as follows

$$\begin{aligned} \vec{a} &= \boldsymbol{\Lambda}_{\Phi}(\tfrac{2\pi}{3}) \\ \vec{a}^2 &= \boldsymbol{\Lambda}_{\Phi}(\tfrac{-2\pi}{3}) \\ 1 &= \boldsymbol{\Lambda}_{\Phi}(0) \\ &= \boldsymbol{\mathcal{I}} \end{aligned}$$

$\boldsymbol{H}_{pnz}$ is worked out to be a maior-Toeplitz[†]

$$\boldsymbol{H}_{pnz} = \begin{bmatrix} \boldsymbol{S}_{abc1} & \boldsymbol{S}_{abc3} & \boldsymbol{S}_{abc2} \\ \boldsymbol{S}_{abc2} & \boldsymbol{S}_{abc1} & \boldsymbol{S}_{abc3} \\ \boldsymbol{S}_{abc3} & \boldsymbol{S}_{abc2} & \boldsymbol{S}_{abc1} \end{bmatrix} \tag{B.9}$$

where

$$\begin{aligned} \boldsymbol{S}_{abc1} &= \boldsymbol{S}_{a\mathcal{T}} + \boldsymbol{S}_{b\mathcal{T}} + \boldsymbol{S}_{c\mathcal{T}} \\ \boldsymbol{S}_{abc2} &= \boldsymbol{S}_{a\mathcal{T}} + a\boldsymbol{S}_{b\mathcal{T}} + a^2\boldsymbol{S}_{c\mathcal{T}} \\ \boldsymbol{S}_{abc3} &= \boldsymbol{S}_{a\mathcal{T}} + a^2\boldsymbol{S}_{b\mathcal{T}} + a\boldsymbol{S}_{c\mathcal{T}} \end{aligned}$$

Finally, each submatrix is described in terms of the coefficients of the original switching function.

$$\begin{aligned} \boldsymbol{S}_{abc1} &= \mathcal{T}\{\boldsymbol{S}_{3n,\forall\, n\in\mathbb{Z}_{\geq 0}}, \boldsymbol{S}_{3n,\forall\, n\in\mathbb{Z}_{<0}}\} \\ \boldsymbol{S}_{abc2} &= \mathcal{T}\{\boldsymbol{S}_{3n+1,\forall\, n\in\mathbb{Z}_{\geq 0}}, \boldsymbol{S}_{3n+1,\forall\, n\in\mathbb{Z}_{<0}}\} \\ \boldsymbol{S}_{abc3} &= \mathcal{T}\{\boldsymbol{S}_{3n-1,\forall\, n\in\mathbb{Z}_{\geq 0}}, \boldsymbol{S}_{3n-1,\forall\, n\in\mathbb{Z}_{<0}}\} \end{aligned} \tag{B.10}$$

where where $\mathcal{T}\{\cdot,\cdot\}$ is defined in 3.9.

B.2 DIRECT PNZ FREQUENCY TRANSFER MATRIX

A less common but more elegant approach to develop an FTM in symmetrical components is to extract the components directly from the switching function.

The switching function in three-phase described in symmetrical components is

$$s(t)_\psi = \sum_{m\in\mathbb{Z}} S_m e^{jm\omega_0 t} e^{jm\psi} \tag{B.11}$$

where ψ takes the value of 0, $\frac{-2\pi}{3}$ and $\frac{2\pi}{3}$ describing each of the three phases.

The input signal, on the other hand is described as

$$u(t)_\psi = \sum_{k\in\mathbb{Z}} U_k e^{jk\omega_0 t} e^{jr_k\psi} \tag{B.12}$$

where $U_k \in \mathbb{C}$ and r_k takes the value of $+1, -1$ or 0 for positive, negative and zero sequence, respectively

To analyse the harmonic transfer in symmetrical components, a representative har-

[†]maior-Toeplitz refers to a large matrix composed of Toeplitz submatrices

monic, $u_k(t)$ extracted from the input signal is used in the analysis.

$$\begin{aligned} y(t)_{k,\psi} &= \sum_{m\in\mathbb{Z}} S_m e^{jm\omega_0 t} U_k e^{jk\omega_0 t} e^{jr_k\psi} e^{jm\psi} \\ &= \sum_{m\in\mathbb{Z}} S_m U_k e^{j(m+k)\omega_0 t} e^{j(m+r_k)\psi} \end{aligned} \tag{B.13}$$

By taking into account three possible cases of symmetrical components for the input, the k^{th} harmonic of the output signal is observed and the harmonic transfer is derived.

Case 1: Positive sequence input For a positive sequence input, $r_k = 1$, the output signal is

$$y(t)_{k,\psi} = \sum_{m\in\mathbb{Z}} S_m U_k e^{j(m+k)\omega_0 t} e^{j(m+1)\psi} \tag{B.14}$$

The output sequence component of the k^{th} harmonic can either be positive, negative or zero sequence depending on the value of $e^{j(m+1)\psi}$. Firstly, the output is positive sequence if $(m+1)\psi$ is equal to $(3n+1)\psi\ \forall n \in \mathbb{Z}$. This means that the transfer from positive sequence to positive sequence is composed of S_m for $m = 3n$. Secondly, the output is negative sequence if $(m+1)\psi$ is equal to $(3n-1)\psi\ \forall n \in \mathbb{Z}$. The transfer from positive sequence to negative sequence is composed of S_m for $m = 3n+1$. Thirdly, the output is zero sequence if $(m+1)\psi$ is equal to $(3n)\psi$. The transfer from positive sequence to zero sequence is composed of S_m for $m = 3n-1$.

Case 2: Negative sequence input For a negative sequence input, $r_k = -1$; the output signal is

$$y(t)_{k,\psi} = \sum_{m\in\mathbb{Z}} S_m U_k e^{j(m+k)\omega_0 t} e^{j(m-1)\psi} \tag{B.15}$$

Using a similar argument as in the previous case, the transfers from negative sequence input to positive, negative and zero sequence is presented in Table B.1.

Case 3: Zero sequence input For a zero sequence input, $r_k = 0$; the output signal is

$$y(t)_{k,\psi} = \sum_{m\in\mathbb{Z}} S_m U_k e^{j(m+k)\omega_0 t} e^{j(m)\psi} \tag{B.16}$$

Finally, the transfers from zero sequence input to positive, negative and zero sequence is also summarised in Table B.1.

For each of these three cases a further three FTMs are developed by taking the Toeplitz transform for each of the selected harmonics vector described. Table B.1 shows a total

Table B.1: Harmonic Coefficients to Generate the FTM in Sequence Components

Input Sequence	Output Sequence	Equation $\forall\, n \in \mathbb{Z}$	Harmonic Coefficients $\boldsymbol{S}_m$
Positive	Positive	$m+1=3n+1$	$m=3n$ $\begin{bmatrix}\dots & S_{-6} & S_{-3} & S_{DC} & S_3 & S_6 & \dots\end{bmatrix}$
	Negative	$m+1=3n-1$	$m=3n+1$ $\begin{bmatrix}\dots & S_{-5} & S_{-2} & S_1 & S_4 & S_7 & \dots\end{bmatrix}$
	Zero	$m+1=3n$	$m=3n-1$ $\begin{bmatrix}\dots & S_{-7} & S_{-4} & S_{-1} & S_2 & S_5 & \dots\end{bmatrix}$
Negative	Positive	$m-1=3n+1$	$m=3n-1$ $\begin{bmatrix}\dots & S_{-7} & S_{-4} & S_{-1} & S_2 & S_5 & \dots\end{bmatrix}$
	Negative	$m-1=3n-1$	$m=3n$ $\begin{bmatrix}\dots & S_{-6} & S_{-3} & S_{DC} & S_3 & S_6 & \dots\end{bmatrix}$
	Zero	$m-1=3n$	$m=3n+1$ $\begin{bmatrix}\dots & S_{-5} & S_{-2} & S_1 & S_4 & S_7 & \dots\end{bmatrix}$
Zero	Positive	$m=3n+1$	$\begin{bmatrix}\dots & S_{-5} & S_{-2} & S_1 & S_4 & S_7 & \dots\end{bmatrix}$
	Negative	$m=3n-1$	$\begin{bmatrix}\dots & S_{-7} & S_{-4} & S_{-1} & S_2 & S_5 & \dots\end{bmatrix}$
	Zero	$m=3n$	$\begin{bmatrix}\dots & S_{-6} & S_{-3} & S_{DC} & S_3 & S_6 & \dots\end{bmatrix}$

of nine transfers from X_{pnz} to Y_{pnz}.

It is worthy of note that the entire FTM derived by extracting the correct harmonic coefficients in the symmetrical components description is identical to B.9 to B.10 which were derived using a transform from abc components to symmetrical components.

B.3 APPLICATION TO TCR MODEL

Based on the elements of the FTM in symmetrical components the structure of the harmonic transfer is as follows

$$\begin{bmatrix}\boldsymbol{Y}_p\\ \boldsymbol{Y}_n\\ \boldsymbol{Y}_z\end{bmatrix} = \begin{bmatrix}\boldsymbol{S}_{abc1} & \boldsymbol{S}_{abc3} & \boldsymbol{S}_{abc2}\\ \boldsymbol{S}_{abc2} & \boldsymbol{S}_{abc1} & \boldsymbol{S}_{abc3}\\ \boldsymbol{S}_{abc3} & \boldsymbol{S}_{abc2} & \boldsymbol{S}_{abc1}\end{bmatrix} \begin{bmatrix}\boldsymbol{U}_p\\ \boldsymbol{U}_n\\ \boldsymbol{U}_z\end{bmatrix} \tag{B.17}$$

where

$$\begin{bmatrix}\boldsymbol{Y}_p\\ \boldsymbol{Y}_n\\ \boldsymbol{Y}_z\end{bmatrix} = \begin{bmatrix}\boldsymbol{Y}_{m=3n+1}\\ \boldsymbol{Y}_{m=3n-1}\\ \boldsymbol{Y}_{m=3n}\end{bmatrix} \qquad \forall n \in \mathbb{Z}$$

The switching function of the TCR as described in 3.38 is an even function with S_m defined for $m = 2n \quad \forall n \in \mathbb{Z}$. This results to a reduction in the harmonic vectors and the FTM as follows

$$\begin{bmatrix}\boldsymbol{Y}_p\\ \boldsymbol{Y}_n\\ \boldsymbol{Y}_z\end{bmatrix} = \begin{bmatrix}\boldsymbol{S}_{m1} & \boldsymbol{S}_{m3} & \boldsymbol{S}_{m2}\\ \boldsymbol{S}_{m2} & \boldsymbol{S}_{m1} & \boldsymbol{S}_{m3}\\ \boldsymbol{S}_{m3} & \boldsymbol{S}_{m2} & \boldsymbol{S}_{m1}\end{bmatrix} \begin{bmatrix}\boldsymbol{U}_p\\ \boldsymbol{U}_n\\ \boldsymbol{U}_z\end{bmatrix} \tag{B.18}$$

where

$$\begin{bmatrix} \boldsymbol{Y}_p \\ \boldsymbol{Y}_n \\ \boldsymbol{Y}_z \end{bmatrix} = \begin{bmatrix} \boldsymbol{Y}_{m=6n+1} \\ \boldsymbol{Y}_{m=6n-1} \\ \boldsymbol{Y}_{m=\pm(6n+3)} \end{bmatrix} \qquad \begin{bmatrix} \boldsymbol{U}_p \\ \boldsymbol{U}_n \\ \boldsymbol{U}_z \end{bmatrix} = \begin{bmatrix} \boldsymbol{U}_{m=6n+1} \\ \boldsymbol{U}_{m=6n-1} \\ \boldsymbol{U}_{m=\pm(6n+3)} \end{bmatrix} \qquad \forall n \in \mathbb{Z}$$

and

$$\begin{aligned} \boldsymbol{S}_{m1} &= \mathcal{T}\{\boldsymbol{S}_{6n,\forall\ n\in\mathbb{Z}_{\geq 0}}, \boldsymbol{S}_{6n,\forall\ n\in\mathbb{Z}_{<0}}\} \\ \boldsymbol{S}_{m2} &= \mathcal{T}\{\boldsymbol{S}_{6n+1,\forall\ n\in\mathbb{Z}_{\geq 0}}, \boldsymbol{S}_{6n+1,\forall\ n\in\mathbb{Z}_{<0}}\} \\ \boldsymbol{S}_{m3} &= \mathcal{T}\{\boldsymbol{S}_{6n-1,\forall\ n\in\mathbb{Z}_{\geq 0}}, \boldsymbol{S}_{6n-1,\forall\ n\in\mathbb{Z}_{<0}}\} \end{aligned} \tag{B.19}$$

Appendix C

SYMMETRICAL COMPONENT OF HARMONICS

A three-phase voltage or current is described either as three distinct single phase variables or a set of symmetrical components. Likewise harmonics of phase variables can be described as symmetrical component harmonics. The transform from phase components to symmetrical components has long been established by Fortescue [21]. However, aside from [4], no other publication has been found to describe the relationship between phase and symmetrical components for harmonic signals. In this appendix, the equivalent symmetrical components of harmonics is derived. The first section uses a set of variables in an order of A-B-C. The second section presents the symmetrical components when the order is A-C-B.

C.1 ABC SEQUENCE SIGNAL

Consider a set of three-phase signals in the order ABC (X^{abc}), the k^{th} harmonic of each phase is individually described as follows:

$$X_{a,k}^{abc}(t) = \frac{V_k}{2}\left(e^{j(k\omega t+\theta_k)} + e^{-j(k\omega t+\theta_k)}\right) \tag{C.1a}$$

$$X_{b,k}^{abc}(t) = \frac{V_k}{2}\left(e^{j(k\omega t+\theta_k-k\frac{2\pi}{3})} + e^{-j(k\omega t+\theta_k-k\frac{2\pi}{3})}\right) \tag{C.1b}$$

$$X_{c,k}^{abc}(t) = \frac{V_k}{2}\left(e^{j(k\omega t+\theta_k+k\frac{2\pi}{3})} + e^{-j(k\omega t+\theta_k+k\frac{2\pi}{3})}\right) \tag{C.1c}$$

Using the transform to symmetrical components as described in references such as [4],

the positive sequence k^{th} harmonic is

$$\begin{aligned}
X_{p,k}^{abc}(t) &= \frac{1}{3}\left(X_{a,k}^{abc} + \vec{a}X_{b,k}^{abc} + \vec{a}^2 X_{c,k}^{abc}\right) \\
&= \frac{V_k}{6}\Big(e^{j(k\omega t+\theta_k)} + \vec{a}e^{j(k\omega t+\theta_k-k\frac{2\pi}{3})} + \vec{a}^2 e^{j(k\omega t+\theta_k+k\frac{2\pi}{3})} \\
&\quad + e^{-j(k\omega t+\theta_k)} + \vec{a}e^{-j(k\omega t+\theta_k-k\frac{2\pi}{3})} + \vec{a}^2 e^{-j(k\omega t+\theta_k+k\frac{2\pi}{3})}\Big) \\
&= \frac{V_k}{6}\Big(e^{j(k\omega t+\theta_k)} + e^{j(k\omega t+\theta_k-(k-1)\frac{2\pi}{3})} + e^{j(k\omega t+\theta_k+(k-1)\frac{2\pi}{3})} \\
&\quad + e^{-j(k\omega t+\theta_k)} + e^{-j(k\omega t+\theta_k-(k+1)\frac{2\pi}{3})} + e^{-j(k\omega t+\theta_k+(k+1)\frac{2\pi}{3})}\Big) \\
&= \begin{cases} \frac{V_k}{2}e^{j(k\omega_0 t+\theta_k)}, & k = 3n+1 \qquad \forall n \in \mathbb{Z} \\ \frac{V_k}{2}e^{-j(k\omega_0 t+\theta_k)}, & k = 3n-1 \end{cases}
\end{aligned} \tag{C.2}$$

Necessarily, the negative sequence for the same k^{th} harmonic is

$$\begin{aligned}
X_{n,k}^{abc}(t) &= \frac{1}{3}\left(X_{a,k}^{abc} + a^2 X_{b,k}^{abc} + aX_{c,k}^{abc}\right) \\
&= \begin{cases} \frac{V_k}{2}e^{-j(k\omega_0 t+\theta_k)}, & k = 3n+1 \qquad \forall n \in \mathbb{Z} \\ \frac{V_k}{2}e^{j(k\omega_0 t+\theta_k)}, & k = 3n-1 \end{cases}
\end{aligned} \tag{C.3}$$

The zero sequence ($X_{z,k}^{abc}$) component for this set of signals is null.

C.2 ACB SEQUENCE SIGNAL

Consider another set of three-phase signals, this time in the negative sequence (X^{acb}), the k^{th} harmonic of each phase is individually described as follows:

$$X_{a,k}^{acb}(t) = \frac{V_k}{2}\left(e^{j(k\omega t+\theta_k)} + e^{-j(k\omega t+\theta_k)}\right) \tag{C.4a}$$

$$X_{b,k}^{acb}(t) = \frac{V_k}{2}\left(e^{j(k\omega t+\theta_k+k\frac{2\pi}{3})} + e^{-j(k\omega t+\theta_k+k\frac{2\pi}{3})}\right) \tag{C.4b}$$

$$X_{b,k}^{acb}(t) = \frac{V_k}{2}\left(e^{j(k\omega t+\theta_k-k\frac{2\pi}{3})} + e^{-j(k\omega t+\theta_k-k\frac{2\pi}{3})}\right) \tag{C.4c}$$

Using the transform to symmetrical components as described in references such as [4],

the negative sequence k^{th} harmonic is

$$\begin{aligned} X_{n,k}^{acb}(t) &= \frac{1}{3}\left(X_{a,k}^{acb} + \vec{a}^2 X_{b,k}^{acb} + \vec{a} X_{c,k}^{acb}\right) \\ &= \frac{V_k}{6}\Big(e^{j(k\omega t+\theta_k)} + \vec{a}^2 e^{j(k\omega t+\theta_k - k\frac{2\pi}{3})} + \vec{a} e^{j(k\omega t+\theta_k + k\frac{2\pi}{3})} \\ &\quad + e^{-j(k\omega t+\theta_k)} + \vec{a}^2 e^{-j(k\omega t+\theta_k - k\frac{2\pi}{3})} + \vec{a} e^{-j(k\omega t+\theta_k + k\frac{2\pi}{3})}\Big) \\ &= \frac{V_k}{6}\Big(e^{j(k\omega t+\theta_k)} + e^{j(k\omega t+\theta_k + (k-1)\frac{2\pi}{3})} + e^{j(k\omega t+\theta_k + (k+1)\frac{2\pi}{3})} \\ &\quad + e^{-j(k\omega t+\theta_k)} + e^{-j(k\omega t+\theta_k - (k-1)\frac{2\pi}{3})} + e^{-j(k\omega t+\theta_k - (k+1)\frac{2\pi}{3})}\Big) \\ &= \begin{cases} \frac{V_k}{2} e^{j(k\omega_0 t+\theta_k)}, & k = 3n+1 \qquad \forall n \in \mathbb{Z} \\ \frac{V_k}{2} e^{-j(k\omega_0 t+\theta_k)}, & k = 3n-1 \end{cases} \end{aligned} \tag{C.5}$$

Necessarily, the positive sequence for the same k^{th} harmonic is

$$\begin{aligned} X_{p,k}^{acb}(t) &= \frac{1}{3}\left(X_{a,k}^{acb} + \vec{a} X_{b,k}^{acb} + \vec{a}^2 X_{c,k}^{acb}\right) \\ &= \begin{cases} \frac{V_k}{2} e^{-j(k\omega_0 t+\theta_k)}, & k = 3n+1 \qquad \forall n \in \mathbb{Z} \\ \frac{V_k}{2} e^{j(k\omega_0 t+\theta_k)}, & k = 3n-1 \end{cases} \end{aligned} \tag{C.6}$$

The zero sequence ($X_{z,k}^{acb}$) component for this set of signals is null.

C.3 ZERO SEQUENCE SIGNAL

Consider another set of three-phase signals, this in-phase with each either characterising a zero sequence, the k^{th} harmonic of each phase is individually described as follows:

$$X_{a,k}(t) = X_{b,k}(t) = X_{c,k}(t) = \frac{V_k}{2}\left(e^{j(k\omega t+\theta_k)} + e^{-j(k\omega t+\theta_k)}\right) \tag{C.7}$$

It is not difficult to show that the equivalent zero sequence component of this set of signals is identical to itself, while both positive and negative sequence components are null.

C.4 APPLICATION TO TCR MODEL

For a six-pulse converter such as the TCR, C.2 is updated to C.8 while C.5 is updated to C.9:

$$X_{p,k}(t) = \begin{cases} \frac{V_k}{2} e^{j(k\omega_0 t + \theta_k)}, & k = 6n-1 \qquad \forall n \in \mathbb{Z} \\ \frac{V_k}{2} e^{-j(k\omega_0 t + \theta_k)}, & k = 6n+1 \end{cases} \tag{C.8}$$

$$X_{n,k}(t) = \begin{cases} \frac{V_k}{2} e^{j(k\omega_0 t + \theta_k)}, & k = 6n+1 \qquad \forall n \in \mathbb{Z} \\ \frac{V_k}{2} e^{-j(k\omega_0 t + \theta_k)}, & k = 6n-1 \end{cases} \tag{C.9}$$

The significance of this is that signals with sequence of either $X^{abc}(t)$ or $X^{acb}(t)$ can be correctly generated if $X_p(t)$ and $X_n(t)$ are properly specified. For the fundamental frequency, where $k = 1$, $X_{p,1} = \frac{V_1}{2} e^{j(\omega_0 t + \theta_1)}$ and $X_{n,-1} = \frac{Vk}{2} e^{-j(\omega_0 t + \theta_1)}$ together results to a three-phase signal with an ABC sequence; whereas $X_{p,1} = \frac{Vk}{2} e^{-j(\omega_0 t + \theta_1)}$ and $X_{n,-1} = \frac{V_1}{2} e^{j(\omega_0 t + \theta_1)}$ together results to a three-phase signal with an ACB sequence.

Appendix D

PULSE AMPLITUDE MODULATION SPECTRUM

This appendix describes the derivation of the Pulse Amplitude Modulation (PAM) spectrum and its corresponding Frequency Transfer Matrix (FTM). The PAM spectrum that was described by Schwartz [60] has been used by Wood [75] and Hume [31] in developing harmonic models for HVDC links.

Pulse Amplitude Modulation FTM A pulse train signal with fixed pulsewidth and whose amplitudes are varied according to a modulating signal is formally defined as a Pulse Amplitude Modulation (PAM) signal [28]. Figure D.1 shows the PAM signal, $PAM(t)$ with period, T, and pulsewidth, μ, resulting from a modulating signal, $m(t)$. In this particular figure, the pulses occur at ϕ after every start of the period. It has been further described in [28] that the PAM signal is a combination of a sampling process at ϕ and a lengthening of pulses to a width μ. The lengthening process is facilitated by using a standard rectangular pulse but shifted to take-off at $\omega t = 0$ instead of centered at $\omega t = 0$. This is shown as $\sqcap_\mu(t)$ in Fig. D.2. where $\sqcap(t)$ is defined as:

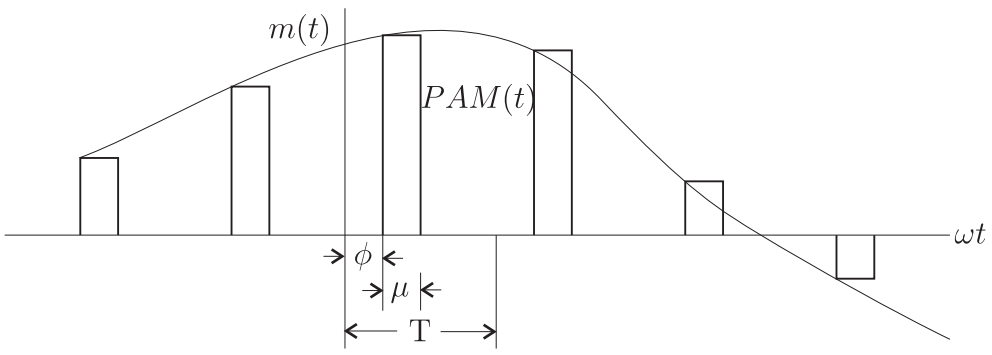

Figure D.1: Amplitude-modulated pulse train

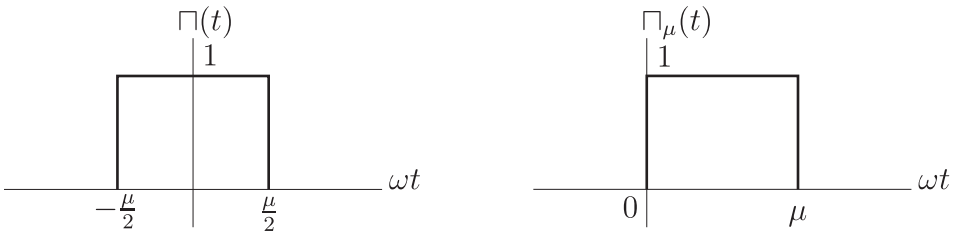

Figure D.2: Rectangular Pulse with shifted version

$$\sqcap(t) = \begin{cases} 1 & \text{if} \quad |t| < \frac{\mu}{2\omega} \\ 0 & \text{elsewhere} \end{cases} \tag{D.1}$$

$$\sqcap_\mu(t) = \begin{cases} 1 & \text{if} \quad 0 < t < \frac{\mu}{\omega} \\ 0 & \text{elsewhere} \end{cases} \tag{D.2}$$

The Fourier transform of the non-periodic function $\sqcap_\mu(t)$ can be easily computed and as special function is presented in a number of publications such as [13]. Furthermore, the discrete frequency representation of this transform is written as:

$$\prod\!\!\!\!\!\!\sqcap_\mu(f_k) = \frac{\mu}{2\pi} sinc\left(k\frac{\mu}{2\pi}\right) e^{-jk\frac{\mu}{2}} \tag{D.3}$$

where k is the integral multiples (harmonics) of the fundamental frequency. This expression, likewise specifies the elements of the harmonic vector of the rectangular pulse. The unmodulated pulse train, $s(t)$, with fixed pulsewidth, μ and takes-off at ϕ is generated by convolving $\sqcap_\mu(t)$ with the time-shifted sampling function, δ_{T_ϕ} presented in 3.19.

$$s(t) = \sqcap_\mu(t) * \delta_{T_\phi} \tag{D.4}$$

In the harmonic domain, D.4 translates into the product of the discrete frequency Fourier transform of $\prod\!\!\!\!\!\!\sqcap(kf)$ with the harmonic vector of δ_{T_ϕ}. Finally, the FTM, $\mathbf{\Lambda}_{PAM}$ which when multiplied by a modulating signal, $m(t)$ produces a PAM signal is computed as:

$$\mathbf{\Lambda}_{PAM} = \left[\prod\!\!\!\!\!\!\sqcap_\mu(f_k)\right] \cdot \left[\boldsymbol{\delta}_{T_\phi}\right]^T \tag{D.5}$$

This FTM applies to a model that includes both positive and negative frequencies. For the model in Chapter 3 where positive frequency-only is used, the procedure in Appendix A has to be applied.

Hume in his thesis, [31] presented the full spectrum of the PAM signal where the FTM corresponding to the unmodulated pulse train can be extracted.

Appendix E

HARMONIC STATE SPACE EQUATIONS BASED ON HARMONIC BALANCE

This volume on Harmonic State Space (HSS) is not complete without presenting a thorough derivation of the HSS dynamic and measurement equations using the principle of harmonic balance. The discussion presented in this appendix closely follows what was presented by Wereley [72] and cited by Love [40]. A similar discussion is also included in a very recent book by Bittanti and Colaneri [9].

Given a Linear Time Periodic (LTP) system, such as a power system with periodically switching electronic converters, the dynamic and measurement equations are written as follows:

$$\dot{x}(t) = A(t)x(t) + B(t)u(t) \tag{E.1}$$

$$y(t) = C(t)x(t) + D(t)u(t) \tag{E.2}$$

If the input to the LTP is an Exponentially Modulated Periodic (EMP) signal,

$$u(t) = \sum_{k\in\mathbf{Z}} U_k e^{(s+jk\omega_0)t} \tag{E.3}$$

where $s = \sigma + j\omega_n$,

The output $y(t)$ and the state-variable $x(t)$ take the same form

$$y(t) = \sum_{k\in\mathbf{Z}} Y_k e^{(s+jk\omega_0)t} \tag{E.4}$$

$$x(t) = \sum_{k\in\mathbf{Z}} X_k e^{(s+jk\omega_0)t} \tag{E.5}$$

whose derivative is

$$\dot{x}(t) = \sum_{k\in\mathbf{Z}} (s + jk\omega_0) X_k e^{(s+jk\omega_0)t} \tag{E.6}$$

In the same manner, the time-periodic characteristics of the A(t), B(t), C(t) and D(t)

can be expressed as Fourier series, for example,

$$A(t) = \sum_{l \in \mathbf{Z}} A_l e^{(jl\omega_0)t} \tag{E.7}$$

Using these forms into E.1

$$\sum_{k \in \mathbf{Z}} (s + jk\omega_0) X_k e^{(s+jk\omega_0)t} = \sum_{l \in \mathbf{Z}} A_l e^{(jl\omega_0)t} \sum_{k \in \mathbf{Z}} X_k e^{(s+jk\omega_0)t} + \sum_{l \in \mathbf{Z}} B_l e^{(jl\omega_0)t} \sum_{k \in \mathbf{Z}} U_k e^{(s+jk\omega_0)t} \tag{E.8}$$

and into E.2

$$\sum_{k \in \mathbf{Z}} Y_k e^{(s+jk\omega_0)t} = \sum_{l \in \mathbf{Z}} C_l e^{(jl\omega_0)t} \sum_{k \in \mathbf{Z}} X_k e^{(s+jk\omega_0)t} + \sum_{l \in \mathbf{Z}} D_l e^{(jl\omega_0)t} \sum_{k \in \mathbf{Z}} U_k e^{(s+jk\omega_0)t} \tag{E.9}$$

Summing all contributions to the k^{th} harmonic, we get the following form of the state-space equation expressed for each harmonic frequency, n:

$$\begin{aligned} (s + jk\omega) X_k &= \sum_{l \in \mathbf{Z}} A_{k-l} X_l + \sum_{l \in \mathbf{Z}} B_{k-l} U_l \\ Y_k &= \sum_{l \in \mathbf{Z}} C_{k-l} X_l + \sum_{l \in \mathbf{Z}} D_{k-l} U_l \end{aligned} \tag{E.10}$$

which is conveniently written as follows:

$$\begin{aligned} s\boldsymbol{X} &= (\boldsymbol{A} - \boldsymbol{N})\boldsymbol{X} + \boldsymbol{B}\boldsymbol{U} \\ \boldsymbol{Y} &= \boldsymbol{C}\boldsymbol{X} + \boldsymbol{D}\boldsymbol{U} \end{aligned} \tag{E.11}$$

where $\boldsymbol{X}$, $\boldsymbol{Y}$, and $\boldsymbol{U}$ are harmonic vectors while $\boldsymbol{A}$, $\boldsymbol{B}$, $\boldsymbol{C}$, and $\boldsymbol{D}$ are Toeplitz matrices of the Fourier coefficients of T-periodic $A(t)$, $B(t)$, $C(t)$ and $D(t)$, respectively. $\boldsymbol{N}$ represents the diffferentiation of the $e^{jn\omega t}$ component of $x(t)$ defined in E.5 and is a diagonal matrix defined as

$$\boldsymbol{N} \triangleq \begin{bmatrix} \ddots & & & & & & \\ & -j2\omega_0 & & & & & \\ & & -j\omega_0 & & & & \\ & & & 0 & & & \\ & & & & j\omega_0 & & \\ & & & & & j2\omega_0 & \\ & & & & & & \ddots \end{bmatrix} \tag{E.12}$$

Appendix F

PRESENTED CONFERENCE PAPERS

The following papers related to this thesis were presented by the author in conferences:

1. Orillaza, J. R. C. and Wood, A. R. W., "Linearized Harmonic Domain Model for Three-phase Thyristor Controlled Reactor", *18th Australasian Universities Power Engineering Conference (AUPEC)*, Sydney, Australia, IEEE/PES, December 2008.

2. Orillaza, J. R. C. and Wood, A. R. W., "Reduced Harmonic State Space Model of TCR", *14th International Conference on Harmonics and Quality of Power (ICHQPS)*, Bergamo, Italy, IEEE/PES, September 2010.

3. Orillaza, J. R., Hwang, M. S. and Wood, A. R., "Switching Instant Variation in Harmonic State-space Modelling of Power Electronic Devices", *20th Australasian Universities Power Engineering Conference (AUPEC)*, Christchurch, New Zealand, IEEE/PES, December 2010.

REFERENCES

[1] *IEEE 100 The Authoritative Dictionary of IEEE Standard Terms 7th Ed.* New York: IEEE Press, 2000.

[2] ABB, "ABB SVC and SVC Light Projects Worldwide," June 2011. [Online]. Available: http://www05.abb.com/global/scot/scot221.nsf/veritydisplay/.../SVC_RefList%20110608.pdf

[3] E. Acha, "Harmonic Domain Representation of Tyristor Controlled Reactors," in *International Conference on AC and DC Power Transmission.* London: IEE, September 1991.

[4] E. Acha and M. Madrigal, *Power System Harmonics Computer Modelling and Analysis.* England: John Wiley & Sons, 2002.

[5] S. Almér and U. T. Jöhnsson, "Harmonic Lyapunov Functions in the Analsyis of Periodically Switched Systems," in *45th IEEE Conference on Decision & Control.* California: IEEE, December 2006.

[6] J. E. R. Alves, Jr., L. A. S. Pilotto, and E. H. Watanabe, "Thyristor-Controlled Reactors Nonlinear and Linear Dynamic Analytical Models," *IEEE Transactions on Power Delivery*, vol. 23, no. 1, pp. 338–346, Jan 2008.

[7] P. M. Anderson, *Analysis of Faulted Power Systems.* New York: Wiley-IEEE Press, 1995.

[8] J. Arrillaga, B. C. Smith, N. R. Watson, and A. R. Wood, *Power System Harmonic Analysis.* West Sussex, England: John Wiley & Sons, 1997.

[9] S. Bittanti and P. Colaneri, *Periodic Systems Filtering and Control.* London: Springer-Verlag, 2009.

[10] L. J. Bohmann and R. H. Lasseter, "Harmonic Interactions in Thyristor Controlled Reactor Circuits," *IEEE Transactions on Power Delivery*, vol. 4, pp. 1919–1926, 1989.

[11] ——, "Stability and Harmonics in Thyristor Controlled Reactors," *IEEE Transactions on Power Delivery*, vol. 5, pp. 1175–1181, 1990.

[12] A. Böttcher and B. Silbermann, *Introduction to Large Truncated Toeplitz Matrices*. New York: Springer-Verlag, 1998.

[13] R. N. Bracewell, *The Fourier Transform and its Applications 3rd Ed.* USA: McGraw-Hill, 2000.

[14] V. A. Caliskan, G. C. Verghese, and A. M. Stanković, "Multifrequency Averaging of DC/DC Converters," *IEEE Transactions on Power Electronics*, vol. 14, pp. 124–133, January 1999.

[15] J. J. Chavez and A. Ramirez, "Dynamic Harmonic Domain Modeling of Transients in Three-phase Transmission Line," *IEEE Transactions on Power Delivery*, vol. 23, pp. 2294–2301, April 2008.

[16] L. O. Chua, "On the Choice of State Variables for the Potential Function in Nonlinear Networks," *IEEE Proceedings*, p. 2110, 1965.

[17] J. Das, *Power System Analysis: Short-circuit, Load Flow and Harmonics*. New York: Marcel Dekker, 2002.

[18] J. de Jesus Chavez, "A Modified Dynamic Harmonic Domain Distribution Line Model," in *Power and Energy Society General Meeting*. MN: IEEE/PES, July 2010.

[19] H. W. Dommel, "Digital Computer Solution of Electromagnetic Transients in Single- and Multiphase Networks," *IEEE Transactions on Power Apparatus and Systems*, vol. PAS-88, pp. 388–399, 1969.

[20] J. H. R. Enslin, W. T. J. Hulshorst, A. M. S. Atmadji, P. J. M. Heskes, A. Kotsopoulos, J. F. G. Cobben, and P. V. der Sluijs, "Harmonic Interaction Between Large Numbers of Photovoltaic Inverters and the Distribution Network," in *Power Tech Conference Proceedings*. Bologna: IEEE, June 2003.

[21] C. L. Fortescue, "Method of Symmetrical Co-ordinates Applied to the Solution of Polyphase Network," in *34th Annual Convention of the AIEE*. NJ: AIEE, June 28 1918.

[22] G. F. Franklin, J. D. Powell, and A. Emami-Naeini, *Feedback Control of Dynamic Systems, 5th ed.* New Jersey: Pearson Prentice Hall, 2006.

[23] H. Garcia and M. Madrigal, "Modelling and Analysis of a TCR-FC Reactive Power Compensator Using the Harmonic Domain," in *Electronics and Automotive Mechanics Conference CERMA*. Mexico: IEEE Computer Society, September 2009.

[24] H. Garcia, M. Madrigal, B. Vyakaranam, R. Rarick, and F. E. Villaseca, "Dynamic Companion Harmonic Circuit Models for Analysis of Power Systems with

Embedded Power Electronis Devices," *Elsevier Electric Power Systems Research*, vol. 81, pp. 340–346, 2011.

[25] L. Gyugyi and B. R. Pelly, *Static Power Frequenecy Converters.* New York: John Wiley & Sons, 1976.

[26] A. E. Hammad, "Analysis of Second Harmonic Instability for Chateauguay HVDC/SVC," *IEEE Transactions on Power Delivery*, vol. 7, pp. 410–415, 1992.

[27] J. F. Hauer and C. W. Taylor, "Information, Reliability, and Control in the New Power System," in *Americal Control Conference.* PA: AACC, June 1998.

[28] S. Haykin, *Communication Systems 4th Ed.* New York: John Wiley & Sons, 2001.

[29] R. He and Z. Cai, "Modeling and Harmonic Analysis of TCSC with Dynamic Phasors," in *Transmission and Distribution Conference & Exhibition: Asia and Pacific.* Dalian, China: IEEE/PES, August 2005.

[30] N. G. Hingorani and L. Gyugyi, *Understanding FACTS Concepts and Technology of Felxible AC Transmission Systems.* New York: IEEE Press, 2000.

[31] D. J. Hume, "Harmonic and Interharmonic Cross Modulation in HVDC Links," Ph.D. dissertation, University of Canterbury, July 2002.

[32] IEEE Special Stability Controls Working Group, "Static Var Compensator Models fro Power Flow and Dynamic Performance Simulation," *IEEE Transactions on Power Systems*, vol. 9, pp. 229–240, 1994.

[33] S. Jiang, A. M. Gole, U. D. Annakkage, and D. A. Jacobson, "Damping Performance Analysis of IPFC and UPFC Controllers Using Validated Small-Signal Models," *IEEE Transactions on Power Delivery*, vol. 26, pp. 446–454, 2011.

[34] J. G. Kassakian, M. F. Schlecht, and G. C. Verghese, *Principles of Power Electronics.* USA: Addison-Wesley, 1991.

[35] E. Kreyszig, *Advanced Engineering Mathematics 5th Ed.* New York: John Wiley & Sons, 1983.

[36] P. Kundur, *Power System Stability and Control.* USA: McGraw-Hill, 1994.

[37] B. C. Kuo, *Automatic Control Systems 7th Ed.* New Jersey: Prentice Hall, 1995.

[38] E. V. Larsen, D. H. Baker, and J. C. McIver, "Low-Order Harmonic Interactions on AC/DC Systems," *IEEE Transactions on Power Delivery*, vol. 4, pp. 493–501, January 1989.

[39] L. T. G. Lima, A. Semlyen, and M. R. Iravani, "Harmonic Domain Periodic Steady State Modeling of Power Electronics Apparatus: SVC and TCSC," *IEEE Transactions on Power Delivery*, vol. 18, pp. 960–967, July 2003.

[40] G. N. Love, "Small Signal Modelling of Power Electronic Converters for the Study of Time-domain Waveforms," Ph.D. dissertation, University of Canterbury, 2007.

[41] M. Madrigal and J. J. Rico, "Operational Matrices for the Analysis of Periodic Dynamic Systems," *IEEE Transactions on Power Systems*, vol. 19, pp. 1693–1695, 2004.

[42] R. M. Mathur and R. K. Varma, *Thyristor-based FACTS Controllers for Electrical Transmission Systems.* New Jersey: IEEE Press, 2002.

[43] P. Mattavelli, A. M. Stanković, and G. C. Verghese, "SSR Analysis with Dynamic Phasor Model of Thyristor-Controlled Series Capacitor," *IEEE Transactions on Power Systems*, vol. 14, pp. 200–208, 1999.

[44] P. Mattavelli, G. C. Verghese, and A. M. Stanković, "Phasor Dynamics of Thyristor-Controlled Series Capacitor Systems," *IEEE Transactions on Power Systems*, vol. 12, pp. 1259–1267, 1997.

[45] F. Milano, *Power System Modelling and Scripting.* London: Springer-Verlag, 2010.

[46] E. Mollerstedt, "Dynamic Analysis of Harmonics in Electrical Systems," Ph.D. dissertation, Lund Institute of Technology, February 2000.

[47] I. J. Nagrath and M. Gopal, *Control Systems Engineering, 2nd Ed.* Singapore: John Wiley & Sons, 1986.

[48] T. Noda, A. Semlyen, and R. Iravani, "Entirely Harmonic Domain Calculation of Multiphase Nonsinusoidal Steady State," *IEEE Transactions on Power Delivery*, vol. 19, pp. 1368–1377, July 2004.

[49] ——, "Harmonic Domain Dynamic Transfer Function of a Nonlinear Time-Periodic Network," *IEEE Transactions on Power Delivery*, vol. 18, pp. 1433–1441, October 2003.

[50] A. V. Oppenheim, A. S. Willsky, and S. H. Nawab, *Signals & Systems 2nd Ed.* New Jersey: Prentice Hall, 1997.

[51] J. R. C. Orillaza, M. S. Hwang, and A. R. Wood, "Switching Instant Variation in Harmonic State-Space Modelling of Power Electronic Devices," in *20th Australasian Universities Power Engineering Conference.* Christchurch, New Zealand: IEEE PES, December 2010.

[52] C. M. Osauskas and A. R. Wood, "A Frequency Domain Model of a Thyristor Controlled Reactor," in *8th International Conference on Harmonics and Quality of Power*. Athens, Greece: IEEE/PES and NTUA, October 1998.

[53] C. Osauskas and A. Wood, "Small-Signal Dynamic Modeling of HVDC Systems," *IEEE Transactions on Power Delivery*, vol. 18, pp. 220–225, January 2003.

[54] L. A. S. Pilotto, J. E. R. Alves, and E. H. Watanabe, "High Frequency Eigenanalysis of HVDC and FACTS Assisted Power Systems," in *Power Engineering Society Summer Meeting*. Washington: IEEE/PES, July 2000.

[55] L. A. S. Pilotto, W. F. Long, and A. A. Edris, "Basic Mechanisms of Control Interactions Among Power Electronic-Assisted Power Systems," in *Transmission and Distribution Conference and Exposition*. Atlanta, Georgia: IEEE/PES, October 2001.

[56] A. Ramirez, "The Modified Harmonic Domain: Interharmonics," *IEEE Transactions on Power Delivery*, vol. 26, pp. 235–241, January 2011.

[57] A. Ramirez, A. Semlyen, and R. Iravani, "Harmonic Domain Characterization of the Resonant Interaction Between Generator and Transmission Line," *IEEE Transactions on Power Delivery*, vol. 20, pp. 1753–1762, April 2005.

[58] J. J. Rico, M. Madrigal, and E. Acha, "Dynamic Harmonic Evolution Using the Extended Harmonic Domain," *IEEE Transactions on Power Delivery*, vol. 18, pp. 587–594, April 2003.

[59] S. R. Sanders, J. M. Noworolski, X. Z. Liu, and G. C. Verghese, "Generalized Averaging Method for Power Conversion Circuits," *IEEE Transactions on Power Electronics*, vol. 6, pp. 251–259, April 1991.

[60] M. Schwartz, W. R. Bennett, and S. Stein, *Communication Systems and Techniques*. IEEE Classic reissue, 1996.

[61] P. Sen, P. Biringer, and R. Segsworth, "Thyristor-Controlled Single Phase Variable Inductor," *IEEE Transactions on Magnetics*, vol. 3, pp. 240–245, September 1967.

[62] J. Serio Gomes, N. Martins, and A. Stankovic, "Improved Controller Design Using New Dynamic Phasor Models of SVCs Suitable for High Frequency Analysis," in *Transmission and Distribution Conference and Exhibition*. Texas: IEEE PES, May 2006.

[63] B. C. Smith, "A Harmonic Domain Model for the Interaction of the HVDC convertor with AC and DC Systems," Ph.D. dissertation, University of Canterbury, May 1996.

[64] A. M. Stanković, P. Mattavelli, V. Caliskan, and G. C. Verghese, "Modeling and Analysis of FACTS Devices with Dynamic Phasors," in *Power and Energy Society Winter Meeting*. Singapore: IEEE/PES, January 2000.

[65] Y. Tang and A. P. S. Meliopoulos, "Power System Small Signal Stability Analysis with FACTS Elements," *IEEE Transactions on Power Delivery*, vol. 12, pp. 1352–1361, 1997.

[66] Task Force on Harmonics Modeling & Simulation IEEE PES Harmonic Working Group, "Characteristics and Modeling of Harmonic Sources – Power Electronic Devices," *IEEE Transactions on Power Delivery*, vol. 16, pp. 791–800, October 2001.

[67] Task Force on Interfacing Techniques for Simulation Tools, "Interfacing Techniques for Time-Domain and Frequency-Domain Simulation Methods," *IEEE Transactions on Power Delivery*, vol. 25, pp. 1796–1807, July 2010.

[68] M. Vahjta, "Some Remarks on Padé-Approximations," in *3rd Symposium on Intelligent Systems in Control and Measurement*. Veszprém, Hungary: TEMPUS, September 2000.

[69] B. Vyakaranam, M. Madrigal, F. E. Villaseca, and R. Rarick, "Dynamic Harmonic Evolution in FACTS via the Extended Harmonic Domain Method," in *Power and Energy Conference at Illinois (PECI)*. Illinois: IEEE/PES, February 2010.

[70] C. L. Wadha, *Network Analysis and Synthesis*. New Delhi: New Age Intl. Ltd., 2006.

[71] N. Watson and J. Arrillaga, *Power Systems Electromagnetic Transients Simulation*. United Kingdom: IEE, 2003.

[72] N. M. Wereley, "Analysis and Control of Linear Periodically Time Varying Systems," Ph.D. dissertation, Massachusetts Institute of Technology, February 1991.

[73] A. R. Wood, D. J. Hume, and C. M. Osauskas, "Linear Analysis of Waveform Distortion for HVDC and FACTS Devices," in *9th International Conference on Harmonics and Quality of Power*. Orlando, Florida: IEEE/PES, October 2000.

[74] A. R. Wood and C. M. Osauskas, "A Linear Frequency-Domain Model of a STATCOM," *IEEE Transactions on Power Delivery*, vol. 19, pp. 1410–1418, 2004.

[75] A. R. Wood, "An Analysis of Non-ideal HVDC Convertor Behaviour in the Frequency Domain, and a New Control Proposal," Ph.D. dissertation, University of Canterbury, November 1993.

[76] P. Wood, *Switching Power Converters*. USA: Litton Educ. Pub., 1981.

ACKNOWLEDGEMENTS

Dear God,

Lord, you establish peace for us; all that we have accomplished you have done for us. [Isaiah 26:12]

Thank you for giving me the privilege to accomplish this research with my supervisor, **Dr. Alan R. Wood**. Thank you for his wisdom to see the fine details in these studies while fully appreciating the big picture and higher value of this work. Thank you, especially for his patience and encouragement during those periods when things are not going well. May you generously bless him and his family as he has been generous to all his students and supervisees.

Thank you for my second supervisor, **Prof. Neville R. Watson** for the valuable discussions and lectures on various power quality issues. Thank you for his inspiration as a God-loving academic.

Thank you for **Prof. Edson H. Watanabe** and **Dr. Nirmal Nair** for their diligent examination of this thesis and for their most welcome critiques to improve the manuscript.

Thank you for the University of the Philippines (UP) and the ERDT program of the Department of Science and Technology for providing the financial support for this foreign fellowship. Thank you for the UP-Electrical and Electronics Engineering Institute for their support for my study leave and taking the extra burden while I was away. May you help us achieve our tasks as we serve our nation.

I appreciate the postgraduate students who have come before me, whose works have both inspired and served as foundations for my research. Thanks for Geoff, Nikki, Chris, Nick, Simon, and Leo. Thank you for the amazing colleagues with whom I share the ups and downs of postgraduate research: for Lance, Mike, Bhaba, Ida, Ali, Kalyan, Parash, Thahira, Andrew, Rowan, Ryan, Shreejan, James, Vijay and Pramhod. May you help them achieve their goals and plans.

Thank you for the management and staff of the EPECentre for their support for the postgrads and for the learning experiences at the Centre. Thank you for Postgraduate Coordinators and the support staff at the UC Electrical and Computer Engineering Department. Thank you for the staff at the previous International Students Support office. May you bless their endeavors as they work to support others.

Thank you for the Christian families we had in Christchurch without whom we would not have survived this long journey. As you know each one of them by name, may you bless them with the kindness they showed us and may your Kingdom advance through their lives.

Thank you for our families in the Philippines for patiently waiting for our return. For sharing the tears in troubles and rejoicing with us in victories.

Most especially, thank you for my most beautiful wife, **Louella** for her patience, understanding and sacrifices throughout these years. It has been a huge privilege that you allowed us to take this research journey together. Thank you for our adoring daughter, **Aila Hauora** and may she appreciate, in due time, the value of her parents' labors in the academe. I love them both so much.

For without your gifts and the life you gave through Your Son, Jesus Christ, I am nothing,

jordan